8

Powder metallurgy of titanium alloys

F.H. (SAM) FROES, Consultant, USA

DOI: 10.1533/9780857098900.2.202

Abstract: The major reason that there is not more widespread use of titanium and its alloys is the high cost. In this paper, developments in one cost effective approach to fabrication of titanium components – powder metallurgy – is discussed with respect to various aspects of this technology. These aspects are the blended elemental approach, prealloyed techniques, additive layer manufacturing, metal injection molding, spray deposition, far from equilibrium processing (rapid solidification mechanical alloying and vapor deposition) and porous materials. Use of titanium powder for sputtering targets, coating, as a grain refiner in aluminium alloys and fireworks are not addressed.

Key words: additive layer manufacturing, blended elemental, compaction techniques, far from equilibrium processing, mechanical properties and shape production, metal injection molding, prealloyed, porous materials, powder metallurgy, spray deposition, titanium.

8.1 Introduction

Titanium alloys are amongst the most important of the advanced materials which are key to improved performance in aerospace and terrestrial systems.[1–5] This is because of the excellent combinations of specific mechanical properties (properties normalized by density) and outstanding corrosion behavior[6–11] exhibited by titanium alloys. However, negating widespread use is the high cost of titanium alloys compared to competing materials. This has led to numerous investigations of various potentially lower cost processes,[1–3] including powder metallurgy (PM) techniques.[1–2,6–10,12,13] In this paper the titanium PM scenario will be reviewed, dividing the various technologies into the categories shown in Table 8.1. Basically the power metallurgy techniques to be discussed are the blended elemental (BE) approach, prealloyed (PA) methods, additive layer manufacturing (ALM), metal injection molding (MIM), spray deposition (SD) and far from equilibrium processing (rapid solidification mechanical alloying and vapor deposition). Powders to be attached to the surface of body implants (to improve the bonding between artificial devices and the human body) will only be discussed briefly, and for fireworks, sputtering targets, coatings and as a grain refiner in aluminium alloys will not be addressed. An indication of where PM fits into the broad scenario of fabrication techniques is shown in Fig. 8.1.

Table 8.1 Categories of titanium powder metallurgy

Category	Features	Status
Additive manufacturing	Powder feed melted with a laser or other heat source	Pilot production
Powder injection molding	Use of a binder to produce complex small parts	Production
Spraying	Solid or potentially liquid	Research base
Near net shapes	Prealloyed and blended elemental	Commercial
Far from equilibrium processes	Rapid solidification, mechanical alloying and vapor deposition	Research base

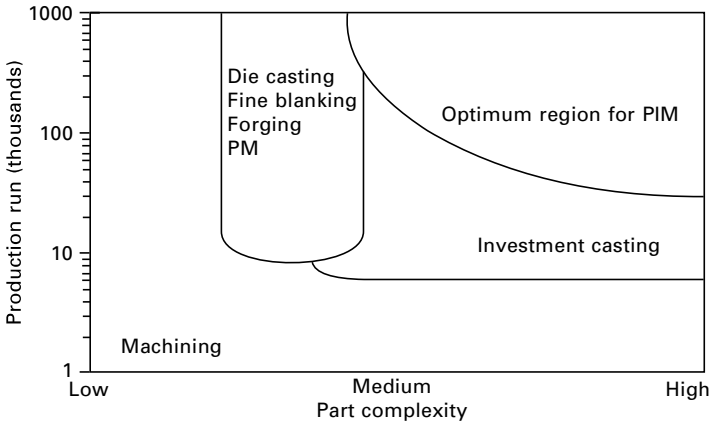

8.1 Diagram showing where powder metallurgy (PM) in general and powder injection molding (PIM) in particular, fit in with other fabrication processes (courtesy of Krebsöge, Radevormwald).

In publications over the past few years[1–3] the cost of fabricating various titanium precursors and mill products has been discussed and it has been pointed out that the cost of extraction is a small fraction of the total cost of a component fabricated by the cast and wrought (ingot metallurgy) approach (Figure 8.2). To reach a final component the mill products shown in the figure must be machined, often with very high buy-to-fly ratios (which can reach as high as 40:1). The generally accepted cost of machining a component is that it doubles the cost of the component (with the buy-to-fly ratio being another multiplier in cost per pound), Fig. 8.3. This means that anything that can be done to produce a component which is closer to the final configuration will result in a cost reduction and hence the attraction of near net shape powder metallurgy components.

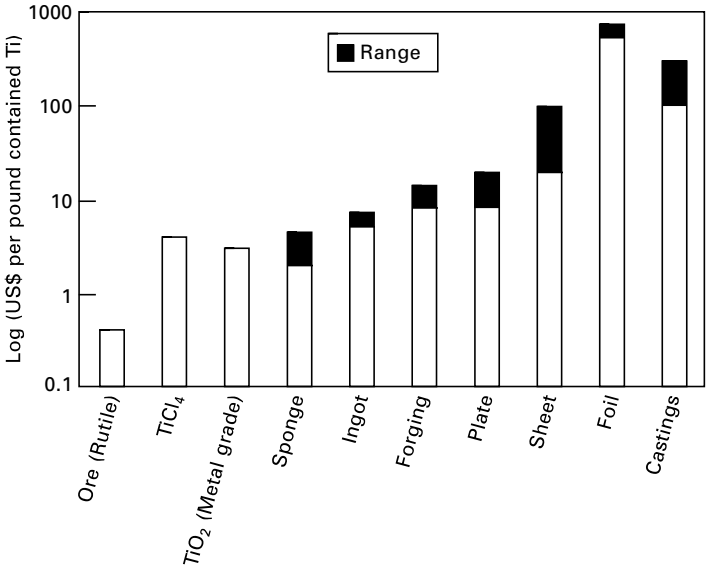

8.2 Cost of titanium at various stages of a component fabrication.

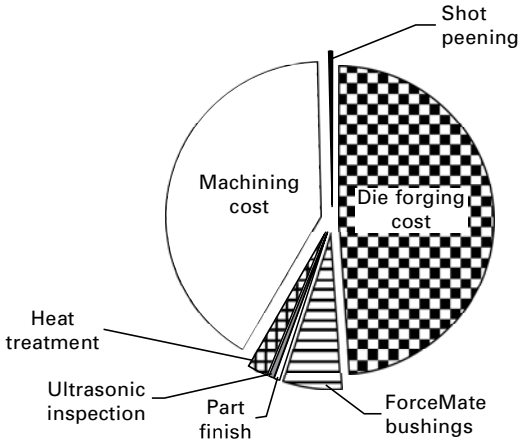

8.3 Manufacturing cost breakdown for Boeing 787 side-of-body chord. (courtesy Boeing).

8.2 Powders

Table 8.2 shows the characteristics of the different types of titanium powders that are either available or under development today. This table is based in part on a recent review of powder production methods co-authored by McCracken.[14] The oxygen level of the hydride–dehydride (HDH) powder can be reduced by deoxidizing with calcium.[14] It is also possible to convert

Table 8.2 Characteristics of different types of titanium powders (modified from Abkowitz *et al.*[15])

Type/process	Elemental or prealloyed	Advantages	Status/ disadvantages
Hunter process (pure sodium)	Elemental	Low cost, excellent for cold press and sinter	Limited availability High chloride
HDH[a] Kroll process (pure magnesium)	Elemental	Lower cost Good compactibility Readily available Low chloride	
HDH powder produced from alloys	Prealloyed	Readily available	High cost Fair compactibility
Atomized	Prealloyed	High purity available	High cost Not cold compactable
REP/PREP[b]	Prealloyed	High purity	High cost Not cold compactable
Armstrong/ International titanium (ITP) powder	Both	Compactable Moderate cost	Processibility/quality Production Scale-up
Fray	Both	TBD	Developmental
MER[c]	Both	TBD	Developmental
CSIRO TiRO[d]	Both	TBD	Developmental

[a]Hydride-dehydride. [b]Rotating electrode powder/plasma rotating electrode powder. [c]MER Corp., Tucson, AZ. [d]CSIRO Melbourne, Australia.

the angular HDH to a spherical morphology using the Tekna process (see later).

The development of new titanium production methods such as the ITP/ Armstrong, Fray, CSIRO and MER processes (see later) shown in Table 8.2 is aimed at lowering the cost of PM titanium powder. However, these powders will not be available for some time and their relative cost and processing characteristics are yet to be established.

There are a number of processes which produce pre-alloyed spherical titanium powder including the following:

- ATI Powder Metals (formerly Crucible Research Center): spherical gas atomized alloy powder, 100 pounds (45 kg) capacity melting furnace, 50 pounds (23 kg) of –100/+325 (–150/+45 μm) Ti-6Al-4V at US$130.00 per pound (US$260 per kg).
- Advanced Specialty Metals: spherical plasma rotating electrode process (PREP) –100/+325 (–150/+45 μm) Ti-6Al-4V for US$189.00 per pound (US$416 per kg).

- Raymor (now includes Pyrogenesis): spherical plasma atomized Ti-6Al-4V powder, –450 to +60 mesh (–30/+250 μm) powder available. Ti-6Al-4V US$118 per pound (US$260 per kg), oxygen 0.09 wt%.
- Baoji Orchid Titanium: spherical PREP, Ti-6Al-4V –70/+325 (–210/+45 μm), 0.13 oxygen max. US$84 per pound (US$185 per kg).
- ALD Vacuum Technologies: spherical gas atomized Ti-6Al-4V electrode induction melting gas atomization.
- Sumitomo Sitex: gas atomized Ti-6Al-4V, oxygen 0.08–0.13 wt%.
- TLS Technik: gas atomized Ti-6Al-4V with 0.13 oxygen. Ti-6Al-4V 100-270 mesh (53–150 μm), O_2 0.13 wt%, US$73 per pound (US$ 161 per kg).
- Affinity International GA and PREP: but they seem to have gone out of business.
- Iowa State University/Ames Lab: experimental gas atomization, cost effective very fine spherical powder produced using a close-coupled high pressure supersonic gas (less than 325 mesh, 45 μm). Plans are to commercialize the process under a company called Iowa Powder Atomization Technologies.
- Tekna induction plasma spheriodization process converts irregular shaped titanium powders to a spherical morphology. Typically an irregular powder with –100/+400 mesh (–150/+37 μm) is converted to a spherical powder in the same size range (but with a significant improvement in tap density and flow rate).
- Quad Cities Manufacturing Laboratory: to establish capabilities for PREP, GA, HDH and the Tekna induction plasma spheriodization process (to convert HDH powders).

The atomized powders are generally prealloyed and spherical (Figure 8.4(a)), sponge fines (a by-product of sponge production) are 'sponge-like' in nature and contain remnant salt (which prevents achievement of full density and adversely affects weldability) and are angular (Fig. 8.4(b)). The HDH powders, which are generally also prealloyed, are angular in nature (Fig. 8.4(c)).[16] Conversion to a spherical morphology using the Tekna process is shown in Fig. 8.4(d).

Four non-melt processes appear to have the greatest potential for scale-up, with an additional process being developed by Advance Materials (ADMA) Products also of potential commercial interest. These four processes are the FFC Cambridge approach, the MER technique, the Commonwealth Scientific and Industrial Research Organization (CSIRO) methods and the ITP/Armstrong process.

In the FFC Cambridge approach, titanium metal is produced at the cathode in an electrolyte (generally $CaCl_2$) by the removal of oxygen from the cathode. This technique allows the direct production of alloys such as Ti-6Al-4V at a

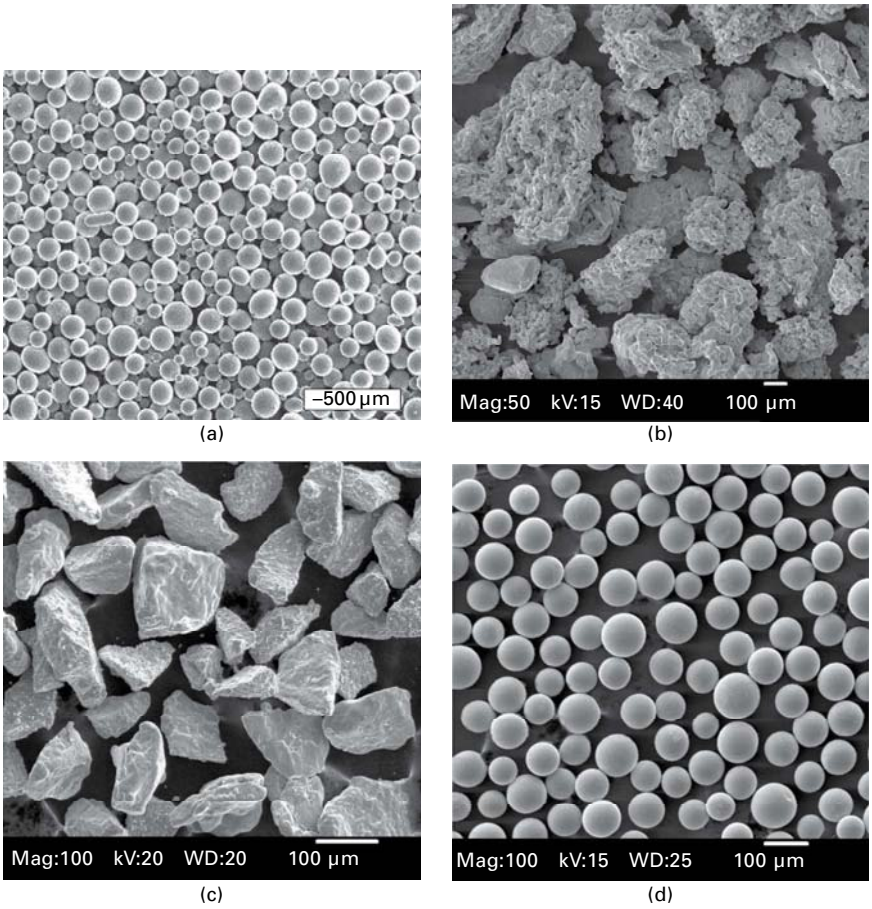

8.4 (a) Scanning electron microscopy (SEM) photomicrograph of a gas atomized prealloyed spherical Ti-6Al-4V (courtesy of Affinity International). (b) SEM photomicrograph of sponge fines produced by the Kroll process (courtesy Ametek). (c) SEM photomicrograph of angular HDH titanium powder. (d) SEM photomicrograph of spherical powder produced by processing angular HDH titanium to a spherical morphology using the Tekna technique.

cost which could be less than the product of the conventional Kroll process.[17] The process is being developed by Metalysis in South Yorkshire, UK.

The MER approach is an electrolytic method, which uses a composite anode of TiO_2, a reducing agent and an electrolyte, mixed with fused halides. Projections are for titanium production at a significantly lower cost than the conventional Kroll process.[18]

The CSIRO technique[19] builds upon the fact that Australia has some of the largest mineral and sand deposits in the world. In this approach, cost-

effective commercially pure titanium is produced in a continuous fluidized bed in which titanium tetrachloride is reacted with molten magnesium (the TiRO^{TM} process). They also have a proprietary process for producing alloys, although details are unavailable at the present time. Continuous production of a wide range of alloys including aluminides and Ti-6Al-4V has been demonstrated on a large laboratory scale. The commercially pure titanium powder produced has been used to fabricate extrusions, thin sheet (Fig. 8.5) by continuous roll consolidation, and cold-sprayed complex shapes including ball valves and seamless tubing (see later). Commercialization of the process is now in the planning stage with a decision to proceed to the pilot plant stage likely to be taken in 2013.

The ITP/Armstrong method[1–3] is continuous and uses molten sodium to reduce titanium tetrachloride, which is injected as a vapor. The resultant powder does not need further purification and can be used directly in the conventional ingot approach.The powder is most efficiently utilized in the powder metallurgy technique. A range of alloys can be produced (including the Ti-6Al-4V alloy) as a high quality homogeneous product suitable for many applications. ITP currently operates an R&D facility in Lockport, Illinois, USA and has broken ground on a four million pound (1.8 million kg) per year expansion in Ottawa, Illinois which is expected to ramp-up production

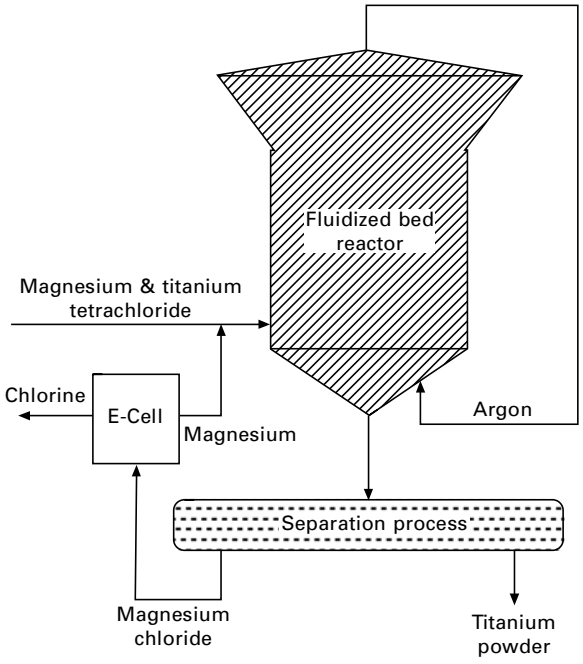

8.5 Schematic of the CSIRO process for producing commercially pure titanium powder.

throughout 2013 and will produce both commercially pure titanium and Ti-6Al-4V alloy powder.

In the ADMA Products approach[20] sponge titanium is cooled in a hydrogen atmosphere rather than the conventional inert gas. The hydrogenated sponge is then easily crushed and in the hydrogenated condition can be compacted to a higher density than conventional low hydrogen sponge, with subsequent hydrogen removal easily accomplished with a simple vacuum anneal. The remnant chloride content of the hydrogenated sponge is reported to be at low levels (helping to avoid porosity and enhancing weldability). There are 14 patents covering this approach.

Estimates of the powder shipments (in all cases per year) that have been made as HDH are: worldwide 1000–2500 MT, USA 200–400 MT and as spherical are: worldwide 150–350 MT, USA 20–50 MT.

8.3 Near net shapes

The techniques generally available for production of near net shapes (NNS) are amenable for use with various types of titanium powders; these include conventional press-and-sinter, elastomeric bag cold isostatic pressing (CIP), and ceramic mold or metal can hot isostatic pressing (HIP). For convenience, NNS will be divided into those produced using blended elemental (BE) powders and those produced from prealloyed (PA) powders.

8.3.1 Blended elemental

The blended elemental (BE) approach is potentially the lowest cost titanium PM process, especially if any secondary compaction step (e.g. HIP) can be avoided.[15,21] In the BE approach, angular titanium sponge fines (or titanium hydride powder) and master alloy composition (generally the 60:40 Al:V variety to produce the Ti-6Al-4V composition) are blended together, cold pressed and sintered to near full density. Use of titanium hydride allows densities very close to 100% to be obtained in components such as an auto connecting rod (Fig. 8.6) with mechanical properties at ingot metallurgy levels.

The blended element PM technology using hydride–dehydride (HDH) titanium powder produced by a Kroll sponge process is the key to the commercial success of Dynamet's PM process.[15] This process is producing a wide range of affordable PM mill product forms and components. Dynamet has developed critical specifications for its titanium and master alloy powders that control morphology, particle size, particle distribution and chemistry. The properties of the PM materials can be adjusted by modifications in these process parameters. The new powders that are under development may provide an opportunity to reduce the costs of PM product further if they can

8.6 Auto connecting rod fabricated via the blended elemental approach using hydrogenated titanium powder (courtesy Orest Ivasishin, Ukrainian Academy of Sciences).

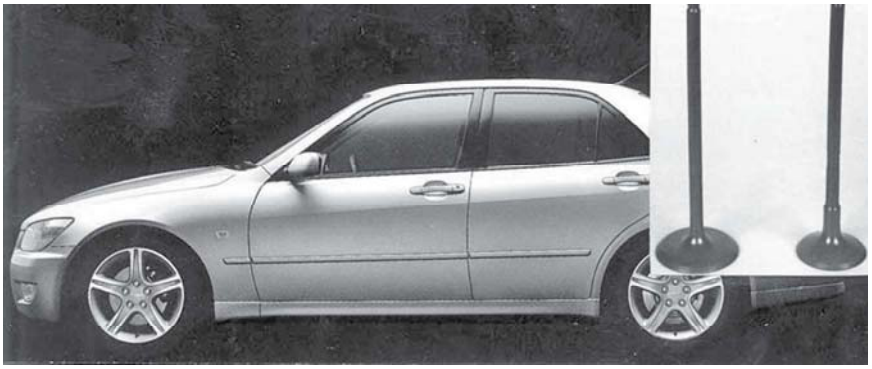

8.7 Toyota Altezza, 1998 Japanese car of the year, the first family automobile in the world to feature titanium valves. Ti-6Al-4V intake valve (left) and TiB/Ti-Al-Zr-Sn-Nb-Mo- Si exhaust valve (right) (courtesy Toyota Central R & D Labs, Inc).

be processed to the necessary density levels with properties equivalent or superior to baseline PM and wrought titanium. Finally, the cost of producing components from those powders must be competitive.

Examples of how the BE approach has been used to produce valves for production models, the Toyota Altezza family automobile, golf club heads and softball bats are shown in Fig. 8.7, 8.8 and 8.9,[1–3] respectively.

Currently, ADMA Products hydrogenated titanium powder manufacturing capacities are 50 000–60 000 lbs/year (22680–2722 kg/year), but they are installing a pilot scale unit which will triple output.[22] Meanwhile, the major aircraft companies and the US Departments of Energy and Defense (DOE

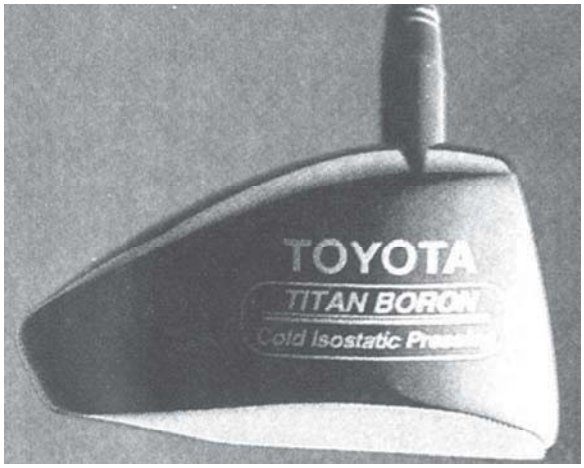

8.8 Titanium metal matrix composite golf club head (reinforced with TiB) (courtesy Toyota Central R & D Labs, Inc).

8.9 Susan Abkowitz of Dynamet Technology, Inc. holds a softball bat with a powder metallurgy titanium alloy outer shell.

and DOD) agencies have tested this material and reported that the properties of the PM Ti alloys meet Aerospace Materials Specification (AMS) and meet or exceed those of titanium wrought alloys made by conventional ingot metallurgy approaches.

8.3.2 The CHIP process

The CIP-Sinter or CHIP (CIP-Sinter-HIP) process,[15] Fig. 8.10, is used by Dynamet Technologies to produce near net shape parts for finish machining

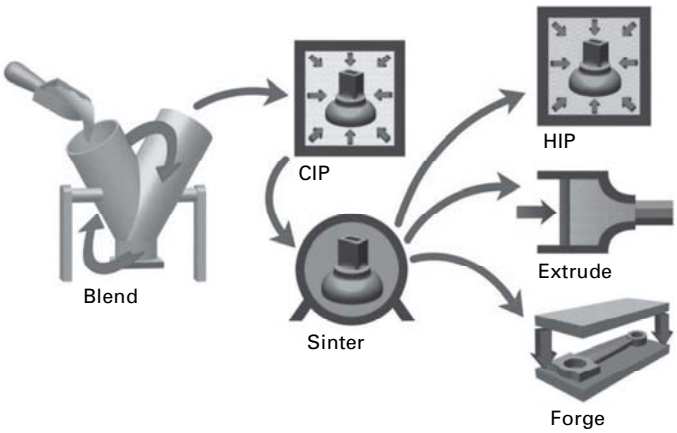

8.10 Schematic of Dynamet Technologies Inc CHIP process.

to high tolerance configurations. These processes can also be used to make forging preforms or mill product shapes for subsequent processing such as billets for casting, extrusion or hot rolling. In the case of as-sintered material, full density is achieved during subsequent processing.

The CHIP process is a green manufacturing technology[15] that has proven to be an acceptable process for producing military, industrial and medical components. This advanced PM process uses titanium powder, typically Kroll process HDH powder, blended with master alloy powder such as an aluminum–vanadium master alloy powder. The blended powder is compacted to shape by cold isostatic pressing (CIP) in elastomeric tooling. With proper selection of powders, well designed CIP tooling and appropriate pressing conditions, a shaped powder compact can be produced and readily extracted from the PM tooling with sufficient green strength for handling. It must also have sufficient uniformity and intimate contact of the powder particles for densification and homogenous alloying in the subsequent sintering process.

A wide range of shapes has been produced with size only limited by the capacity of the equipment. The size of the CIP is usually the limiting factor since vacuum furnaces and HIP units are available in larger sizes than are high pressure CIP units. Size capability also depends on the powder fill characteristics, product configuration and by tooling parameters. Successful products can range from a few grams to hundreds of kilos.

The major cost benefits of this clean, energy efficient manufacturing process are that it uses relatively low cost raw materials, avoids costly melt processes and results in relatively little material lost during processing. The capability to produce to a near net shape conserves raw material and also reduces costs for machining to finished parts. The cold pressed compacts are sintered in vacuum to high or nearly full density. Alloying of the titanium

with the desired other elements is accomplished by solid state diffusion during the sintering process. By selecting the proper powders and sintering parameters, a homogeneous alloyed material with sufficiently high density, free of interconnected porosity, is achieved.

The sintering process was historically established to reach a minimum density level at which the material had no interconnected porosity. At this density threshold the material could be hot isostatically pressed (HIP) without the processing expense of HIP encapsulation, making the HIP process economically viable. Through recent developments the capability to reach greater than 98% sintered density has been achieved. This results in as-sintered tensile properties (Table 8.3)[15] that are equivalent to wrought properties and superior to castings. This reduces the need for the HIP operation and further strengthens the economic advantage of this PM CIP-Sinter manufacturing technology.

8.3.3 ADMA Products hydrogenated titanium process

The use of titanium hydride powder instead of titanium sponge fines has led to the achievement of essentialy100% density, using a simple cost-effective press-and-sinter technique, in complex parts.[20,21] In this work, hydrogenated non-Kroll powder (by cooling the sponge produced in a Kroll process with hydrogen rather than the conventional inert gas, a lower cost titanium hydride powder has been produced by ADMA Products) was utilized along with 60:40 Al:V master alloy to produce components made from the Ti-6Al-4V alloy. The press-and-sinter densities achieved using this novel fabrication technique are shown in Fig. 8.11. The associated microstructure and typical mechanical properties are shown in Fig. 8.12 and Table 8.4 (after cold pressing, sintering, forging and annealing), respectively. The mechanical properties compare well with those exhibited by cast-and-wrought product. The low cost of this process in combination with the attractive mechanical properties make this approach well suited to the cost-obsessed automobile industry. The parts shown in Fig. 8.13 have already been fabricated and a cost estimate of less than US$3.00 for an 0.32 kg (0.705 lb) connection link has been made.[23]

Table 8.3 Ti-6Al-4V alloy: ASTM E-8 tensile properties

	Theoretical density (%)	Ultimate tensile strength (MPa) (ksi)	Yield strength (MPa) (psi)	Elongation (%)
AMS 4928 (min)		896 (130)	827 (120)	10
Typical wrought		965 (140)	896 (130)	14
Typical PM CIP-Sinter	98%	951 (138)	841 (122)	15
Typical PM CHIP	100%	965 (140)	854 (124)	16

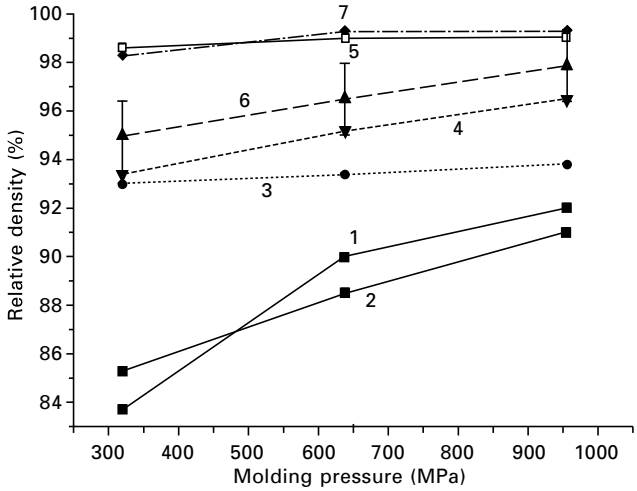

8.11 Density of Ti-6Al-4V compacts after sintering. Conditions 5 and 7 used hydrided powder and show by far the highest and most uniform densities.

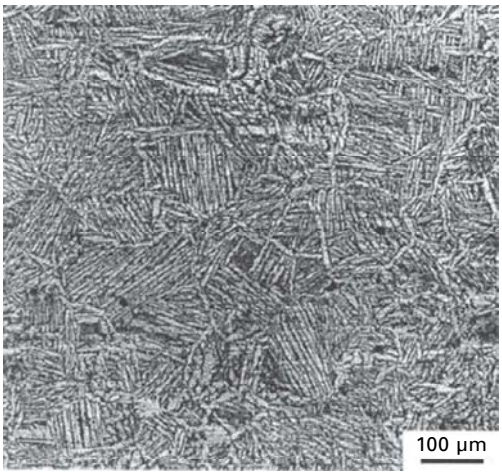

8.12 Microstructure of sintered Ti-6Al-4V material.

Table 8.4 Room temperature tensile properties of a hydrogenated titanium compact (after dehydrogenation)

PM Ti-6Al-4V	Ultimate tensile strength (MPa) (ksi)	Yield strength (MPA) (ksi)	Elongation (%)	Reduction of area (%)
3.5 cm (1.376″) thick	994–1028 (144–149)	911–938 (132–136)	14.0–15.5	34–38
ASTM	897 (130)	828 (120)	10	25

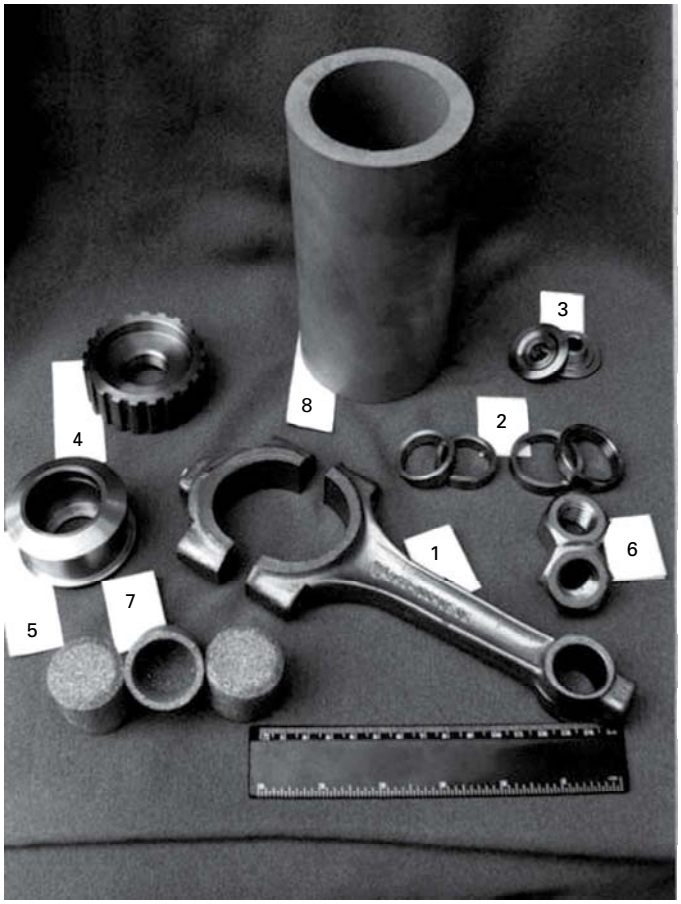

8.13 Ti-6Al-4V parts produced using a press-and-sinter approach and titanium hydride: (1) connecting rod with big end cap, (2) saddles of inlet and exhaust valves, (3) plate of valve spring, (4) driving pulley of distributing shaft, (5) roller of strap tension gear, (6) screw nut, (7) embedding filter, fuel pump, and (8) embedding filter (courtesy Ukrainian Academy of Sciences).

In Kroll's process, the removal of the Ti sponge from the retort and its subsequent crushing is time and energy intensive. In comparison, ADMA's process produces TiH_2 which, unlike Ti sponge, is very friable (see Fig. 8.14) and easily removed from the retort with no need for an expensive sizing operation. ADMA's vacuum distillation processing time is also at least 80% less than in Kroll's process since phase transformations/lattice parameter changes of the hydride sponge, in the presence of hydrogen, accelerate the distillation removal of $MgCl_2$. Finally, atomic hydrogen is released during sintering–dehydriding of the TiH_2 powder and acts as a

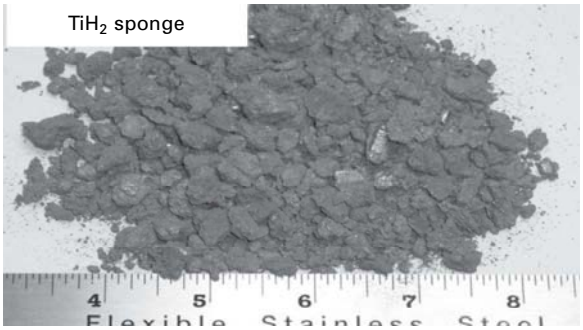

8.14 TiH_2 powder (courtesy of ADMA Products).

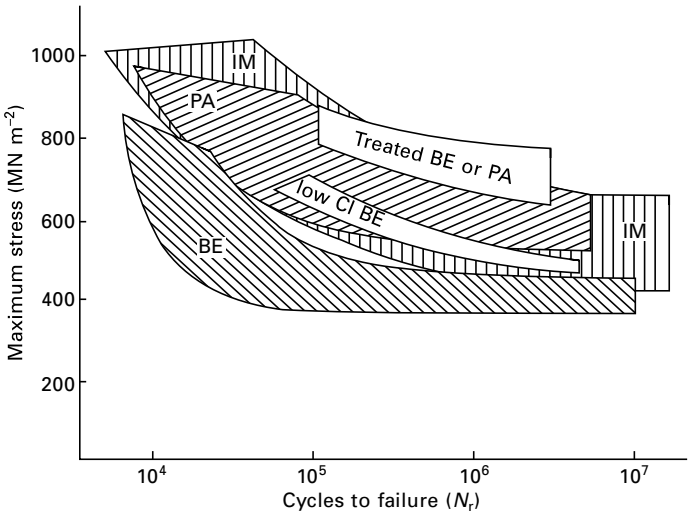

8.15 Fatigue data scatterbands of conventional BE, low chloride BE, treated low chloride BE, and PA, compared with wrought annealed material.

scavenger for impurities (e.g. oxygen, chlorine, magnesium etc) resulting in titanium alloys with low interstitials that at least meet the properties of ingot metallurgy alloys.

A comparison of the *S–N* fatigue behavior of BE and prealloyed material with cast-and-wrought product is shown in Fig. 8.15.[12]

Powders can be subsequently fabricated to other product forms, such as titanium sheet, (Fig. 8.16). Alloy sheet can be fabricated in a similar manner by adjusting the feedstock to a mixture of titanium powder and alloying additions.

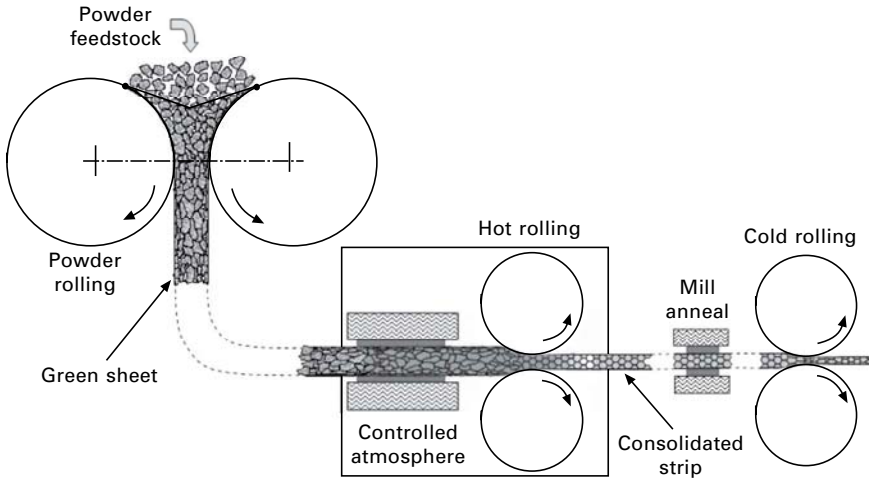

8.16 Schematic of the process used to produce commercially pure titanium sheet at CSIRO.[19]

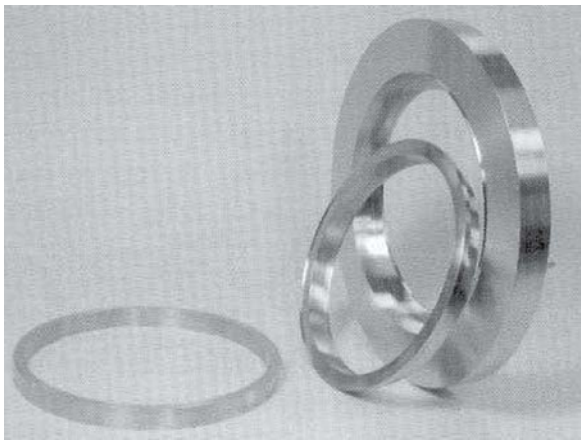

8.17 Finished titanium MMC ring for spin pit testing (courtesy IMT-Bodycote).

8.3.4 Metal matrix composites (MMC)

Both continuously and discontinuously reinforced titanium components have been produced using PM approaches. Figure 8.17 shows a finished titanium MMC ring for spin pit testing fabricated from HIP densified plasma sprayed tapes.

The blended elemental technique has also been used by Dynamet Technologies for the fabrication of MMCs utilizing particulate and a combined cold and hot isostatic pressing (CHIP) combination or forging, extrusion

and rolling of the CHIP preform.[15] The CermeTi family of titanium alloy matrix composites incorporates particulate ceramic (TiC or TiB2) (Fig. 8.18) or intermetallic (TiAl) as a reinforcement with minimal particle/matrix interaction. The mechanical properties of CermeTi material are shown in comparison with PM Ti-6Al-4V in Table 8.5.[15] A seven layer armor and a dual hardness gear have been made by Dynamet Technologies from CermeTi material.

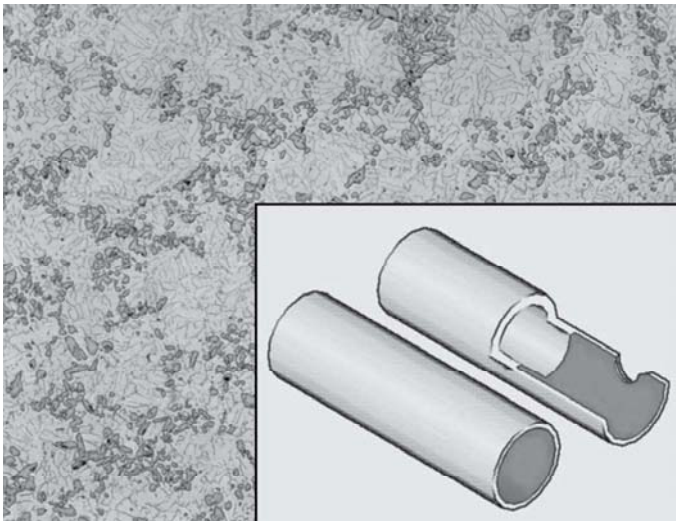

8.18 Microstructure of CermeTi material, TiC reinforcement (top) and parts fabricated from this material (bottom) (courtesy Dynamet Technology Inc.).

Table 8.5 Typical properties of CermeTi® versus Ti-6Al-4V

	Ultimate tensile strength (MPa) (ksi)	Yield strength (MPa)	Elongation (%)	Hardness (Rc)
Ti-6Al-4V PM	965 (140)	896 (130)	14	36
CermeTi®-C MMC (Ti-64+TiC)	1034 (150)	965 (140)	3	42

8.3.5 Prealloy

The prealloyed approach (PA) involves use of prealloyed powder, generally spherical in shape, which has been produced by melting, either by a technique such as the plasma rotating electrode processing (PREP) or gas atomization (GA), followed by hot consolidation (generally by hot isostatic pressing).[12] The mechanical properties are superior to ingot material (because of the

refined microstructure and lack of directionality, see later). Powders are poured either into a metal can (with metal inserts) or into a ceramic mold (sealed in a can filled with a secondary pressing media) and compacted in a hot isostatic processing (HIP) unit.

The mechanical properties of PA compacts, fabricated using the ceramic mold process, for example the Ti-6Al-4V alloy, are at least at cast and wrought (ingot metallurgy) levels, including fatigue behavior, Fig. 8.15.[12] The PA approach has been used to produce large and complex parts such as the nacelle frame, impeller and engine mount support shown in Fig. 8.19.

More recently, the advantage to be gained by the near net shape PM approach for difficult to process alloys such as the intermetallic Ti-Al-type compositions has been recognized.[24,25] Components produced from this type of alloy include the shapes shown in Fig. 8.20. The shapes are demonstration parts, the links, which demonstrate the amenability of the process to production of composite concepts, are in production. Another item produced from gamma-material is sheet produced from powder via a pack-rolling approach [26] which has been produced for systems such as the X series of NASA vehicles (Fig. 8.21).

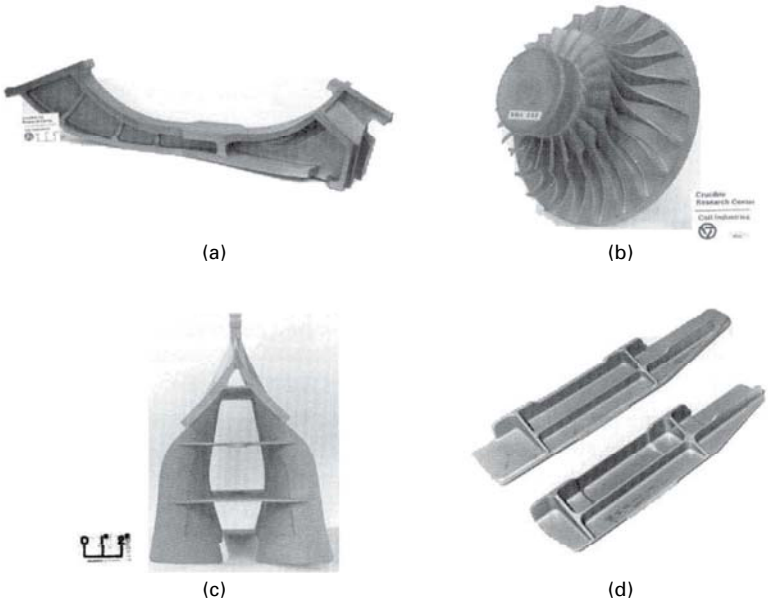

8.19 Components produced from prealloyed titanium powder, using HIP and the ceramic mold process; (a) a nacelle frame for F14A, Ti-6Al-6V-2Sn, (b) radial impeller for F107 cruise missile engine, Ti-6Al-4V, (c) a complex airframe component for the stealth bomber, Ti-6Al-4V and (d) engine mount support, Ti-6Al-4V (courtesy of Crucible Materials Corporation).

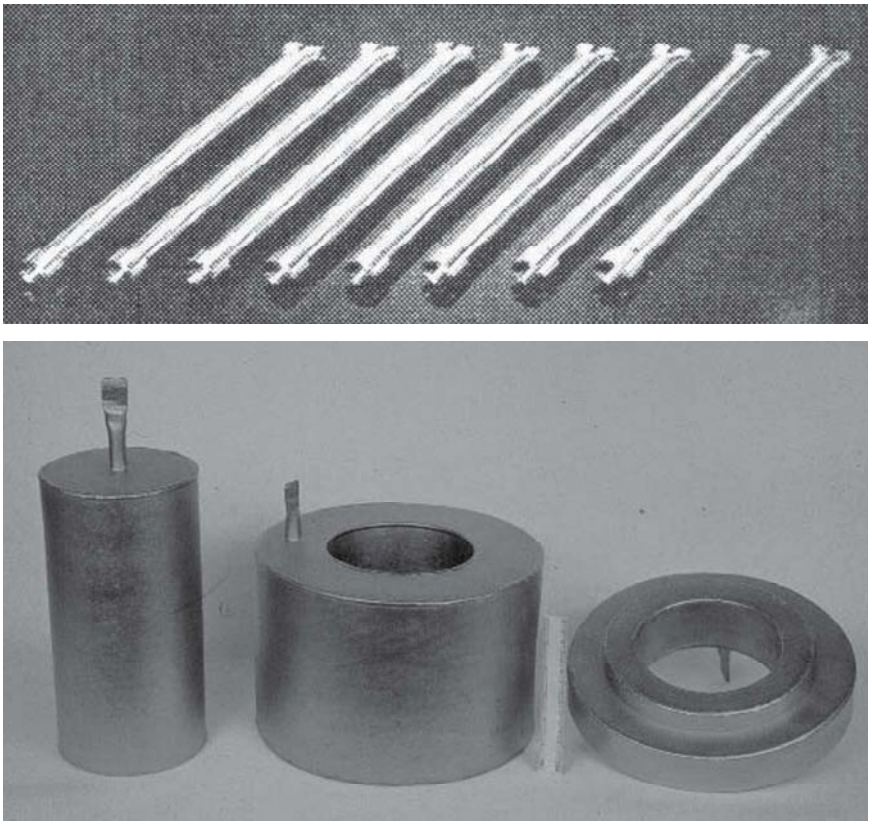

(a) (b) (c)

8.20 (Top) Gamma titanium aluminide shapes made using prealloyed gas atomized powder followed by HIP (left to right), (a) billet for subsequent forging, (b) forging or to be machined, (c) a near net sonic shape for an engine application; and (bottom) exhaust nozzle compression links for the F110 engine (power system for the F-16 Falcon), consisting of continuous SiC fibers in a Ti-6Al-2Sn-4Zr-2Mo matrix.[25]

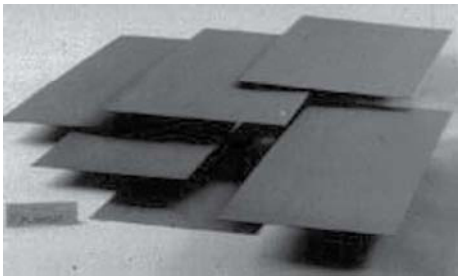

8.21 PM titanium aluminide sheet (courtesy Plansee Aktiengesellschaft).

Partly because of concerns that ceramic particles could get into the titanium parts fabricated using the ceramic mold process, no parts are currently in production using this approach. However parts produced using a shaped metal can and removable mild steel inserts (removed by chemical dissolution), Figs 8.22 and 8.23, are production ready.[27]

Despite the 30–35% volume shrinkage (typical for HIP of PA powders), advanced process modeling allows 'net surfaces' to be achieved and minimal machining stock on the 'near net surfaces'. Also these near net shape titanium parts can be made up to the size of existing HIP furnaces, that is up to 2 m, which is considerably larger than the capabilities of the other technologies discussed in this paper.

These parts exhibit mechanical properties superior to conventional cast and wrought (ingot metallurgy) components (Figs 8.24 and 8.25 and Table 8.6). Figure 8.24 shows actual tensile strength levels obtained in cast and

8.22 Near net shape Ti-6Al-4V engine component fabricated using the prealloyed metal mold method (courtesy Synertech PM).

8.23 Selectively net shape ELI Ti-6Al-4V impeller for a turbo-pump of a rocket engine. Fabricated using the prealloyed metal method (courtesy Synertech PM/P&W Rocketdyne).

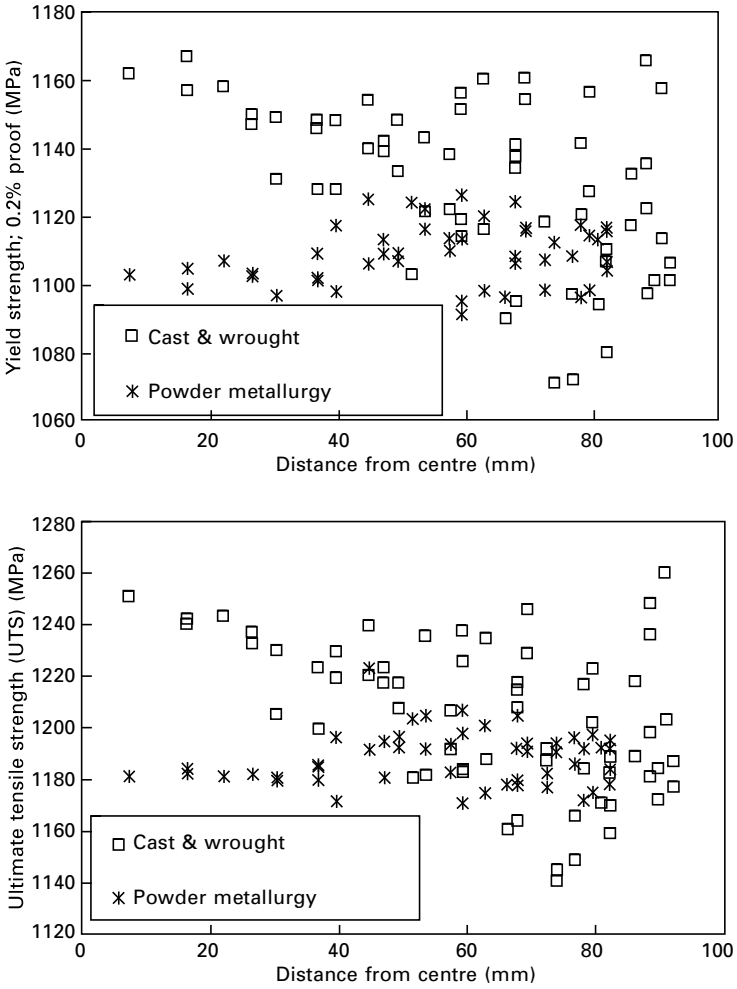

8.24 Comparison of ingot and powder metallurgy tensile properties (courtesy Prof. Igor Polkin, VILS, Russia).

wrought product compared to data from PM product. However the minimum values (which are used in design) for the PM material is above that for the conventionally fabricated material (Fig. 8.25). Fracture toughness of the PM product is superior to cast and wrought material (Table 8.6).

8.4 Additive layer manufacturing and powder injection molding

In the additive layer manufacturing approach, powder is laid down in successive layers and melted under the control of a computer to produce

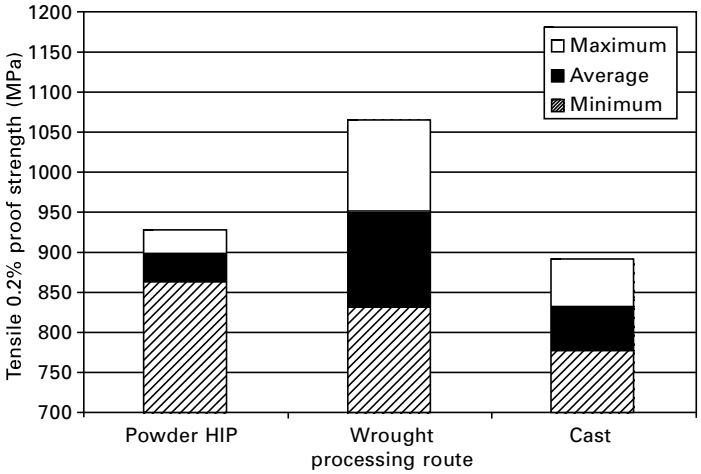

8.25 Comparison of Ti-6Al-4V powder HIP and wrought tensile properties (courtesy of Wayne Voice, Rolls-Royce).

Table 8.6 Fracture toughness of PM material and conventionally forged material (courtesy Dr. Wayne Voice, Rolls-Royce, UK)

Specimen	K_{IC} (MN $m^{-3/2}$)
1	94.0
2	96.5
3	92.5

Forged Ti-6Al-4V K_{IC} = 55 $MNm^{-3/2}$

virtually any shape; the mechanical properties are still being optimized. AeroMet Corporation's Lasform technique (Figs 8.26–8.27) features shorter lead times and greatly reduced buy-to-fly ratios (minimal machining required). This PM fabrication approach has been studied by Boeing to produce large 10 foot x 3 foot substrates, which would then be built-up.[28] However the Aeromet equipment is no longer in operation.

The strength of ALM Ti-6Al-4V is 160 ksi (1104 MPa) with 5–6% elongation 'as-formed' and after a HIP step is 140 ksi (965 MPa) with 15% elongation, equivalent to cast and wrought levels (data courtesy of B. Dutta, the POM Group).

The *S–N* fatigue performance of ALM is at or even a little above conventional material levels. However the main issue influencing growth in deployment of ALM for titanium alloys relates to raw material supply. First, with material cost being typically 40–50% of total manufacturing cost for ALM titanium, material cost is a major issue. The material supply chain is an issue for both powder and wire; sustainable sources are not always

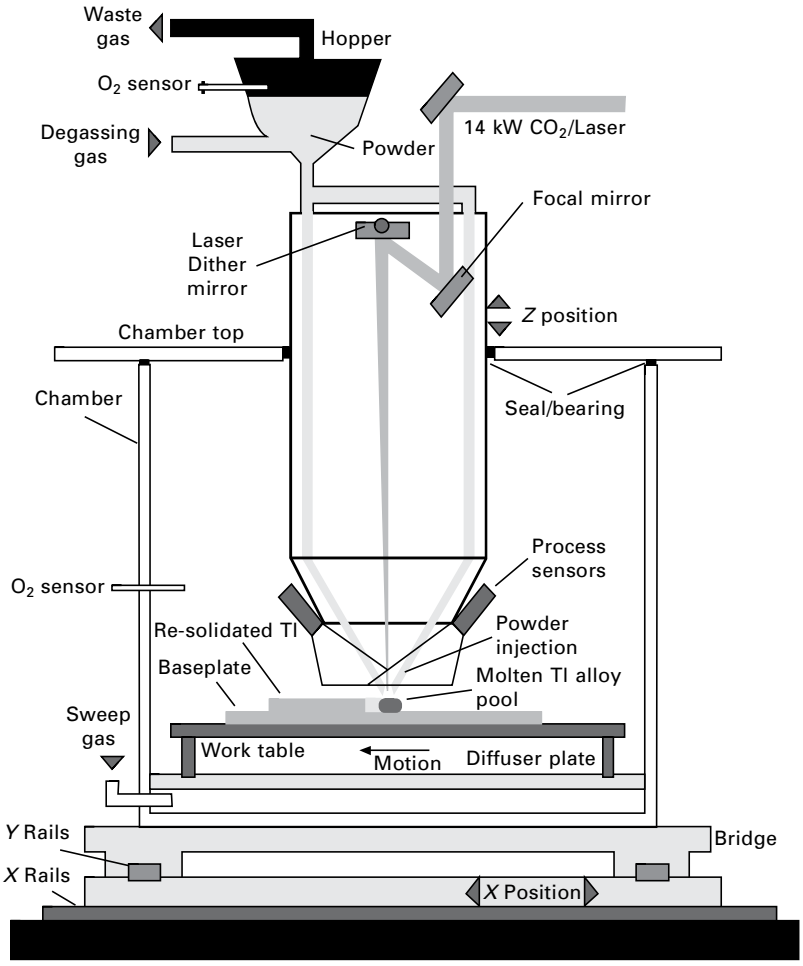

8.26 Schematic of the Lasforming System (courtesy AeroMet Corp.).

available and supplies of certain alloys have limited availability.[29] Typical parts fabricated by ALM are shown in Figs 8.29–8.32.[29] The advantage of attaching features is demonstrated in Figs 8.33 and 8.34, and the capability of using ALM in repair of a part is illustrated in Fig. 8.35.[29]

Metal powder injection molding (PIM) is based upon the injection molding of plastics; the process has been developed for long production runs of small (normally below 400 g) complex-shaped titanium parts in a cost-effective manner. This technique involves melting and pelletization of a mixture of titanium powder and a binder which are injected into a die, the binder removed chemically/thermally, and finally the part is sintered. By increasing the metal (or ceramic) particle content, the process evolved into a process for production of high density metal, intermetallic or ceramic components (Fig. 8.36).[30,31]

8.27 Examples of Lasform shapes (courtesy AeroMet Corp.). A further example of an ALM component is shown in Fig. 8.28.

8.28 Additive layer manufacturing. Sandwich structure aerofoil demonstrator produced at the Centre for Additive Layer Manufacturing (CALM) using an electron beam chamber and powder feed.

This method allows the fabrication of components with good mechanical properties provided the chemistry (particularly oxygen) is controlled.[32,33] Typical shapes are shown in Fig. 8.37. By incorporating a porous layer on the surface of body implant parts Praxis are able to cause bone ingrowth and an improved bonding between the implant and the bone.[34]

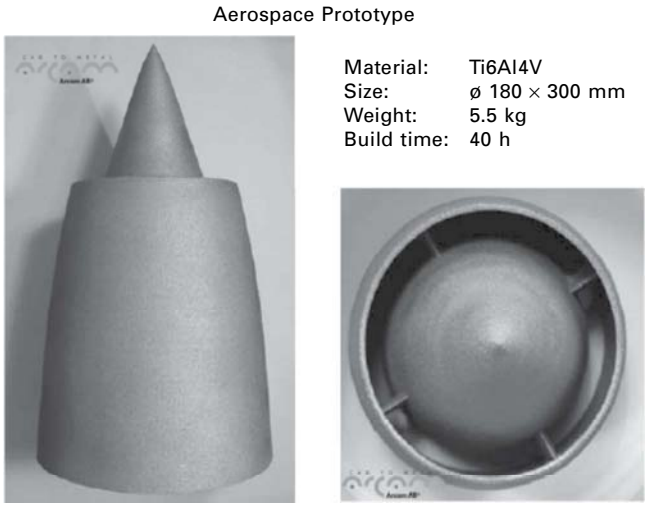

8.29 Aerospace application for ALM.

8.30 Medical implant application for ALM.

The majority of the early work on developing a viable titanium PIM process was plagued by the unavailability of suitable powder, inadequate protection of the titanium during elevated temperature processing and less than optimum binders for a material as reactive as titanium.[31] However, some PIM practitioners have now learned what the titanium community has long known – that titanium is the universal solvent and must be treated accordingly.[7–11,35]

Titanium has a high capacity to form interstitial solutions readily with a wide range of commonly encountered elements including carbon, oxygen and nitrogen, which has presented several challenges for titanium PIM development efforts. These interstitial solutions are undesirable since they

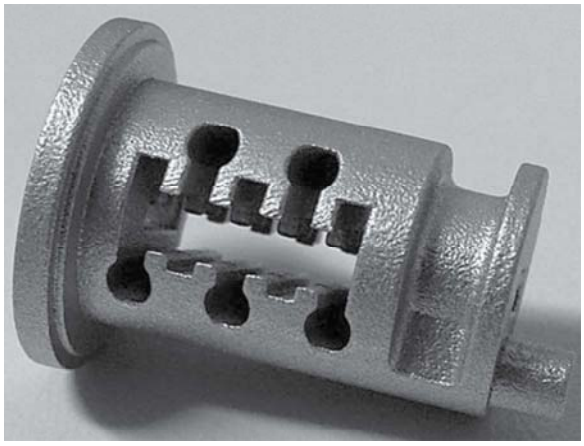

8.31 Lock barrel prototype fabricated by ALM.

8.32 Automotive pulley prototype fabricated by ALM.

significantly degrade the ductility of sintered titanium PIM parts. Therefore, it is advantageous to use a binder, which can be completely removed from the green PIM part without leaving these detrimental impurities behind. This is particularly true when fabricating structural aerospace and medical implant parts, which can require oxygen impurity levels below 300 ppm to meet ASTM F 167 Standards.

Unfortunately, unlike conventional ceramic and ferrous alloy PIM processing, there is a significantly narrower processing window between the debinding cycle and the temperature where impurity diffusion becomes significant within titanium. In general this requires that the titanium PIM binder be essentially removed from the green part at temperatures typically below 260°C to prevent introducing impurities into the sintered parts. Additionally, the binder must exhibit high chemical stability and not undergo catalytic decomposition in the presence of titanium metal powder surfaces

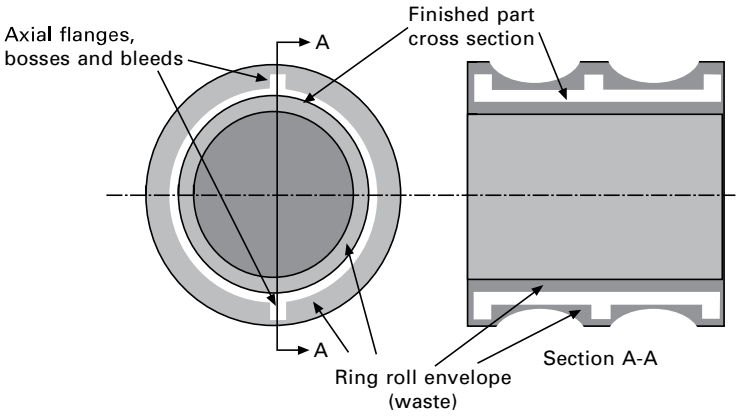

8.33 Material waste in machining features on a forged preform in conventional manufacture. Discrete features like axial flanges and bosses produce a disproportionate increase in forging size and weight.

8.34 Fan case produced by adding features by ALM to a forged preform.

during molding operations, even when held for long isothermal holds within the injection molding machine.

Attempts to adapt conventional ceramic and metal PIM binder systems for titanium processing have met with limited success. This is due to the fact that these systems often employ significant amounts of thermoplastic polymer within their formulations. Unfortunately, even some of the more

8.35 ALM repair of gas turbine components.

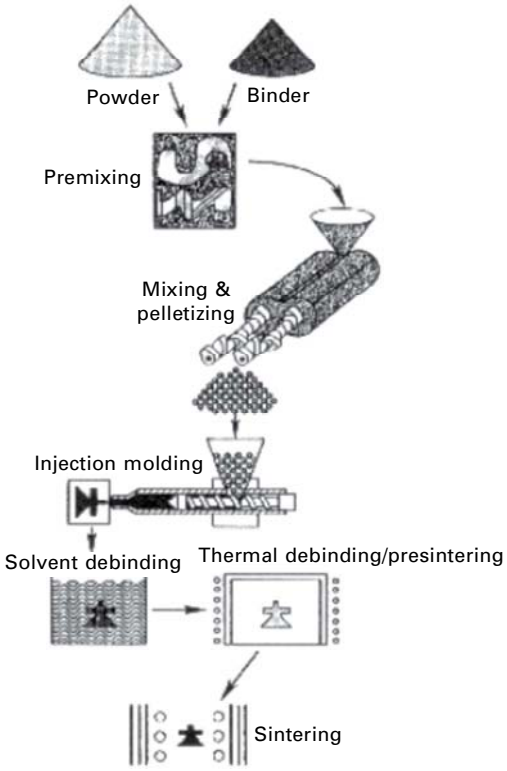

8.36 Schematic of the steps involved in powder injection molding, in which a polymer binder and metal powder are mixed to form the feedstock which is molded, debound and sintered.

8.37 Titanium MIM components (courtesy of Praxis Technology).

well-known polymer binders known for their ability readily to thermally unzip to their starting monomers (e.g. polymethylmethacrylate, polypropylene carbonate, poly-α-methylstyrene) still tend to introduce impurities into the sintered titanium PIM bodies because their depolymerization occurs close to those temperatures where impurity uptake is initiated. Alternative binder systems based upon catalytic decomposition of polyacetals are promising but require expensive capital equipment to handle the acid vapor catalyst as well as suitable means of eliminating the formaldehyde oligomers that form as polymer decomposition by-products. However, there are a number of binder systems which appear to have the necessary characteristics to be compatible with titanium.[34]

Currently titanium PIM parts run up to a foot in length, but parts over three or four inches (about 50 g weight) are not common, Fig. 8.37. The limiting factors at this time are dimensional reproducibility and chemistry. Owing to the shrinkage, large parts become dimensionally more difficult to make because of loss of shape during shrinkage. If the parts have flat surfaces to rest on the setter they come out fairly consistently. But parts with multiple surfaces that require setters in complex shapes become less practical as the size goes up. Further, large overhanging areas become difficult to control dimensionally owing to the effects of gravity. With increasing experience, the packing density of titanium powder mixes will be increased, especially when new binders become available and the shrinkage can be decreased making the dimensional problems less of a factor.

The current estimate is that worldwide titanium PIM part production is currently at about the 3–5 ton per month level.[31] This market is poised for expansion. What is needed is low cost (less than US$20/lb or US$44/kg) powder of the right size (less than about 40 μm) and good purity (which is maintained throughout the fabrication process). For non-aerospace applications, the purity level of the Ti-6Al-4V alloy can be less stringent; for example, the oxygen level can be up to 0.3 wt% while still exhibiting acceptable ductility levels (the aerospace requires a maximum oxygen level of 0.2 wt%).[11] For the CP grades, oxygen levels can be even higher; up to at least 0.4 wt% (Grade 4 CP titanium has a specification limit of 0.4 wt%).[11] In fact, the Grade 4 CP titanium (UTS 550 MPa (80 ksi)) while having a lower strength than regular Ti-6AL-4V (UTS 930 MPa (135 ksi)) may well be a better choice for many potential PIM parts where cost is of great concern. Grade 4 would allow use of a lower cost starting stock and a higher oxygen content in the final part. Further into the future, the beta alloys with their inherent good ductility (body centered cubic, bcc structure) and the intermetallics with attractive elevated temperature capability are potential candidates for fabrication by PIM. The science, technology and cost now seem to be in the market for titanium PIM to show significant growth.

8.5 Spraying and research-based processes

Spray forming can involve either molten metal [36] or solid powder. Because of its very high reactivity, the challenges associated with molten metal spraying of titanium are quite considerable. However, both spray forming in an inert environment and under reactive conditions have been achieved with appropriately designed equipment.[13] A segmented cold-wall crucible, combined with induction heating and an induction-heated graphite nozzle was used to produce a stream of molten metal suitable for either atomization, to produce powder or spray forming (Fig. 8.38).

Recently there has been increased interest in cold-spray forming involving solid powder particles.[37] Cold spray (<500°C) can produce both monolithic 'chunky' shapes and coated components. In this process, solid powder is introduced into a deLaval-type nozzle and expanded to achieve supersonic flow (Fig. 8.39). Powders are in the range of 1–50 μm, at relatively low temperatures (<500°C) with a velocity in the range of 300–1200 m s^{-1}. Both monolithic 'chunky' shapes and coated components can be produced (Fig. 8.40)[19] and the coatings can be applied even to the inside of tubular components. The density of the sprayed region is less than full density, but this can be increased to 100% density by a subsequent HIP operation.

This technique is also very useful in bonding together normally difficult to bond metals such as titanium and steel (Fig. 8.41).

Rapid solidification (RS), mechanical alloying (MA) and vapor deposition

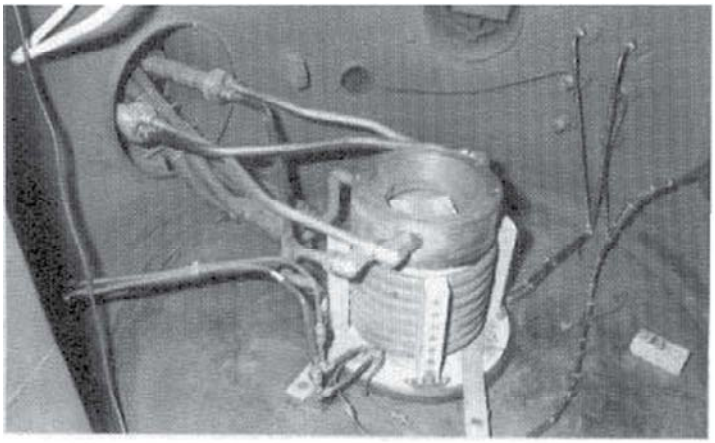

(a)

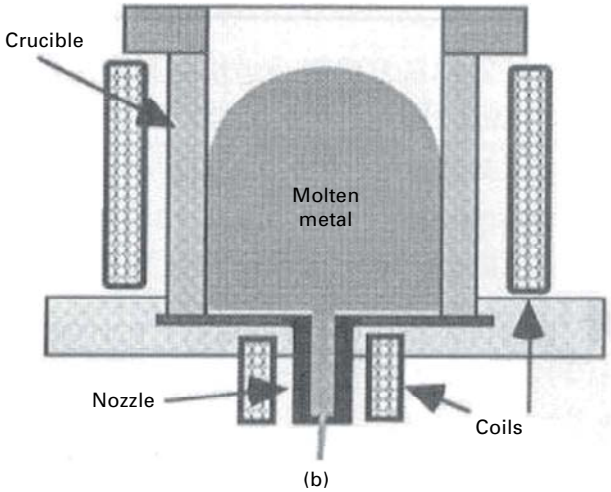

(b)

8.38 (a) Cold-wall induction bottom-pour (CWIBP) crucible installed in a plasma cold hearth furnace, (b) schematic of the CWIBP system.

(VD) all fall in the category of 'far from equilibrium processes'.[13] Novel constitutional (such as extension of solubility levels) and microstructural (in particular microstructural refinement and production of very stable dispersions of second phase particles) effects can be obtained by all three processes, however commercial processes are not on the near horizon. An example of the fine dispersion of second phase particles which can be obtained by RS is shown in Fig. 8.42(a) and nanograined material produced by MA in Fig. 8.42(b).[38,39] These nanograins show surprisingly good stability on exposure to elevated temperatures, especially when yttria particles are dispersed throughout the matrix.

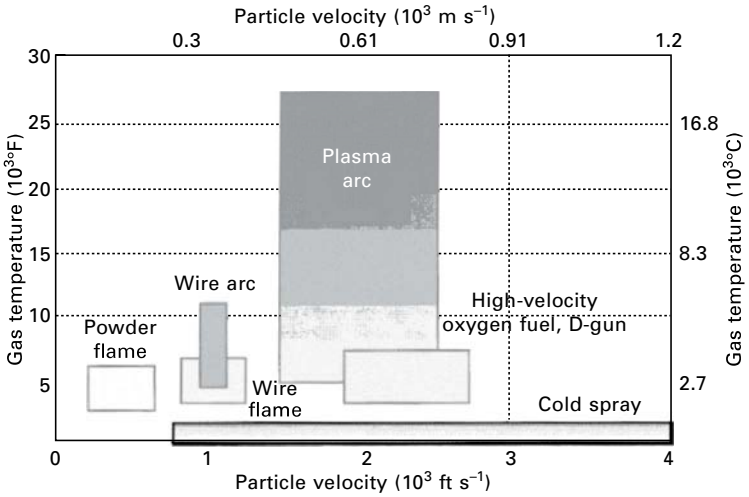

8.39 Temperature versus velocity regimes for common thermal spray processes compared to temperature and velocity in cold spray technology.

8.40 Titanium heat pipe connectors produced by cold spraying (courtesy of M. Jahedi, CSIRO).

The VD approach can be used to alloy together normally virtually immiscible Mg with Ti to create low density alloys akin to Al-Li alloys, and fabricate layered structures at the nano-level (Fig. 8.43).[40]

Also, currently in the research base are thermohydrogen processing (THP)[13,41] and porous structures.[42] By intentionally adding hydrogen to a titanium alloy such as Ti-6Al-4V with a normal PM microstructure, the

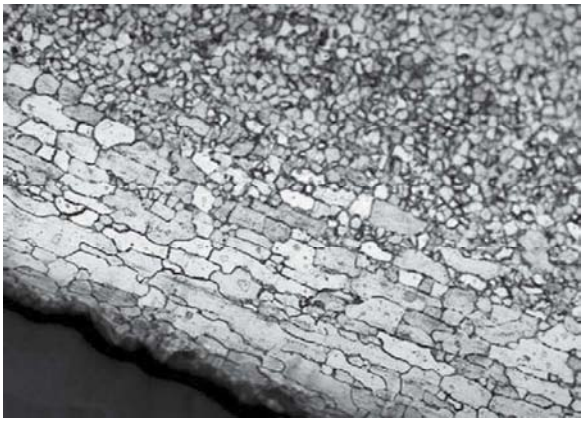

8.41 Optical photomicrograph showing the excellent bonding of titanium to steel (courtesy Ktech).

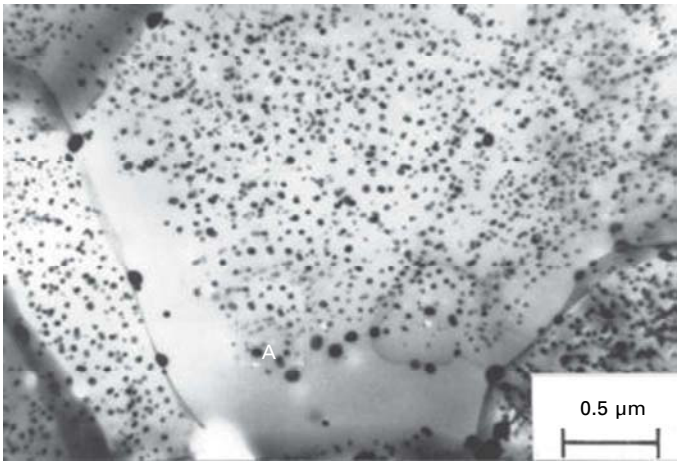

(a)

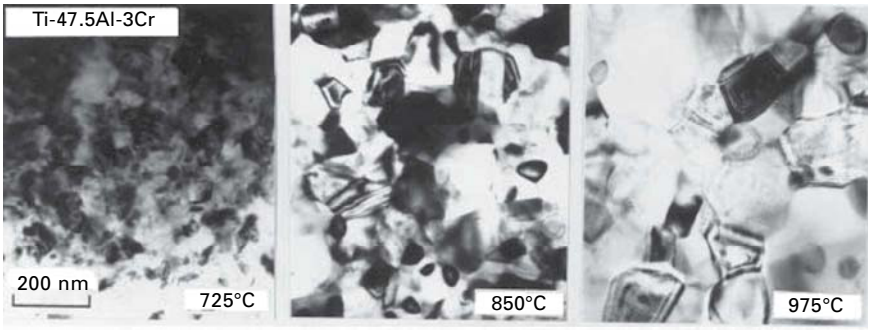

(b)

8.42 Titanium aluminide intermetallic alloys exhibiting (a) a fine dispersion of second phase erbia particles (Ti3Al based alloy) and (b) nanograins after HIP at the temperatures indicated (TiAl based alloy).

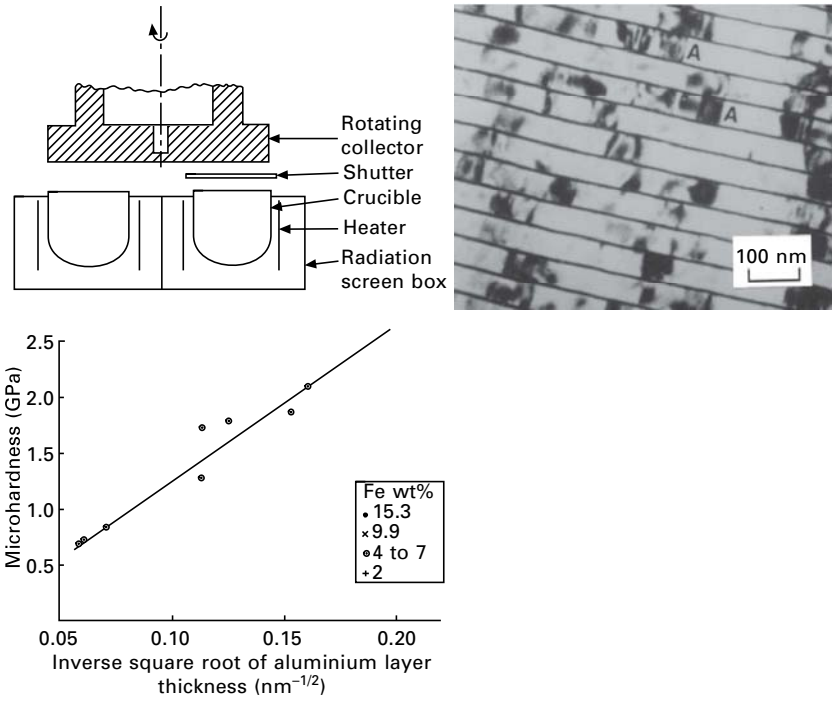

8.43 Schematic cross section of rotating collector used in vapor deposition of layered nanostructured materials (top left). Increase in hardness with decreasing layer spacing (bottom left), and layered nanostructured consisting of layers of Al and Fe (top right).

microstructure can be refined in the dehydrogenated conditions (Fig. 8.44) with an enhancement in mechanical properties.[41]

A novel type of porous low density titanium alloy can be produced by HIP consolidation of alloy powder in the presence of an inert gas such as argon (Fig. 8.45).[13] The tensile strength decreases in a linear manner as the porosity level increases, following the 'rule of mixtures' relationship at least up to 30% porosity level. This material exhibited excellent damping characteristics suggesting a generic area of application. There may also be applications in body implants with the foam integrated in various locations to facilitate growth of bone/flesh into the porous regions promoting a stronger joint. Tensile testing of the bond between foam and dense material indicated a bond strength in excess of 85 MPa well above the Food and Drug Administration (FDA) requirement of 22 MPa for porous coatings on orthopedic implants.

Porous structures with a potential use in honeycomb structures or in sound attenuating or firewall applications are now possible with very precisely controlled porosity levels and architecture using a novel blended metal–plastic approach. (Fig. 8.46).[42]

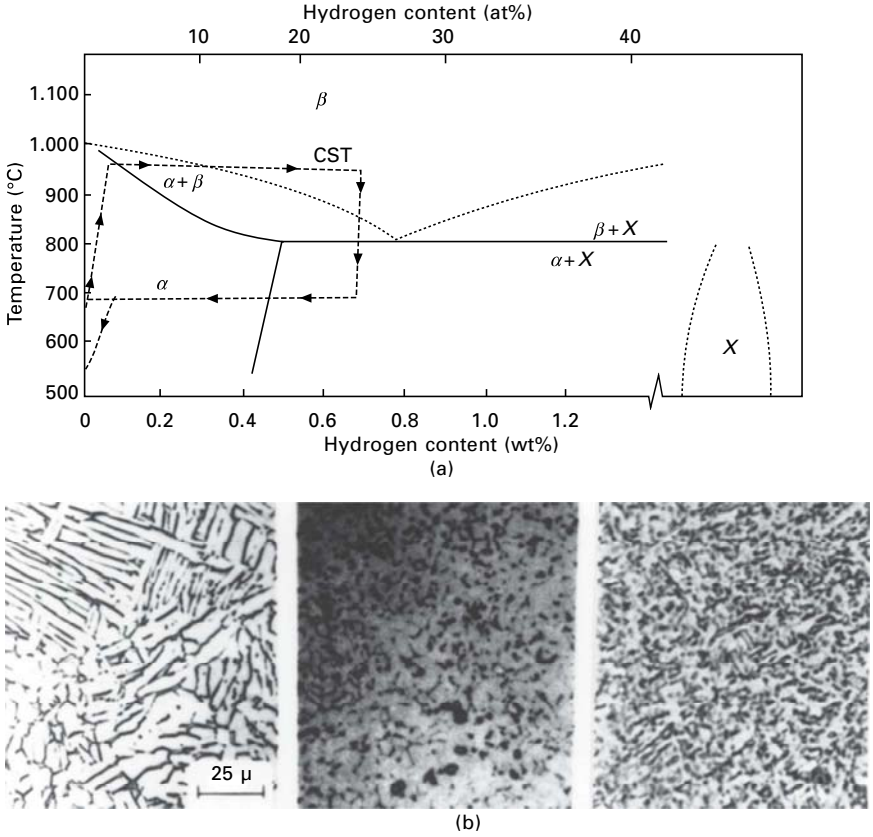

8.44 (a) Pseudo binary phase diagram for Ti-6Al-4V. X represents the hydride phase and CST (constitutional solution treatment) is one possible thermohydrogen processing treatment, and (b) refinement of the microstructure of Ti-6Al-4V powder compact using the thermochemical processing technique, (left) as HIP coarse alpha laths, (center) hydrogenated then compacted, (right) hydrogenated in compacted state. The latter two conditions are after dehydrogenation, both showing a refined alpha microstructure, (center) equiaxed grains, (right) fine alpha laths.

8.6 Future trends

Over the past 30 years, a great deal of money, much of it from US government sources, has been spent in attempting to circumvent the high cost of titanium components for aerospace and terrestrial applications. However, despite a few successes with lower integrity, BE parts and recent advances in PIM, the overall market is small; in total perhaps 20 000 pounds per year maximum worldwide.

However, a variety of high quality, low cost powders should be available

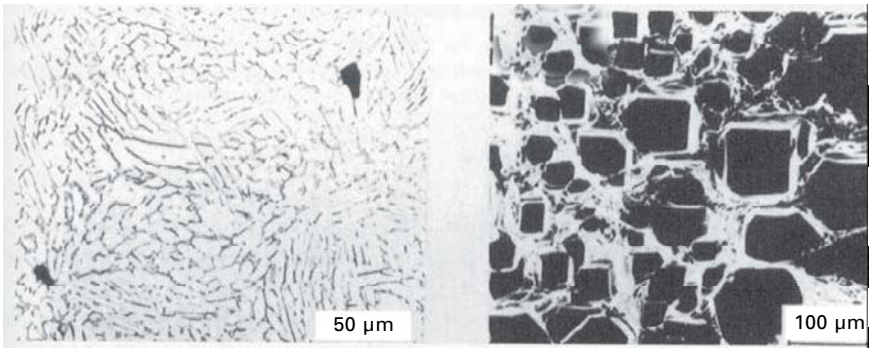

8.45 (a) Optical micrograph of pores in HIP Ti-6Al-4V containing argon after annealing at 700°C (1290°F), and (b) SEM of sample containing up to 40% porosity after an anneal in excess of 1000°C (1830°F).

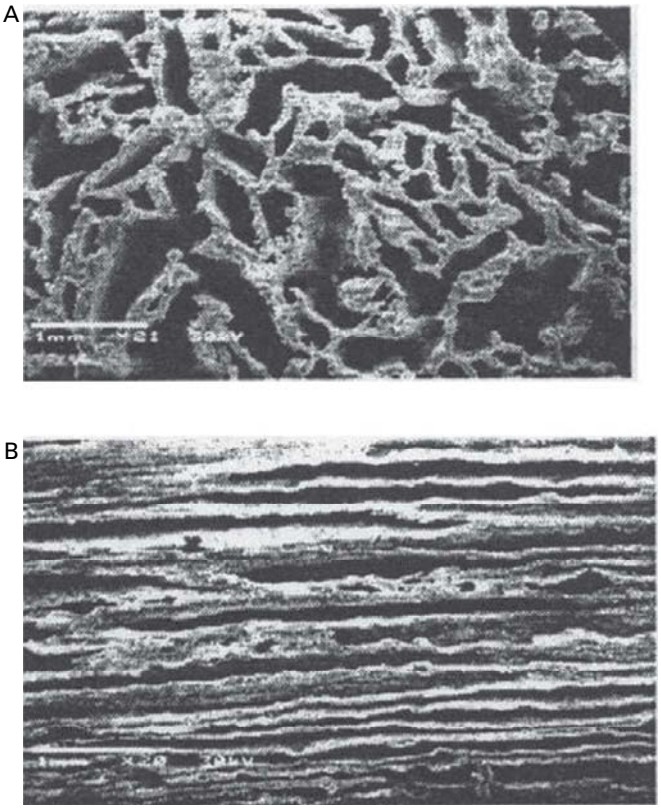

8.46 Micrographs of foams produced by die compaction (A) and extrusion (B). A, cross section is perpendicular to the compaction direction; B, cross section is parallel to the extrusion direction.

8.47 Cold press, sinter and hot rolled preform (weighing 95 kg (210 pounds)) for commanders hatch forging (Bradley Fighting Vehicle) (courtesy of ADMA Products).

soon. There have also been a number of developments, which should lead to a reasonable growth of products produced by the PM method. There appear to be three areas where significant growth can occur: (a) small parts (less than 1 pound in weight) by PIM, (b) larger parts using the BE and PA techniques and (c) generally larger parts using the ALM approach. Early entrants to the PIM marketplace naively largely ignored what every good titanium metallurgist knows – that titanium is the universal solvent. This fact should be clear to current titanium PIM practitioners and growth should be healthy in this area. Blended elemental applications are likely to grow especially with innovative approaches such as use of hydrogenated powder to produce uniformally high densities[20,21] including large armored vehicle parts (Fig. 8.47).

There are barriers to overcome using the PA approach; here the competition is with critical components produced by the ('tried and true') cast-and-wrought or direct casting approach.[43] Recent developments suggest that immediate applications for PA titanium is in complex parts, very difficult to fabricate TiAl intermetallic alloys, and in metal matrix composite concepts.[24,25] The ALM approach should also see significant growth, in competition with the BE and PA techniques. The research-based techniques mentioned in this paper all show promise, but have yet to approach commercial fruition.

8.7 Acknowledgements

The author recognizes useful discussions with Joe Fravel, Serge Grenier, Mitch Godfrey, G. N. Hayek Jr., Andy Hanson, Larry LaVoie, John (Qiang)

Li, Tim McCabe, Steve Miller, John Moll, Vladimir Moxson, Vladimir Duz, Takashi Nishimura, Hiroaki Shiraishi, Tessa Stillman, Yoshy Takada, Bruno Unternährer, Jim Withers and Fred Yolton. We also acknowledge the contribution of Mrs Marlane Martonick for assistance in formatting and typing the text.

8.8 References

1 Froes F H (Sam), Imam M A and Fray D (eds), *Cost Affordable Titanium*, TMS, The Minerals, Metals and Materials Society, Warrendale, Pa, 2004.
2 Gungor M N, Imam M A and Froes F H (Sam) (eds), *Innovations in Titanium Technology*, TMS, Warrendale, Pa. 2007.
3 Imam M A, F H Froes and Dring K F (eds), *Cost-Affordable Titanium III* TMS, Warrendale, Pa. 2010.
4 Congress of the US Office of Technology Assessment, *Advanced Materials by Design* (June 1988).
5 Materials Science and Engineering – *Forging Stronger Links to Users*, NMAB, National Academy Press publication NMAB-492, Washington DC, 1999.
6 Froes F H, Eylon D and Bomberger H (eds) *Titanium Technology: Present Status and Future Trends*, TDA, Dayton, OH, 1985.
7 Froes F H (Sam), Yau T-L and Weidenger H G, 'Titanium, Zirconium and Hafnium', *Materials Science and Technology – Structure and Properties of Nonferrous Alloys*, Chapter 8, KH Matucha (ed.), VCH Weinheim, FRG, 1996, 401.
8 Froes F H (Sam), 'Titanium', *Encyclopedia of Materials Science and Engineering*, Chapters 3.3.5a–3.3.5e, P. Bridenbaugh (ed.) Elsevier, Oxford, UK, 2000.
9 Froes F H (Sam), 'Titanium alloys', *Handbook of Advanced Materials*, Chapter 8, James K. Weasel (ed.), McGraw-Hill Inc., New York, NY, 2000.
10 Froes F H (Sam), 'Titanium metal alloys', *Handbook of Chemical Industry Economics, Inorganic*, Jeff Ellis (ed.), John Wiley and Sons, New York, 2000.
11 Boyer R R, Welsch G and Collings E W (eds), *Materials Properties Handbook: Titanium Alloys*, ASM International, Materials Park, OH, 1994.
12 Froes F H and Eylon D, 'Powder metallurgy of titanium alloys', *International Materials Reviews*, 1990, **35**, 162.
13 Froes F H and Suryanarayana C, 'Powder processing of titanium alloys', *Reviews in Particulate Materials*, A. Bose, R.M. German and A. Lawley (eds), MPIF, Princeton, NJ, 1993, **1**, 223.
14 McCracken C G, 'Manufacture of hydride-dehydride low oxygen Ti-6Al-4V (Ti-6-4) powder incorporating a novel powder de-oxidation step', *Euro P/M Conference 2010*.
15 Abkowitz S M, Abkowitz D, Fisher H, and Main D H (2011), 'Affordable P/M titanium – Microstructure, properties and products', *MPIF Conference*, 2010.
16 McCracken C G, private communication February 14, 2012.
17 Bertolini M, private communication April 21, 2010.
18 Withers J, private communication, May 29, 2011.
19 Barnes J E, private communication, November 7, 2011.
20 Abakumov G I, Duz V A and Moxson V S (2010), 'Titanium alloy manufactured by low cost solid state PM processes for military, aerospace and other critical applications,' ITA Conference.

21 Ivasishin OM, Savvakin DV, Froes FH, Moxson VS and Bondareva KA, *Mater Technol*, 2002, **17**(1), 20–5.
22 Moxson V S, private communication, October 17, 2011.
23 Moxson V S, ADMA Corp., private communication, October 31, 2011.
24 Moll J H and McTiernan B J 'A powder metallurgy approach to fabrication of Ti-Al-type intermetallics', *MPR*, 2000, January, 18–26.
25 Moll J H 'Fabrication of titanium intermetallics via a powder metallurgy approach', JOM, 2003, **52**(5), 32.
26 Clemens H, Schretter P, Wurzwallne K, Bartels A and Koeppe C (2003), *Structural Intermetallics*, R. Darolia (ed) TMS, Warrendale, Pa, 2003, 205.
27 Samarov V, private communication, March 17, 2011.
28 Arcella F and Froes F H (Sam), 'Production of titanium aerospace components from powder using laser forming', *JOM*, 2000, **52**(5), 28.
29 Sears J (2011), reported at PowderMet, San Francisco, May 18–21.
30 German RM, *Powder Metallurgy Science*, 2nd edition, MPIF, Princeton, NJ, 1994, chapter 6, p. 192 *et seq*.
31 Froes F H (Sam) and German R M, *Metal Powder Report*, 2000, **55**(6) 'Titanium powder injection molding (PIM)', 12.
32 German R 'Powder injection molding of titanium components', *Powder Injection Molding Int*, 2009, **3**(4), 21–37.
33 Baril E 'Titanium alloys by powder injection molding', Powder Injection Molding Int, 2010, **4**(4), 22–32.
34 MacNeal T, private communication, May 2, 2011.
35 Froes F H (Sam) 'Advances in titanium metal injection molding', *TMS Symposium on Innovations in Titanium Technology*, Gungor M N, Imam M A and Froes F H (Sam) (eds), Orlando, Fl, February 25–March 1, 2007, 157–66.
36 Froes F H (Sam) (Feb 2000) 'Conference report: Fourth International Conference on Spray Forming', Baltimore, Maryland, October 24–26, 1999, *Light Metals Age*, vol. 58, p. 72.
37 Segal L A E, Papyrin A N, Conway Jr J C and Shapiro D (Sept 1998), 'A review of cold forming of metals', JOM, **50**(9), 52.
38 Srisukhumbowornchai N, Senkov O N, Froes F H, Öveçoglu M L and Hebeisen J (1997), 'Stability of nanocrystalline structures in a Ti-47.5Al-3Cr (at %) alloy produced by mechanical alloying and hot isostatic pressing', *Synthesis/Processing of Lightweight Metallic Materials – II*, CM Ward-Close, F.H. Froes, D.J. Chellman and S.S. Cho (eds), TMS, Warrendale, Pennsylvania, 1997, 243.
39 Trivedi P B, Baburaj E G, Geng A, Ovecoglu M L, Patankar S and Froes F H, 'Grain size control in Ti-48Al-2Cr-2Nb with yttrium additions', *J. Alloys and Compounds*, 2003, March, 100–6.
40 Ward-Close M, private communication, Nov 11, 2003.
41 Froes F H, Senkov O N and Qazi J I, 'Hydrogen as a temporary alloying element in titanium alloys : thermohydrogen processing', *Int. Mater Rev*, 2004, **49**(3–4), 227–245.
42 R. Loutfy (2000), MER Corp., Tucson, AZ, unpublished work.
43 Machiavelli, *II Principe*, 1513.

9
Metal-based composite powders

N. LLORCA-ISERN and C. ARTIEDA-GUZMÁN,
Universitat de Barcelona, Spain

DOI: 10.1533/9780857098900.2.241

Abstract: Since the early 1990s considerable effort has been devoted to the development of metal-based composite powders (MeCP). Reinforcements in MeCP can vary from intermetallic to ceramic or polymer, depending on composition and can also be microstructured or nanostructured, depending on the size of the constituent materials. Composite powders can be used at the macro- and microscale to produce dense composite objects, composite coatings, to provide a combination of properties in one component or to provide specific properties to withstand extreme conditions in service. In addition to this, technology for the synthesis of nanodevices has also evolved. Metal composite powders are produced by a variety of methods based on solid-, liquid- and gas-phase synthesis and mechanosynthesis. Functionality and design are the current drivers for the development of metal composite powders.

Key words: applications, gas-phase synthesis, liquid-phase synthesis, metal composite powders, solid-phase synthesis.

9.1 Introduction

The objective of this chapter is to provide an overview of metal-based composite powders (MeCPs), including the processes for their synthesis, the most frequently employed composite systems, the linking between composite powders and the common applications of MeCPs. Some future trends will also be discussed.

The main reason for producing composite powders is, of course, to optimise the properties of a product, but they have the added advantage of making it easy to combine dissimilar materials that are difficult to obtain by conventional composite production. Composite powders can also be used to advantage in components where extremes of size are necessary, such as nanotechnology and large dimension objects, for which the need to ensure size-related properties is critical.

From the macroscale and microscale points of view, the objectives when using composite powders are focused on the need to produce a dense composite object, a composite coating, a combination of different properties, or to ensure that certain properties are present even in severe service conditions. In addition to this, the production of nanodevices in nanoscience and nanotechnology can be considered a breakthrough for the composite powder sector.

Solid-phase and liquid-phase sintering are the consolidation processes that are most often used to achieve these objectives. Liquid-phase sintering is particularly common: metals (such as copper) or polymers are used as a wetting reinforcement matrix to produce the metal matrix composites (MMCs) and polymer matrix composites (PMCs). Composite coatings can be made using composite powders as the raw material (a direct composite process) or by mixing the different constituents during the coating process (an indirect composite process).

Composite materials are produced by a variety of methods. Conventional melting and casting techniques are not ideal for producing composites because they are unable to ensure uniformity of dispersoids. It is therefore recommended that powder metallurgy (PM) is used for the production of such materials. PM techniques are known to allow distribution of the reinforcement particles, but without the segregation phenomena typical of the casting processes (Fogagnolo *et al.*, 2004; Khakbiz and Akhlaghi, 2009). Mechanical synthesis (MS), also known as mechanical alloying (MA), is another widely used preparation technique for obtaining composite powders.

Macroparticles, microparticles and nanoparticles are always formed in a medium, which may be in the gas, liquid, or solid phase. Classification that is based on the media in which the particles are formed is perhaps the most important and most widely used. By focusing on the media in which the particles are formed, many issues that are common to all of the techniques within each specific medium are included. The media and the different techniques for particle syntheses are usually classified as gas phase, liquid phase or solid phase.

Gas phase: vapour condensation, vapour reaction (flame synthesis, chemical vapour reactions) and aerosol (spray pyrolysis or vapour pyrolysis, flame-aerosol pyrolysis). These techniques use precursors in order to activate the reactions. Two points must be taken into account: the precursor must be dissolved in the fluid, but not react with it and the product must not dissolve in the fluid, nor react with it. In the aerosol process, the main difference between spray and flame pyrolysis is the source of heat. In spray pyrolysis, the aerosol is carried by the gas into a preheated furnace, where the liquid droplets undergo solvent evaporation, solute precipitation, solute decomposition and oxide sintering in order to gain the final particles. In flame-aerosol pyrolysis, heat is supplied by the burning fuel gases and organic solvents that are in direct contact with the precursor.

Liquid phase: chemical precipitation and coprecipitation, hydrothermal, solvothermal (non-hydrolytic), forced hydrolysis, sol–gel, microwave heating, reduction in solution and electrochemical. The chemical composition of the particles can be tailored in the liquid phase. Surface controlling agents can be added during or after particle formation in order to control the size and to prevent agglomeration.

Solid phase: mechanical milling, mechanochemical processing, cryochemical processing, self-combustion and solid-state synthesis. The kinetic energy from a grinding medium is transferred to a coarse-grained metal, ceramic, or polymeric sample material with the purpose of reducing size or alloying or combining immiscible systems. The severe plastic deformation induced by these high-energy processes leads to the nanostructuration of the components. The self-combustion method has been widely used in the synthesis of ceramic particles.

In all gas-phase and liquid-phase synthesis methods and most solid-phase methods, their most significant and basic part is a chemical reaction. These include, but are not exclusive to: reduction (redox) reactions, oxidation (redox) reactions, precipitation and coprecipitation reactions, hydrogenation or condensation, and addition or displacement reactions. Temperature, pressure, catalysation or a particular atmosphere are important factors. The name of the process is sometimes based on one of these precise parameters, which results in a long list of different terms which can cause confusion when trying to find or decide on a method for producing a particular composite powder. Consequently, there is considerable interest in simplifying the classification; as suggested above, a simple option is the medium in which the formation of the composite particle takes place.

9.2 Metal-based composite powder production

Although there are different techniques for producing metal-based composite powders, three groups are generally recognised. These are mechanosynthesis, sol–gel methods and pyrolysis.

9.2.1 Solid phase: mechanosynthesis

Mechanical alloying (MA) is a low-temperature powder processing method that was developed in the 1960s (Benjamin, 1988), but which reached its full commercial status in the 1980s (Fisher and Haeberle, 1988). Originally, MA was developed to produce oxide dispersion strengthened steels (ODS) and Ni-based superalloys (Benjamin, 1990), but nowadays it is used in the production of aluminium, copper alloys (Fogagnolo *et al.*, 2002), iron or refractory metals and especially intermetallics (Benn *et al.*, 1988). In the last two decades, different mechanical routes have been developed with the aim of producing advanced materials using mechanical energy to achieve chemical reactions or structural changes and involving the milling of the constituents (e.g. pure metals, or compounds or blends) (Chinicas, 2006).

Mechanical milling (MM), mechanical alloying (MA) or mechanosynthesis (MS) and mechanochemical synthesis (MCS) or reactive milling (RM) refer

to processes involving the mechanical energy that is produced in vibratory mills, attritor mills, tumbling ball mills or planetary ball mills. With the exception of mechanical milling, in which no chemical changes are produced, the processes involve chemical or metallurgical reactions, which are either direct or induced by the high energy of the process. High energy ball milling chemical reactions are one of the most effective ways of synthesising composites and nanocomposites of various classes of compounds, for example metals, oxides, nitrides, borides, carbides, salts and organic compounds, in reactions involving activation in solids, and displacement or redox reactions between a reactive metal and metal oxide.

Important research was done by Schaffer and McCormick (1989) on the relationship of the diffusion rate to the diffusion path and they demonstrated that the solid-state reaction of copper oxide by calcium with an enthalpy of –473 kJ mol^{-1} of CaO produced pure Cu. On the other hand, the reduction of iron oxide by aluminium for the synthesis of nanomagnetic composites has been studied by Takacs (2002) and the combustion reaction was detected empirically. For example, the presence of fine Al_2O_3 particles in a copper matrix not only increases the hardness of this material, but it also diminishes the grain growth rate at temperatures near the melting point of copper. It is well known that the amount, size and distribution of reinforcing particles plays a critical role in enhancing or limiting the overall properties of the composite. This effect was also observed by other researchers in NiTi/Al_2O_3 nanocomposites (Mousavi *et al.*, 2009). Adding reinforcement particles to the matrix does not always produce a fine and homogenous composite distribution. To achieve a fine distribution of nanosized Al_2O_3 particles, the internal oxidation and MA are often used.

Dispersing fine reinforcement particles in a metallic matrix or a nanostructured matrix is beneficial to the mechanical properties of the composite. However, the former alone is not always recommended when changes in the physical properties may be involved, but fine and well-distributed reinforcement with a nanostructured matrix can overcome this limitation. Different theories have been developed in order to explain the effect of inclusions, for example the effects on the magnetic properties. The chemical precursors typically consist of mixtures of oxides, chlorides and/or metals that react either during milling or during subsequent heat treatment to form a composite consisting of ultrafine particles within a matrix. Since high-energy milling processes significantly reduce the size of the crystals involved, research is now focused on the production of nanocomposite powders. Thus the direct consequences are, first, the possibility of synthesising the particles of the composite system *in situ* or *ex situ* and, second, producing them with microstructural refinement at the nanometre scale. This is why the majority of the literature from the past ten years deals with the production of nanocomposite or nanostructured composite powders.

The capacity of the MA technique to produce composite powders with a uniform distribution of nanoparticles within the matrix alloy has resulted in the synthesis of a variety of nanocomposite systems such as the Mg/carbon nanotube (CNT) (Huang *et al*., 2007), Mg/Cr_2O_3 (Vijay *et al*., 2006), Cu/Fe_3C (Correia *et al*., 2007), Co/Al_2O_3 (Li *et al*., 2007) Zn/Al_2O_3 (Karimzadeh *et al*., 2008) or Ni/AlN (Chung *et al*., 2003).

Mechanochemical processing is a relatively new technique in the preparation of nanosized materials. It has been shown that enhanced reaction rates can be achieved and dynamically maintained during milling as a result of microstructural refinement and mixing processes accompanying repeated fracture, welding and deformation of particles during collision events (Suryanarayana, 2001; Schaffer and McCormick, 1991). MA or MM can be used as an initial step prior to other synthesis techniques and also as the final step following the synthesis method. This will be discussed with examples in the next part of the chapter.

Mechanochemical synthesis (MCS) or reactive milling (RM) reactions fall into two categories as suggested by Botta *et al*., (2001), namely:

(i) Those which occur during the mechanical activation process and where the reaction enthalpy is highly negative. The adiabatic temperature (at heat release) is T_{ad} = 1300–1800K.
(ii) Those which occur during subsequent thermal treatment and where the reaction enthalpy is only moderate. The adiabatic temperature is T_{ad} < 1300K.

The first type of reaction takes place in two distinct modes of reaction kinetics, that is, either a combustion reaction or a progressive reaction (Takacs, 2002). The latter reaction may extend to a very small volume of powder mixture resulting in a gradual transformation ($T_{adiabatic}$ < 1800K). The former is a self-propagating combustion reaction that can be initiated when the reaction enthalpy is sufficiently high ($T_{adiabatic}$ > 1800K) (Munir, 1988; Botta *et al*., 2001). The combustion reaction can be ignited by the aforementioned high-energy ball milling. In addition to the energy dissipated by the collision events, the reaction enthalpy will also contribute to the temperature rise during milling and will ultimately cause thermal instability and combustion. Since diffusion and thus reaction rates depend on temperature, the overall rate of reaction is affected by the reaction enthalpy. Schaffer and McCormick (1991) stated that in reactions that may involve the combustion effect, it is required that the adiabatic temperature, T_{ad}, be at least 1800K. The adiabatic temperature is a measure of the local heat generated by the reaction and is often taken as a measure of the driving force. Thus the value of T_{ad} can be used as a suitable criterion for anticipating the occurrence of a self-propagating combustion reaction in ball milling processes. It is worth noting that if the matrix system is diluted, T_{ad} will decrease. The value of

T_{ad} for any reaction, taking into consideration the dilution effect, can be calculated from the reaction enthalpy ΔH_r:

$$\Delta H_r + \sum \int_{T_0}^{T_m} C_{p,S} + \sum \Delta H_t + \sum \int_{T_m}^{T_{ad}} C_{p,L} = 0 \qquad [9.1]$$

where $C_{p,S}$ and $C_{p,L}$ are the mean heat capacities in the solid and liquid phases of the products respectively, T_0, T_m and T_{ad} are the initial, melting and adiabatic temperatures respectively and the ΔH_t is the state transformation enthalpy.

Nanostructured materials inherit relatively large interfacial energy (Gleiter, 2000). When such nanostructures are generated by extensive plastic deformation, for example by high-energy ball milling (HEBM), the stored energy in the material also becomes significant. These factors enhance the chemical reactivity of the milled product and in some cases novel metastable phases form in the course of HEBM (Koch and Whittenberger, 1996; Suryanarayana, 2001; Zhang, 2004).

When mechanochemical synthesis involves a reduction reaction, mechanical milling alone may not be sufficient for the reduction reaction to take place completely, for example if the reaction enthalpy is moderately high. Thus, a combination of mechanical and thermal treatment makes the material system a likely candidate for the synthesis of nanocomposites. Some composite systems involve post thermal treatment in an inert or a reactive atmosphere in order to form the final composite structure; this is a two-step synthesis.

Other composites can be synthesised by a displacement reaction. A reaction can take place thermodynamically at room temperature if its ΔG^0_{298} has a high negative value (it is highly exothermic) and provided the kinetics are fast. In this regard MA can enhance the kinetics of the reaction by creating a high diffusivity path, providing an extensive interface area between reactants and by the dynamic removal of reaction products from the interfaces through repeated fracturing and cold welding of powder particles. MA also increases the number of dislocations and grain boundaries and this shortens the diffusion paths.

The reinforcement particles are incorporated into the matrix by means of a high-energy process (HEM). It allows the production of diverse combinations of metals and reinforcement components and has led to the development of novel materials that cannot be produced by melting metallurgy (Ag/SnO_2, Al/SiC, $MCrAlY/SnO_2$, $NiCrBSi/TiB_2$, and Stellite/VC, among others).

In the effort to produce nanoparticles, some new innovations have been added to these traditional methods, such as introducing reactive materials into the milling process and combining milling with solid-state synthesis. Some new approaches include the extraction of soluble molecules from a uniform molecular solid mixture by acid/base leaching or evaporation in order to leave molecular skeleton residues that become nanoparticles.

When mechanochemical synthesis includes a combustion process that is induced inside a vial, which is similar to thermally ignited self-propagating high-temperature synthesis (SHS), it is called a mechanically induced self-sustaining reaction (MSR) (Takacs, 2002; Lu and Li, 2005; Kim *et al*., 2006). The synthesis of ternary carbonitride phases that could be employed as master alloys has produced, via different methods such as thermal treatments (Pastor, 1988), self-sustaining high-temperature synthesis (Munir and Ealamloo, 1994; Yeh and Chen, 2005, 2007, Yeh and Liu, 2006), or mechanochemical synthesis (Córdoba *et al*., 2005, 2007a). Recently, MSR synthesis has been proposed as a reliable and easy method for obtaining high purity quaternary $Ti_yNb_{1-y}C_xN_{1-x}$ carbonitrides (Córdoba *et al*. 2007b, 2009). If a second MA step for mixing them with refractory, iron or Co–Ni alloys is carried out, novel cermet-like powders can be produced.

Limitations of mechanosynthesis

The first potential limitation is the low productivity of the high-energy ball mills, which makes it difficult to introduce mechanochemistry in large-scale technology. The advent of horizontal attritor mills with different types of milling media has overcome this problem to a certain extent. The second limitation is contamination from the milling media and the reaction of the milling media or the milled products with the atmosphere in which the synthesis is performed. The latter shortcoming can be minimised if the time for intensive mechanical activation is sufficiently short and this is possible when mechanocomposites are used as precursors for traditional synthesis methods. In this way, all of the advantages of the mechanochemical approach are conserved, while the limitations may be reduced significantly. The oxidation of pure metals seems to be inevitable during milling. Fortunately, recent research reveals that when the grain sizes of the powders are reduced to the nanometre scale, the bulk sintered part can achieve nearly full densification (Lee and Kim, 1995; Kim and Moon, 1998; Kim *et al*., 2004a). High-energy ball milling offers a large number of possible routes for synthesising new materials and is a promising method for industrial scale-up synthesis.

9.2.2 Liquid phase: sol–gel technology

In this chemical process, a colloidal solution (sol) gradually evolves towards the formation (gellation) of a gel-like dual phase system, formed by a continuous network of a solid in a continuous network of fluid. It is a wet chemical technique widely used in materials science and more specifically in ceramic engineering. A drying process removes the remaining solvent and a final sintering thermal treatment can be carried out if further polycondensation or densification is needed.

Varma *et al*. (1990) prepared Ag–YBCO superconductors from composite powders via the citrate gel route. The raw materials were cupric nitrate, yttrium nitrate, barium nitrate, silver nitrate and citric acid. The nitrates were dissolved, a stoichiometric amount of citric acid was added, and the pH value was adjusted. The mixture was concentrated to a viscous state in a steam bath and an oven to obtain a citrate gel. The gel was then thermally decomposed in air and the powder was ground, pressed and sintered in a static air atmosphere. Nanostructured Ni–Y_2O_3/ZrO_2 composite powders were synthesised by Grossmann *et al*. (1995) employing the sol–gel method. The characteristics of the powder can be controlled through choice of the oxidation and reduction conditions, and homogeneously dispersed nickel within a ZrO_2 matrix could be generated. Ragunathan *et al*. (1993) synthesised W–Cu composite powders at lower temperatures than those required for the methods that are more commonly used. Greater control of the chemistry and homogeneity are possible with sol–gel synthesis.

9.2.3 Gas phase: pyrolysis

This synthesis route is capable of forming nanoparticles once a sufficient degree of supersaturation of condensable products has been reached in the vapour phase. Once nucleation occurs, the growth of particles is fast and takes place by coalescence; depending on the temperature, spherical or agglomerated particles are produced. The process has been successfully employed in synthesising various nanometre-scale materials including metals, simple and complex metal oxides, carbides, nitrides, rare earth doped oxides and multi-elemental glasses, among others. Laser pyrolysis is a gas-phase synthesis method where a flowing reactive gas is heated rapidly with a laser.

Spray pyrolysis was used to fabricate Ag–TiO_2 composite powders for application in oxide barrier filaments of superconducting multifilamentary tapes. The composite powders were prepared from an aqueous solution of TiO_2 and $AgNO_3$ (Matsumoto *et al*., 2002). Majumdar *et al*. (1998) synthesised Ag–SiO_2 and Ag–CuO by spray pyrolysis using mixtures of aqueous silver nitrate and colloidal silica, resulting in high purity and a high level of compositionally homogenous composite powders.

9.3 Copper- and aluminium-based composite powder systems

MMCs refer to a kind of material in which rigid ceramic or another high-strength metal or alloy reinforcements are embedded in a ductile metal or alloy matrix. MMCs combine metallic properties, such as ductility and toughness, with characteristics such as high strength, moduli leading to greater strength in shear and compression, and to higher service temperature capabilities.

The attractive physical and mechanical properties that can be obtained with MMCs, such as a high specific modulus, strength, and thermal stability, have been documented extensively (Tjong and Ma, 2000; Flom and Arsenault, 1986; Nardone and Prewo, 1986; Mortensen *et al*., 1988).

Interest in MMCs for use in the aerospace and automotive industries, as well as other structural applications, has increased over the past 20 years. This is a result of the availability of relatively inexpensive reinforcements and the development of various processing routes which result in reproducible microstructures and properties (Chou *et al*., 1985). *In situ* MMC powders with a wide range of matrix materials (including aluminium, titanium, copper and iron) and second-phase particles (including borides, carbides, nitrides, oxides and their mixtures) can be produced.

Since the objective of the reinforcement is to increase the stiffness and strength of the matrix, metallic or ceramic particles are used in the synthesis of metal composite powders. With their large elastic modulus and high strength, ceramic particles are ideal reinforcing particles. In principle, many ceramic powders meet these requirements, but there are other restrictions which influence the choice of the reinforcement for a particular composite. Many of the ceramic particles of interest are thermodynamically unstable when they are in contact with pure metals and will react to form compounds at the interface between the particles and the surrounding matrix (Mortensen, 2007, p 490). There are other factors that should be considered, in addition to reaction stability, when choosing an appropriate reinforcement. If the composite is made by MA or milling of solid powders, the ratio of the metal powder size to that of the reinforcing particles is important if a uniform distribution of the reinforcement is to be achieved. In general, if the size ranges of the metal and ceramic particles are similar, the reinforcement distribution will be more uniform. The reinforcing particles in composite materials with metal alloy matrices, metal carbides (SiC, TaC, WC, B_4C, TiC), metal nitrides (TaN, ZrN, Si_3N_4, TiN), metal borides (TaB_2, ZrB_2, TiB_2, WB) and metal oxides (ZrO_2, Al_2O_3, ThO_2) are applied.

In the following sections, a selection of metallic matrices and the most commonly used reinforcements are analysed.

9.3.1 Copper-based composite powders

Copper and copper alloys constitute one of the major groups of commercial materials. They are widely used in engineering because of their excellent properties, for example, outstanding resistance to corrosion, easy production, high conductivity and good fatigue resistance (Davis, 2001, p 4). The main problem with copper alloys is the low intrinsic strength of these materials; for this reason, they need to be alloyed with different insoluble elements to achieve particle strengthening. Potential alloying elements that can be used

to reinforce copper include Cr, W, Ta, Nb, Mo and V. On the other hand, copper can also be strengthened by reinforcement with ceramic particles such as TiC and NbC. These reinforcements not only increase the microhardness of copper but they also maintain this microhardness at elevated temperatures (Hussain *et al*., 2008).

Sheibaina *et al*. (2009) suggested that copper matrix composites were promising candidates for application in electrical sliding contacts where good wear resistance and high thermal and electrical conductivity are needed. For example, the trend in the development of electrode materials for high-current applications is to design copper matrix composites containing high melting temperature components. These can be produced by dispersing hard particles like oxides, carbides or nitrides into the copper matrix, using either liquid-state or solid-state techniques (Tjong and Lau, 2000; Lee and Lee, 1999).

There are some publications focused on the production of pure Cu matrix nanocomposites such as Cu–Al_2O_3 (Wu and Li, 2000; Ying and Zhang, 2000), Cu–MgO (Mulas *et al*., 1999), Cu–TiB_2 (Dong *et al*., 2002), Cu–ZnO (Castricum *et al*., 2001) and Cu–MnO (Sheibani *et al*., 2009), using an MA method. Very few methods used copper alloy as the matrix (Cu(Mo)), yet it seems that the presence of a nanocrystalline Cu(Mo) alloy as a matrix and the homogenous distribution of Al_2O_3 reinforcements can be helpful in achieving better mechanical properties in a nanocomposite. However, the wettability of the reinforcement from Cu is higher when it is pure.

The mechanochemical reduction of copper oxide with different reductants such as Fe, Al, Ti, Ca, Ni and C has already been studied (Schaffer and McCormick, 1990, 1991; Sheibani *et al*., 2007). The products were usually a mixture of copper with dispersed oxides particle, that is copper matrix composites. When this process is combined with mechanical milling (reactive milling), nanostructured composites with a uniform distribution of reinforcement particles are synthesised.

Cu–15 wt% Mo/30 vol% Al_2O_3 nanocomposites can be synthesised by a displacement reaction between Al and MoO_3 in a Cu–22.5 wt% MoO_3–8.5 wt% Al powder mixture according to the following reaction (Sabooni *et al*., 2010):

$$MoO_3 + 2Al \rightarrow Al_2O_3 + Mo \qquad [6.2]$$

$$\Delta G^0_{298} = -915 \text{ kJ mol}^{-1}; \Delta H^0_{298} = -966 \text{ kJ mol}^{-1}$$

The very high negative value of ΔG^0_{298} (–915 kJ mol^{-1}) indicates that this reaction can thermodynamically take place at room temperature. However, the kinetics may delay the reaction. MA can enhance the kinetics of the reaction owing to the repeated fracturing and cold welding of powder particles. Immediate formation of Al_2O_3 is promoted by dynamically formed high Al/MoO_3 interface areas, as well as the short circuit diffusion path that is provided by increasing the number of defects (such as dislocations and

grain boundaries) during MA (Heidarpour *et al*., 2009). It has been found by different researchers that MA induces the dissolution of metallic atoms into the crystal lattice of the accompanying metal. The relative crystallography, size of atoms and affinity will enhance this process or make it more difficult. Also the presence of ceramic particles will influence the diffusion path (Llorca-Isern *et al*., 2010).

There have also been studies of the *in situ* formation of Cu–MnO nanocomposite powder by mechanochemical reactions between CuO and Mn. Particular attention has been paid to the mechanism of this process and its structural evolution and morphological variation during mechanical milling. Since T_{ad} in this reaction is well above the melting point of Cu, 1358K, it is certain that Cu is completely melted during the combustion reaction. This is in agreement with the observation made by Zhang and Richmond (1999) regarding the spherical morphology of the Cu particles undergoing phase separation from AlO_3.

Pure copper, iron and cobalt together with Al_2O_3 powder were mixed in a planetary ball mill in order to form Cu–Fe–Co/Al_2O_3 composite powders. The reaction stages and resulting magnetic properties were analysed in order to determine the influence of the ceramic powder on the process and properties, compared to the metallic system. Al_2O_3 interacts with the metallic dissolution of Fe and Co atoms in Cu, resulting in a barrier to the progress of the atomic diffusion. Figure 9.1 shows a (CuFeCo) metallic aggregate after mechanical milling. It has a plastic appearance with almost flat surfaces, as welding is the predominant process in these kinds of mechanical alloys. However, in

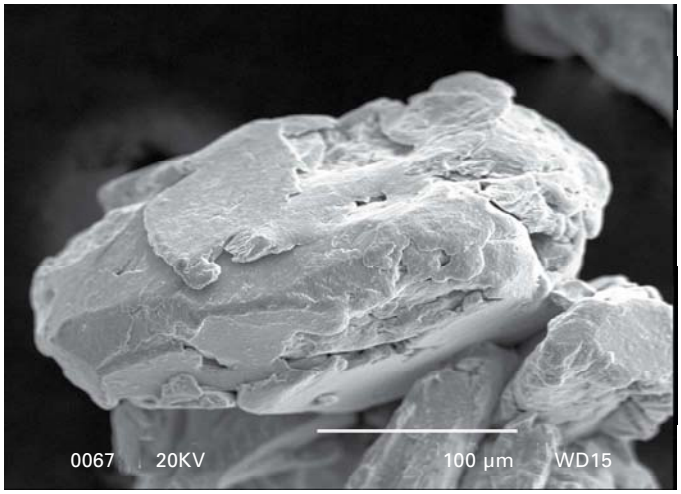

9.1 Scanning electron microscopy (SEM) micrograph of the metallic Cu–Fe–Co aggregate after HEBM showing ductile features of the powder.

Fig. 9.2, the aggregate of a metallic system with 3% Al_2O_3 acting as a barrier to the plastic deformation hampers the mobility of dislocations generated by the mechanical process, resulting in increased fragility of the material so that eventually it will fracture. Consequently the fracture aspect of this composite powder is not plastic but brittle (Llorca-Isern *et al.*, 2010).

An aggregate of composite powder (CuFeCo + 10% Al_2O_3) processed by HEBM is shown in Fig. 9.3(a) and (b). Owing to their hardness and brittleness, ceramic particles are broken and refined during the mechanical process. Al_2O_3 particles are then trapped between deformed metallic particles, hindering the progress of diffusion. In Fig. 9.3(a) and (b), the alumina particles can be seen as dark spots embedded within the metallic matrix; as the milling time favours fracturing, there are different sizes of particles.

Concerning the magnetic properties, the composite powder showed that the presence of alumina increases its coercivity (H_c) and remanence (M_r). The processed metallic powder presents magnetic domains with defined block wall contours showing a dendritic morphology, as can be seen in the Fig. 9.4(a); this was also observed by Zeng *et al.* (2007) who suggested that this morphology was typical for the magnetic domains of metals processed by MA. Looking at the morphology of the magnetic domains in Fig. 9.4(b) (obtained by the authors), corresponding to the composite powders (metallic system with 10% alumina), two features are notable: first, the diffused block wall contours and, second, the different branched forms adopted by the magnetic domains. The magnetic domains of composite powders are less homogenous and present diffused features that are probably caused by

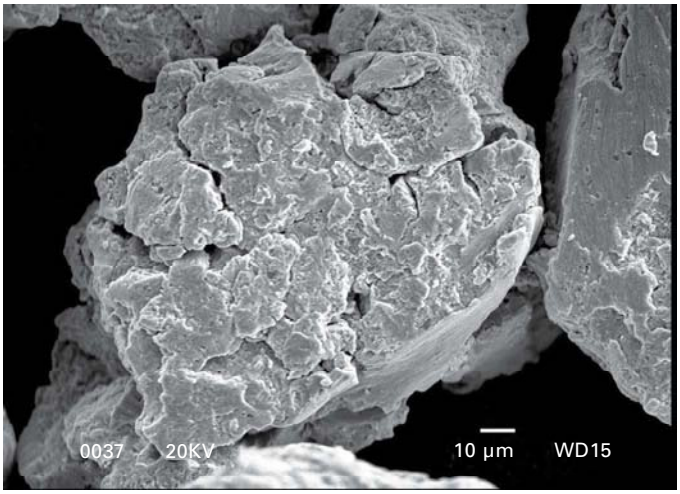

9.2 SEM micrograph of the composite Cu–Fe–Co and 3% alumina (%w) after HEBM showing brittle features of the metal-based composite powder.

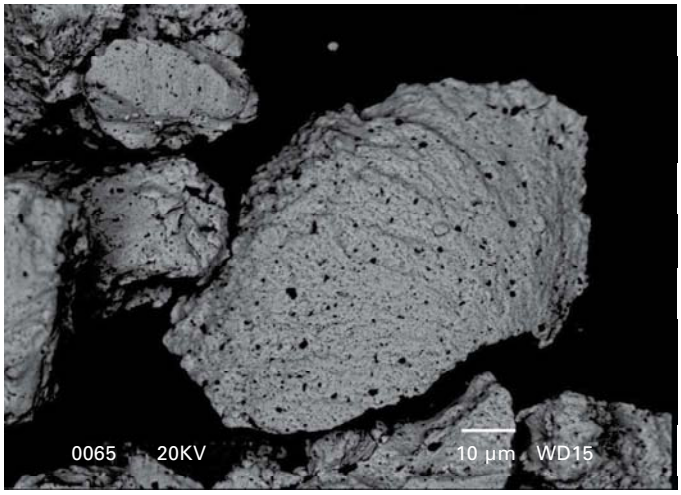

(a)

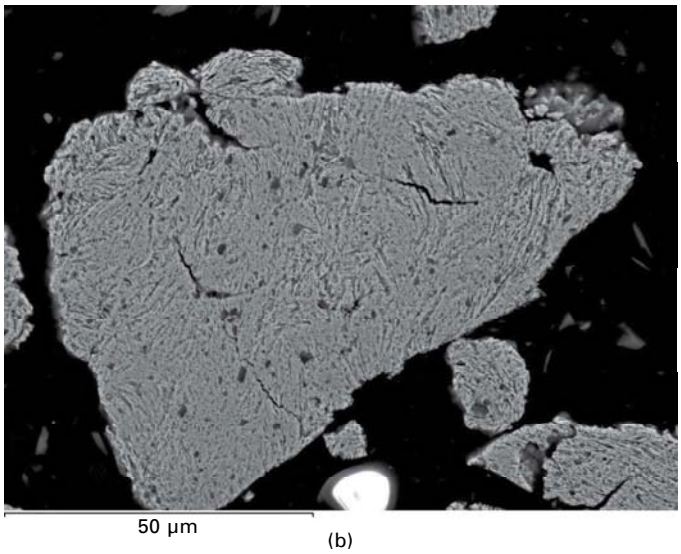

(b)

9.3 (a) SEM-BSE (back scattered electron) micrograph of Cu-Fe-Co and 10% alumina (%w) aggregate after HEBM. The dark spots correspond to the alumina particles embedded in the metallic matrix. (b) SEM-BSE cross-section micrograph of Cu-Fe-Co and 10% alumina (%w) after HEBM. The dark spots correspond to the alumina particles in the metal composite powder.

pinning the alumina particles, hindering the orientation and reorientation of the magnetic dipoles in these domains.

In some studies, (Lee *et al.*, 2001; Korác *et al.*, 2007), Cu–Al_2O_3 nanocomposite powders were synthesised via the thermochemical or

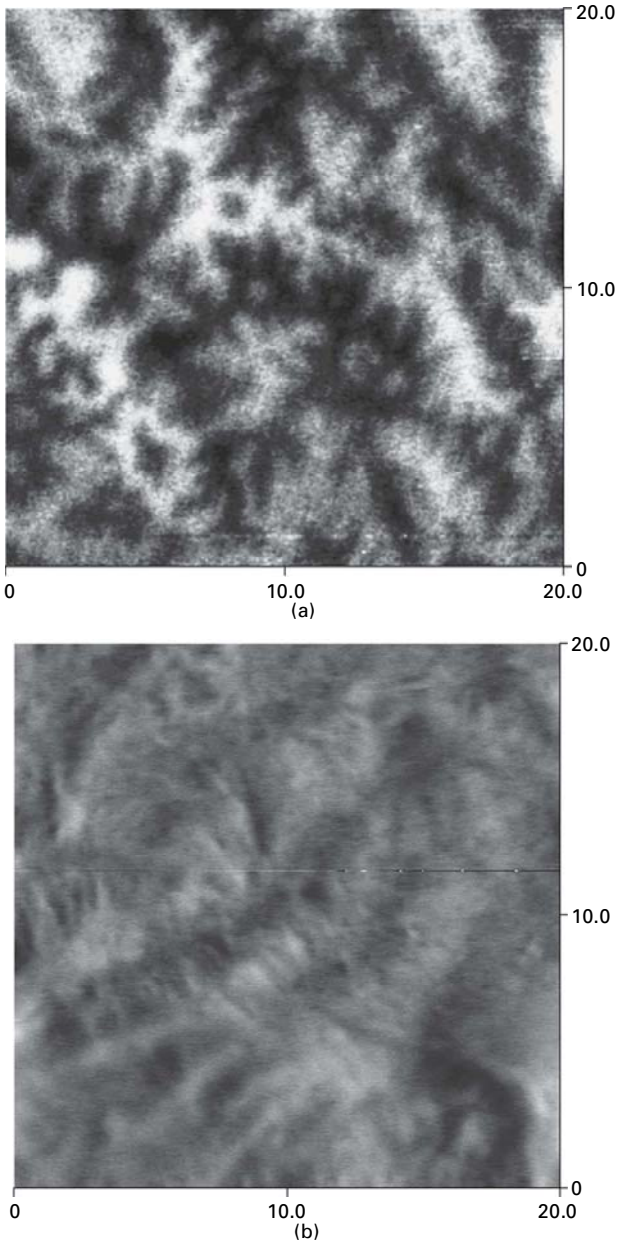

9.4 (a) Magnetic domains characterized by MFM (D3100 Veeco magnetic force microscope) after HEBM in Cu–Fe–Co metallic powder. Image area of 20 μm × 20 μm. (b) Magnetic domains characterized by MFM (D3100 Veeco magnetic force microscope) after HEBM in Cu–Fe–Co and 10% Al_2O_3 (%w) metal composite powder. Image area of 20 μm × 20 μm.

chemical route, in which the input materials are in a liquid state. Owing to the development of contemporary materials with advanced properties, there has been considerable interest in this synthesis method for the production of ultra-fine and nanocomposite powders (Jena *et al.*, 2001).

9.3.2 Aluminium-based composite powders

Aluminium-based matrix composites (AMC) that have been reinforced with hard ceramic particles have received considerable interest because they are relatively easy to process and can offer nearly isotropic properties in comparison to fibre-reinforced composites. In addition, these composites exhibit high strength and stiffness, creep resistance and superior wear resistance, and also provide good electrical and thermal conductivity. All of these properties make particle reinforced AMCs attractive for a wide range of applications in the automotive, aerospace and transport industries. Reinforcement particles used in AMCs include nitrides, borides, carbides and oxides (Everett and Higby, 1991).

The one-step *in situ* production of aluminium matrix composite powders has been successfully realised by means of mechanical alloying. The composite material powders were manufactured by simultaneously mixing the elemental powders in the appropriate percentages to obtain the aluminium alloy matrix and the selected carbides. In this case, the elemental powders used for the aluminium alloy were aluminium, copper, silicon and magnesium. Two different carbides were used as reinforcement for the composite material: VC and TiC (Ruiz-Navas *et al.*, 2006).

Aluminium alloys manufactured by MA show better properties, especially at higher temperatures, than alloys obtained by atomisation or conventional means (Last and Garret, 1996). The reasons for this include the reduction of grain size (Van Meter *et al.*, 1992), the high level of work hardening and the fine dispersion of precipitates (mainly oxides) in the microstructure (Mishra *et al.*, 1992; McCormick and Froes, 1998). Numerous aluminium alloys are manufactured by MA (Li and Lai, 1998), including alloys from the 6xxx (Mukai and Ishikawa, 1995) and 7xxx (Polkin and Borzov, 1995) series. Aluminium matrix composite powders that have been reinforced with SiC and Al_2O_3 (Faure and Brune, 1987; Bhadury *et al.*, 1996; Ravikiran and Surappa, 1997) have been obtained in order to improve the wear behaviour of the aluminium alloy matrix. More recent studies have considered the possibility of adding intermetallics, which is a potential success owing to their hardness and compatibility with the matrix (González-Carrasco *et al.*, 1994; Torralba *et al.*, 1997; Adamiak *et al.*, 2004).

Aluminium alloys have reasonable strength and ductility with corresponding workability. Therefore, these alloys have been widely used for the synthesis of nanocomposites with different nano-sized ceramic particulates such

as Al_2O_3 (Arami *et al*., 2008; Razavi-Hesabi *et al*., 2006), CNT (Pérez-Bustamante, 2008) and $MoAl_x$ (Maiti and Chakraborty, 2008) by MA. The 6xxx series of Al–Mg–Si alloys (i.e. 6061) is a good choice as the matrix alloy owing to its excellent mechanical properties, good weldability and corrosion resistance.

Even though the *in situ* composites have significant advantages, some synthesis routes may lead to composites with an inhomogeneous microstructure with various unstable and/or undesirable phases (Lü *et al*., 2000, 2001; Tee *et al*., 2001). These undesirable phases might drastically reduce the mechanical properties. For example, Tjong *et al*. (2005) have studied the mechanical properties of *in situ* Al–10 wt% TiB_2 and found that the formation of an Al_3Ti phase has a negative impact on the mechanical performance of *in situ* composites. They proposed that the elimination of the intermetallic Al_3Ti phase is a primary task for developing *in situ* Al–TiB_2 composites with superior mechanical performance. Recently, Sadeghian *et al*. (2011) used a two-step MA process and obtained *in situ* formation of TiB_2 particles in the Al matrix with a fine and uniform distribution, thus preventing the formation of undesirable compounds. Consequently, strict control of the process may ensure the synthesis.

Based on the Al–Ce/Al_2O_3 system, Reddy *et al*. (2007) concluded that mechanical milling is not sufficient for the reduction reaction when the reaction enthalpy is moderately high. They suggested that a combination of mechanical and thermal treatment would make the material system a likely candidate for the synthesis of nanocomposites. The chemical redox reaction of this system is:

$$3CeO_2 + 4Al \rightarrow 2Al_2O_3 + 3Ce \qquad [9.3]$$

Boron carbide (B_4C) is one of the hardest and lightest materials and thus a candidate for reinforcing light ductile metals. However, owing to the poor wettability of B_4C with the molten Al alloys, it is difficult to produce dense Al–B_4C composites by liquid-phase approaches. It has been reported that Al requires a temperature as high as 1100°C in order to wet the B_4C surface completely. Processing at such high temperatures leads to the formation of a series of components by chemical reactions between these two phases (Shorowordi *et al*., 2003; Lee and Kang, 2001). Ye *et al*. (2006b,c) have optimised the cryomilling technique for processing composite powders that consist of particulate B_4C reinforcement in different aluminium matrices. It has been reported that Al–B_4C composites prepared by consolidation of the cryomilled powder particles exhibited better wear resistance (Tang *et al*., 2008) and improved mechanical properties (Ye *et al*., 2006a) when compared to the unreinforced alloys. The effect of interfacial debonding on the mechanical properties of Al–B_4C composites consolidated by different thermomechanical techniques was reported in another study (Zhang *et al*.,

2006). However, in the aforementioned studies, cryomilling was used to prepare the Al–B_4C composite powders by using micrometre-sized B_4C particles. Nano-sized boron carbide particles can be produced from commercially available boron carbide particles and mechanically alloyed with Al6061 to synthesise the corresponding nanocomposite powder successfully (Khakbiz and Akhlaghi, 2009).

9.4 Other metal-based composite powders

9.4.1 Iron-based composite powders

The main advantages of the PM route for iron-based systems are raw material savings, low energy costs, higher content of alloying elements and the possibility of ceramic particle additions. However, the materials produced by this technique generally suffer from the problem of contaminated matrix-reinforcement interfaces. Consequently, techniques involving *in situ* generation of the reinforcing phases are preferred as the synthesis route for these materials. As a result, the reinforcement surfaces are likely to be free from gas absorption, oxidation or other detrimental surface reaction contamination, and the interface between the matrix and the reinforcement bond tends to be stronger (Zhang *et al*., 1999). Some of these technologies include liquid–solid or liquid–liquid reactions, and self-propagation high-temperature synthesis (SHS). *In situ* formation of dual carbides (TiC and other carbides) in ferrous composites has already been studied. For example, Dogan and Hawk (1995) formed *in situ* TiC and $(Cr,Fe)_7C_3$ carbides in Fe-based composites; Farid *et al*. (2007) synthesised *in situ* TiB_2 and TiC in stainless steel matrix composites; Jiang *et al*. (2000) produced *in situ* (TiW) Cp/Fe composites, and Fu and Xu (2010) produced VC as an alternative addition to TiC/Fe matrix composites, producing dense (Ti,V)C/Fe-matrix composites by an *in situ* reaction combined with planetary ball mixing techniques.

The strategy applied for iron-based materials is usually to use reinforcement particles which conform to precipitation in the initial matrix alloy. This can be applied when high-alloyed initial powders are needed, for example if Fe-Cr-B has to be reinforced by CrB_2 (Lampke *et al*., 2011).

Crisan and Crisan (2011) studied Fe and Fe_3O_4 (magnetite) powders obtained by ball milling. They demonstrate that the nanocomposite powder undergoes an incomplete redox reaction during preparation with formation of FeO. Magnetite and iron powders are gradually transformed via redox reactions and, at the end of the heating stage, wursite is the main phase observed in the sample.

9.4.2 Titanium-based composite powders

Titanium matrix composites (TiMCs) that have been reinforced with ceramic particles have considerable potential for structural applications in the aerospace, transportation and industrial sectors, primarily because of their superior stiffness, toughness, elevated temperature resistance and excellent specific strength. Many reinforcements are used in TiMCs, including SiC, Al_2O_3, TiO_2, TiC, TiB, TiB_2 and rare earth oxides. In addition, elements of rare earth added to the TiMCs can greatly increase the strength of the matrix alloy at high temperatures. Rare earth oxide is produced from the rare earth element and solid solution oxygen in a matrix alloy; it is beneficial for grain refinement, fatigue resistance and thermal stability (Zhang *et al*., 2004b).

Titanium alloys are the metallic biomaterials that are most commonly used for medical implants owing to their good biocompatibility, high chemical stability in the physiological environment and excellent mechanical properties. For these reasons, effort has been devoted to synthesising titanium alloy–hydroxyapatite (Ti6Al4V/HA) composites. HA has poor mechanical properties that are improved by the Ti alloy. Plasma spraying is the most popular technique for adding a coating of HA to the titanium substrate. The brittle nature of the HA layer often results in wearing of the coating. The development of Ti6Al4V/HA composite powders aims to solve such problems. Thian *et al*. (2001) studied the formation of Ti6Al4V/HA composite powders using a technique called the 'ceramic slurry approach', which was employed to produce Ti6Al4V/HA composite powders; the outer layer consists of a biocompatible HA surface and the inner core consists of mechanically strong Ti6Al4V. Ti6Al4V can also be reinforced with TiC. Ar-atomisation produces a composite powder containing very small TiC particles, as proposed by Hu and Loretto (1994).

The use of innovative reinforcement materials plays an important role in the production of composite materials with outstanding properties. Several studies present nanometre-scale reinforcements as potentially successful materials for the production of metal matrix composites. A few works present titanium MMCs (TiMCs) strengthened with nano-carbon reinforcements. Montealegre *et al*. (2011) studied the behaviour of TiMCs reinforced with nano-carbon materials, CNTs and nanodiamonds (NDs), which were produced via powder metallurgy under different processing conditions. It was shown that TiMCs with a well distributed and small reinforcing phase presented the best flexural strength (1473 MPa for TiMCs with NDs hot pressed at 900°C, compared to 400 MPa for titanium pure matrix (Boyer *et al*., 1994; Kondoh *et al*., 2009)).

Research was carried out by Joshi *et al*. (2002). A titanium composite powder (Ti–TiO_2) was produced by *in situ* metal oxidation during MA. Begin-Colin *et al*. (1993) obtained metal–ceramic composite powders of Al_2O_3–Ti

by MA using TiO_2 and Al as raw materials. These are both examples of TiMC powders.

9.4.3 Intermetallic-based composite powders

Different groups of intermetallics are considered in this section: primarily Fe_3Al, Ti_3Al, NiAl and Ni_3Al. In general, intermetallics are obtained by self-propagated high-temperature synthesis and then milled. In particular, Fe_3Al-based intermetallics possess attractive properties, including considerable hardness, high melting points, relatively low densities compared with Fe-based and Ni-based alloys, and excellent oxidation and corrosion resistance (Matsuura *et al*., 2006). As a result, these compounds are useful for many structural applications, including gas metal filters, heating elements, heat treatment fixtures, high-temperature dies and moulds and cutting tools (Knibloe *et al*., 1992; Yoshimi and Hanada, 1997). Addition of a third alloying element such as Ti or Cr to the Fe_3Al intermetallic compound can lead to an improvement in mechanical properties, including ductility at room temperature and creep resistance at high temperatures, chemical stability and tribological behaviour by solid solution and/or precipitation hardening, as well as grain boundary strengthening (Zhu *et al*., 2000; Fortnum and Mikkola, 1987; Mendiratta *et al*., 1987).

It has also been shown that the dispersion of a hard second phase material (e.g. Al_2O_3) within the matrix can enhance the mechanical properties (Whelham, 1998). Intermetallic reinforced alumina composites exhibit several advantages such as high strength, good wear resistance and improved fracture toughness (Schicker *et al*., 1999; Horvitz *et al*., 2002). Khodaei *et al*. (2009) synthesised Fe_3Al–Al_2O_3 nanocomposites by MA of an Al and Fe_2O_3 powder mixture and reported that prior to the Fe_2O_3–Al combustion reaction, the powder particles attained a nanocrystalline structure. This promotes the Fe_2O_3–Al reaction by providing high diffusivity paths.

Mechanical alloying of Fe, Al and TiO_2 powder mixtures led to the formation of (Fe, Ti)$_3$Al–Al_2O_3 nanocomposites. Rafiei *et al*. (2009) found that the TiO_2 oxide is gradually reduced by Al during milling. This reaction led to the formation of crystalline Ti and amorphous Al_2O_3:

$$4Al + 3TiO_2 \rightarrow 3[Ti]_{Fe} + 2Al_2O_3 \qquad [9.4]$$

The $\Delta G°_{298}$ for reaction [9.4] has a very high negative value (–498.22 kJ mol^{-1}) indicating that this reaction can take place thermodynamically at room temperature.

Upon further milling, Ti (reduced from TiO_2) and the remaining Al were dissolved into an Fe lattice and formed an Fe(Al,Ti) solid solution that transformed to an (Fe,Ti)$_3$Al intermetallic compound with a disordered DO_3 structure at longer milling times. Annealing the final structure led

to the crystallisation of amorphous Al_2O_3 and ordering of the $(Fe,Ti)_3Al$ matrix. If extra Fe and Al is added to the starting powder mixture to obtain an $(Fe,Ti)_3Al$ matrix, it will dilute the starting mixture and consequently T_{ad} will be lowered. Thus, the reaction mode can change from self-propagation combustion to a gradual or progressive mode of reaction.

There have been several studies into the preparation of titanium aluminide and iron aluminide matrix nanocomposites by MA. Zhang *et al.* (2004a) reported that MA of an Al–TiO_2 powder mixture leads to the formation of a range of Ti-based composites including $Ti(Al,O)/Al_2O_3$, $Ti_xAl_y(O)/Al_2O_3$ and $Ti_3Al/TiAl$. Forouzanmehr *et al.* (2009) synthesised the $TiAl/Al_2O_3$ nanocomposite by MA of an Al and TiO_2 powder mixture and reported that TiO_2 is gradually reduced by Al during ball milling.

TiAl-based intermetallics have received considerable interest regarding various applications in the aerospace, automotive and energy production industries, owing to their relatively low densities, high specific strength, excellent oxidation and corrosion resistance and adequate creep resistance at high temperatures. Therefore, the TiAl-based alloys most commonly studied have a composition of 44–48% Al and contain additions of other elements (such as Nb, Cr, W, Si, B, etc) to improve the creep and/or oxidation properties and tensile ductility. Compounds such as Al_2O_3, TiB_2, Ti_5Si_3 and Ti_2AlC have been identified as compatible and thermochemically stable reinforcing phases for the γ-TiAl matrix (Ward-Close *et al.*, 1996; Ramaseshan *et al.*, 1999).

Yeh and Shen (2009) carried out a study of TiAl–Ti_2AlC *in situ* composite preparation with a broad range of compositions, conducted by self-propagating high-temperature synthesis (SHS) of compressed samples with a mixture of elemental powders. Several carbide NiAl intermetallic composite powders have been produced by simultaneous reaction synthesis of the carbide and the intermetallic, with the objective of enhancing metallic cermets by replacing the metallic binder with NiAl (McCoy and Shaw, 1994).

NiAl has also been reinforced with TiB_2 or Al_2O_3, the latter produced by mixing NiO and Al, and it was mechanically alloyed to produce the composite powder (Cheng, 1994; Oleszak, 2001). Ni_3Al and NiAl intermetallics have been used as reinforcement of Al 2124 aluminium alloy, showing higher thermal stability and better mechanical properties than the same metallic alloy reinforced with common ceramics (Torres *et al.*, 2002).

9.4.4 Refractory-based composite powders

A wide variety of refractory materials are available. These materials can be classified in three general families of refractories, in terms of their chemical composition:

- oxide refractories
- non-oxide refractories
- composite refractories.

Concerning metal-based refractories, silver-based refractory contact materials produced by powder metallurgy are used extensively as contact materials owing to their properties, which include high conductivity, good resistance to welding and corrosion, high melting temperatures and hardness. Ag–65 wt% W composite is widely used in air circuit breakers in the 50–100 Å range (Lee, 1997). Findik and Uzun (2003) studied the effect of graphite additions on electrical conductivity and hardness of a 60 wt% Ag–37 wt% WC–3 wt% C contact material produced by powder metallurgy.

Tungsten and molybdenum are two refractory metals that have attracted great interest for high-temperature applications in industries such as consumer electronics, aerospace, telecommunications, medicine and defence, owing to their excellent heat resistance. The high melting temperatures of the metals (3422°C for tungsten and over 2623°C for molybdenum), however, makes it extremely difficult to process the materials by melting and casting. Conventionally, tungsten and molybdenum-based alloys and composites are produced by a powder metallurgical method, followed by minor machining or grinding, if necessary.

An important refractory metal-based composite is the W–Cu system, which has superior thermal management properties and a high microwave absorption capacity. It is predominantly used for heavy-duty electrical contacts and arcing resistant electrodes. Tungsten–copper alloy powders are used in many fields on account of the high electric and thermal conductivities of copper and the high melting point of tungsten. Good thermal and electrical conductivity and a low thermal expansion coefficient contribute to making these composites advanced engineering materials. However, because the W–Cu system exhibits mutual insolubility, W–Cu powder compacts have a bad sintering capacity, even when using liquid-phase sintering at above the melting point of the Cu phase. For this reason, it has been reported that W–Cu composite powders can be produced by ball milling (Gaffet *et al.*, 1991), oxide co-reduction (Gusmano *et al.*, 2001), freeze-drying technique (Xi *et al.*, 2010), mechano-chemical methods (Kim *et al.*, 2004b) and MA (Xiong *et al.*, 1995; Doré *et al.*, 2004; Alam, 2006). However, only a few reports are available on the synthesis of W–Cu composite powders through chemical routes (Ardestani *et al.*, 2009; Hashempour *et al.*, 2010). Compared to MA processes, chemical synthetic approaches have the advantage of better control of particle size, shape and distribution through adjustment of the reaction parameters.

Sahoo *et al.* (2011) addresses the synthesis of W–Cu nanocomposites by a multivariate route, comprising polyol and thermal decomposition processes.

W–Cu nanocomposite powders were synthesised by simultaneous reduction of $Cu(acac)_2$ by polyethyleneglycol (PEG-200) and decomposition of $W(CO)_6$ in diphenyl ether. The composition of the resultant W–Cu nanocomposites could be easily altered by adjusting the ratio of metal precursors, since both are solid powders.

9.5 Applications

Among the diversity of applications in which Me-based composite powders have been used, we can identify four sectors that continue to be employed and probably will be considered in the immediate and mid-range future. First, the enhanced electrical properties are welcomed for the production of electrodes or parts of SOFCs (solid oxide fuel cells) (Changsheng *et al.*, 2011). Second, the magnetic properties of Fe–Co-based metallic alloys have been successfully applied by combining them with some oxides, particularly alumina, in order to strengthen and stabilise the grain size of the metallic matrix. Another example of where the magnetic properties were the key part of the system was the result of combining Fe and ferrite. Taking into account that MA was used as the production method, the magnetic domains can be highly influenced by the process and thus internal stresses and grain/domain size are the key factors to be controlled. Microelectronics and sensor devices are among the most frequent applications of this type of composite powder. Nanocomposite powders can help to produce higher efficacy in doped semiconductors.

When mixing magnetic metals or alloys with polymers, metal-based polymer composite powders can offer magnetic properties that are strongly related to powder particle size and will produce soft magnetic composites. In particular, Nowosielski (2007) studied high energy milling of amorphous ribbons of metallic $Fe_{78}Si_9B_{13}$ and $Fe_{73.5}Cu_1Nb_3Si_{13.5}B_9$ glasses. After annealing to the point of nanocrystallising them, they were mixed with a polymer and finally consolidated.

Biomedicine is the third sector where objects produced from metal-based composite powders find a market. It is well known that HA-ceramic composite powders are in great demand for bone restructuration, but some attempts have also been carried out to combine Ti–Al–V with HA. Biocompatibility and inert bioreactivity are the objectives for any material to be used in this sector.

Structural properties can be enhanced by Me-composite powder-based materials for applications where these properties are essential; however, other functions may also be crucial, thus affecting material selection. The sintering step for the production of composite material products is nowadays well known, as confirmed by the increasing number of scaled-up laboratory processes. Thus, general structural requirements compose the fourth main group of applications (Neikov *et al.*, 2009).

CNT reinforced metal-matrix consolidated composites are still at the research stage. However, there are several potential applications for these composites. Owing to their high strength, wear resistance and low density, these applications are piston rings, gears and cylinder liners in the automobile industry, and aircraft brakes and landing gear in the aerospace industry. If they also have a low coefficient of thermal expansion, structural radiators in space applications or devices in electronic packaging are also potential applications for these materials. Microelectromechanical systems (MEMS), sensors, batteries and energy storage systems need a high elastic modulus, large surface area, reduced response times and high current density, characteristics that can also be found in some metallic composite powder combinations (Bakshi *et al.*, 2010). CNTs have better strength and stiffness than carbon fibres and hence have the potential to replace carbon-fibre reinforced MMCs in various applications. Overcoming the challenges in processing will result in efficient use of the mechanical properties and will result in the strongest MMCs known to mankind.

9.6 Future trends

It is worth noting that nanocomposites have their own particular route and applications in nanotechnology. Among these applications, supercapacitors, thermoelectric materials, templates, sensors, biosensors and controllers appear to be the future for this family of materials. Much research has been undertaken into utilising CNTs as reinforcement for composite materials since their discovery by Iijima in 1991. However, CNT-reinforced MMCs have received little attention. These composites are being prepared for use in structural applications because of their high specific strength, as well as their use as functional materials owing to their excellent thermal and electrical conductivities.

Since 1970, carbon-fibre reinforced composites have been extensively used for a wide array of applications such as aircraft brakes, space structures, military and commercial planes, lithium batteries, sporting goods and structural reinforcement in construction. In the last decade, a number of studies have been carried out using CNT as reinforcement in different materials, namely polymers, ceramics and metals. Bakshi *et al.* (2010) studied journal articles published on CNT-reinforced composites in the last decade and found that the majority of research had been carried out into reinforcement of polymers by CNT. This can be attributed primarily to the relative ease of polymer processing, which often does not require the high temperatures for consolidation that are needed for metals and ceramic matrixes. This is surprising considering the fact that most of the structural materials used today are metals. Also, the number of publications on different metal matrix-CNT composites from 1997 to 2008 was plotted and it could be observed that

there has been an increase in the number of publications on that topic since 2003. In addition, the metal matrixes in CNT-reinforced MMCs that were most used in the last decade were Al, Ni and Cu.

CNT-reinforced metal matrix (MM-CNT) composites are prepared by a variety of processing techniques. Since realising that the most critical issues in the processing of CNT-reinforced MMCs are (i) dispersion of CNTs and (ii) the interfacial bond strength between CNT and the matrix, many researchers have adopted modified steps in their approaches. Powder metallurgy is the most popular and widely applied technique for preparing MM-CNT composites by MA. Esawi and Morsi (2007) used MA for the first time to generate a homogenous distribution of 2 wt% CNT within Al powders. Milling for up to 48 hours led to good dispersion of CNTs but resulted in the formation of large spheres (>1 mm) owing to cold welding. Yang and Schaller (2004) achieved a homogeneous distribution of CNT in a Mg matrix by mechanically mixing the powders in an alcohol and acid mixture, followed by sintering at 823K.

Electrodeposition and electroless deposition are the second most important techniques for the deposition of thin coatings onto MM-CNT composites, as well as for deposition of metals onto CNTs. Walid (2008) researched CNT–Cu composite powders; different CNT volume fractions were prepared in an alkaline citrate bath by electroless copper deposition. The composite powders produced were heat treated and sintered using a spark plasma technique. The CNTs were implanted into the copper particles. To achieve better dispersion in the Cu matrix, the CNTs were electrolessly coated with Ni before hot pressing at 1373K, which ultimately resulted in improved mechanical and wear properties for the composite (Deng *et al.*, 2007).

A novel approach (Xu *et al.*, 2010) was developed to obtain uniformly dispersed CNT reinforcement in Al matrix composite powders. The process involved *in situ* synthesis of carbon nanostructures on the surface of aluminium powders through Friedel–Craft alkylation, and a homogenous dispersion of the CNTs in the aluminium powders was obtained.

The critical issues for mechanical properties in MM–CNT composites are the homogeneous distribution of CNTs in the metal matrix and the interfacial reaction and bonding to the matrix so that they work as effective reinforcement.

9.7 References

This chapter has aimed to reflect the continuing research and effort that has broadened our knowledge and understanding of Me-based composite powders. There are several key books to consult, including: the *Handbook of Non-Ferrous Metal Powders: Technologies and Applications* (Neikov *et al.*, 2009), the *ASM Metals Handbook: Powder Metallurgy* (Eisen *et al.*, 1998), and the *Concise Encyclopaedia of Composite*

Materials (Kelly, 1994 and Mortensen, 2007). The authors would like to thank the valuable contributions of all of the authors and collaborators.

Adamiak M, Fogagnolo JB, Ruiz Navas EM, Dobrzanski LA and Torralba JM (2004), 'Mechanically milled AA6061/(Ti_3Al)P MMC reinforced with intermetallics – the structure and properties', *J Mater Proc Technol*, **155–6**, 2002–6.

Alam SN (2006), 'Synthesis and characterization of W–Cu nanocomposites developed by mechanical alloying', *Mater Sci Eng*, **433**, 161–168.

Arami H, Simchi A and Seyed Reihani SM (2008), 'Mechanical induced reaction in Al–CuO system for *in-situ* fabrication of Al based nanocomposites', *J Alloys Compd*, **465**, 151–6.

Ardestani M, Rezaie HR, Arabi H and Razavizadeh H (2009), 'The effect of sintering temperature on densification of nanoscale dispersed W\20–40wt% Cu composite powders', *Int J Refract Met Hard Mater*, **27**, 862–7.

Bakshi SR, Lahiri D and Agarwal A (2010), 'Carbon nanotube reinforced metal matrix composites – a review', *Int Mater Rev*, **55**, 41–64.

Begin-Colin S, de Araujo Pontes LR, Le Caer G, Pianelli A, Mocellin A and Matteazzi P (1993), 'Synthesis of metal-ceramic composite powders (Al_2O_3-Ti) by mechanical alloying', in *Proceedings International Conference Mechanochemistry*, Tkacova K (ed), Kosice.

Benjamin JS (1988), 'The mechanical alloying process', *Mod Dev Powder Metall*, **21**, 397–414.

Benjamin JS (1990), 'Mechanical alloying – A perspective', *Metal Powder Rep*, **2**, 122–7.

Benn RC, Mirchandani PK and Watwe AS (1988), 'Intermetallic systems produced by mechanical alloying', *Mod Dev Powder Metall*, **21**, 479–93.

Bhadury A, Gopinathan V, Ramakrishnan P and Miodownik AP (1996), 'Microstructural changes in a mechanically alloyed Al –6.2 Zn–2.5 Mg– 1 Cu alloy (7010) with and without particulate SiC reinforcement', *Metall Mater Trans*, **27**, 3718–26.

Botta WJ, Tomasi R, Pallone EMJA and Yavari AR (2001), 'Nanostructured composites obtained by reactive milling', *Scr Mater*, **44**, 1735–40.

Boyer R, Collings EW and Welsch G (1994), *Material Properties Handbook: Titanium Alloys*, ASM International, Ohio.

Castricum HL, Bakker H and Poels EK (2001), 'Oxidation and reduction in copper/zinc oxides by mechanical milling', *Mater Sci Eng*, **304–6**, 418–23.

Changsheng D, Hongfei L, Kazuhisa S and Toshiyuki H (2011), 'Co-precipitation synthesis and characterization of NiO-$Ce_{0.8}Sm_{0.2}O_{1.9}$ nanocomposite powders: effect of precipitation agents', *J Nanosci Nanotechnol*, **11**(3), 2336–43.

Cheng T (1994), 'Mechanical alloying of NiAl-based composites and cold sintering phenomenon', *Scr Metall Mater*, **31**(11), 1599–604.

Chicinas I (2006), 'Soft magnetic nanocrystalline powders produced by mechanical alloying routes', *J Optoelectron Adv Mater*, **8**, 439–48.

Chou TW, Kelly A and Okura A (1985), 'Fibre-reinforced metal matrix composites' *Composites*, **16**, 187–206.

Chung KH, He J, Shin DH and Schoenung JM (2003), 'Mechanisms of microstructure evolution during cryomilling in the presence of hard particles', *Mater Sci Eng*, *A*, **356**, 23–31.

Córdoba JM, Sayagués MJ, Alcala MD and Gotor FJ (2005), 'Synthesis of titanium carbonitride phases by reactive milling of the elemental mixed powders', *J Am Ceram Soc*, **88**, 1760–4.

Córdoba JM, Sayagués MJ, Alcala MD and Gotor FJ (2007a), 'Monophasic $Ti_yNb_{1-y}C_xN_{1-x}$ nanopowders obtained at room temperature by MSR', *J Mater Chem*, **17**, 650–653.
Córdoba JM, Sayagués MJ, Alcala MD and Gotor FJ (2007b), 'Monophasic nanostructured powders of niobium, tantalum, and hafnium carbonitrides synthesized by a mechanically induced self-propagating reaction', *J Am Ceram Soc*, **90**, 381–7.
Córdoba JM, Avilés MA, Sayagués MJ, Alcalá MD and Gotor FJ (2009), 'Synthesis of complex carbonitride powders $Ti_yMT_{1-y}C_xN_{1-x}$ (MT: Zr, V, Ta, Hf) via a mechanically induced self-sustaining reaction', *J Alloys Comp*, **482**, 349–55.
Correia JB, Marques MT, Carvalho PA and Vilar R (2007), 'Hardening in copper-based nanocomposites', *J Alloys Compd*, **434–5** (31), 301–3.
Crisan O and Crisan AD (2011), 'Phase transformation and exchange bias effects in mechanically alloyed Fe/magnetite powders', *J Alloys Comp*, **509**, 6522–7.
Davis JR (2001), *Copper and Copper Alloys*, ASM International, Ohio.
Deng CF, Zhang XX, Wang DZ and Ma YX (2007), 'Calorimetric study of carbon nanotubes and aluminum', *Mater Lett*, **61**, 3221–3.
Dogan ON and Hawk JA (1995), 'Abrasion resistance of *in-situ* Fe-TiC composites', *Scr Metall*, **33**, 953–8.
Dong SJ, Zhou Y, Shi YW and Chang BH (2002), 'Formation of a TiB_2-reinforced copper-based composite by mechanical alloying and hot pressing', *Metall Mater Trans*, **33A**, 1275–1280.
Doré F, Martin CL and Allibert CH (2004), 'Apparent viscosity of W–Cu powder compacts during sintering', *Mater Sci Eng*, **383**, 390–398.
Eisen WB, Ferguson BL, German RM, Iacocca R, Lee PW, Madan D, Moyer K, Sanderow H and Trudel Y (eds) ASM Handbook volume 7: Powder Metallurgy: Technologies and Applications, (1998), ASM International, The Materials Information Society, Ohio.
Esawi A and Morsi K (2007), 'Dispersion of carbon nanotubes (CNTs) in aluminum powder', *Composites: Part A*, **38**, 646–650.
Everett RK and Higby PL (1991), 'Expansivity of diboride-particulate/aluminium composites', *Scr Metall Mater*, **25**, 625.
Farid A, Guo S, Cui F-e C, Feng P and Lin T (2007), 'TiB_2 and TiC stainless steel matrix composites', *Mater Lett*, **61**, 189–191.
Faure JF and Brune G (1987), 'New PM aluminium alloys for wear and sliding applications', *Metal Powder Rep*, **42**, 101–103.
Findik F and Uzun H (2003), 'Microstructure, hardness and electrical properties of silver-based refractory contact materials', *Mater Des*, **24**, 489–492.
Fischer JJ and Haeberle RM (1988), 'Commercial status of mechanically alloyed materials', *Mod Dev Powder Metall*, **21**, 461–477.
Flom Y and Arsenault RJ (1986), 'Deformation of SiC/Al composites', *J Metal*, **38**, 31–34.
Fogagnolo JB, Amador D, Morales F, Ruiz-Navas E and Torralba JM (2002), 'Powder characterization of Al–Cu produced by mechanical alloying', *Adv Powder Metall Part Mater*, **1**, 191–7.
Fogagnolo JB, Robert MH, Ruiz-Navas EM and Torralba JM (2004), '6061 Al reinforced with zirconium diboride particles processed by conventional powder metallurgy and mechanical alloying', *J Mater Sci*, **39**, 127–32.
Forouzanmehr N, Karimzadeh F and Enayati MH (2009), 'Synthesis and characterization of $TiAl/_{\alpha}$-Al_2O_3 nanocomposite by mechanical alloying', *J Alloys Compd*, **478**, 257–9.
Fortnum RT and Mikkola DE (1987), 'Effects of molybdenum, titanium and silicon

additions on the D03 = B2 transition temperature for alloys near Fe_3Al', *Mater Sci Eng*, **91**, 223–31.
Fu S and Xu H (2010), 'Microstructure and wear behaviour of (Ti,V)C reinforced ferrous composite', *J Mater Eng Perform*, **19**, 825–828.
Gaffet E, Louison C, Harmelin M and Faudot F (1991), 'Metastable phase transformations induced by ball-milling in the Cu–W system', *Mater Sci Eng*, **134**, 1380–1384.
Gleiter H (2000), 'Nanostructured materials: basic concepts and microstructure', *Acta Mater*, **48**, 1–29.
González-Carrasco JL, García-Cano F, Caruana G and Liebich M (1994), 'Aluminum/Ni_3Al composites processed by powder metallurgy', *Mater Sci Eng*, **183**, 5–8.
Grossmann J, Rose K and Sporn D (1995), 'Processing, properties and microstructural design of sol–gel derived nanostructured Ni–Y_2O_3/ZrO_2', *Ceram Trans* **51**, 713–717.
Gusmano G, Bianco A and Polini R (2001), 'Chemical synthesis and sintering behaviour of highly dispersed W/Cu composite powders', *J Mater Sci*, **36**, 901–907.
Hashempour M, Rezaie HR, Razavizadeh H, Salehi MT, Mehrjoo H and Ardestani M (2010), 'Investigation on fabrication of W\Cu nanocomposite via a thermochemical coprecipitation method and its consolidation behavior', *J Nano Res*, **11**, 57–66.
Heidarpour A, Karimzadeh F and Enayati MH (2009), '*In situ* synthesis mechanism of Al_2O_3–Mo nanocomposite by ball milling process', *J Alloys Compd*, **477**, 692–695.
Horvitz D, Gotman I, Gutmanas EY and Claussen N (2002), '*In situ* processing of dense Al_2O_3–Ti aluminide interpenetrating phase composites', *J Eur Ceram Soc*, **22**, 947–954.
Hu D and Loretto MH (1994), 'Microstructural characterisation of a gas atomized Ti6Al4V-TiC composite', *Scr Metall Mater*, **31**(5), 543–548.
Huang ZG, Guo ZP, Calka A, Wexler D and Liu HK (2007), 'Effects of carbon black, graphite and carbon nanotube additives on hydrogen storage properties of magnesium', *J Alloys Compd*, **427**, 94–100.
Hussain Z, Othmana R, Longa BD and Umemotob M (2008), 'Synthesis of copper–niobium carbide composite powder by *in situ* processing', *J Alloys Comp*, **464**, 185–189.
Jena PK, Brocchi EA and Motta MS (2001), '*In situ* formation of Cu–Al_2O_3 nano-scale composites by chemical routes and studies on their microstructures', *Mater Sci Eng*, *A*, **313**, 180–186.
Jiang WH, Fei J and Han XL (2000), '*In Situ* Synthesis of (TiW)Cp/Fe Composites', *Mater Lett*, **46**, 222–224.
Joshi PB, Marathe GR, Murti NSS, Kaushik VK and Ramakrishnan P (2002), 'Reactive synthesis of titanium matrix composite powders', *Mater Lett*, **56**, 322–328.
Karimzadeh F, Enayati MH and Tavoosi M (2008), 'Synthesis and characterization of Zn/Al_2O_3 nanocomposite by mechanical alloying', *Mater Sci Eng*, *A*, **486**, 45–48.
Kelly A (1994), Concise Encyclopaedia of Composite Materials, London, Elsevier Science.
Khakbiz M and Akhlaghi F (2009), 'Synthesis and structural characterization of Al–B_4C nano-composite powders by mechanical alloying', *J Alloys Comp*, **479**, 334–1.
Khodaei M, Enayati MH and Karimzadeh F (2009), 'Mechanochemically synthesized Fe_3Al–Al_2O_3 nanocomposite', *J Alloys Compd*, **467**, 159–162.
Kim JC and Moon I (1998), 'Sintering of nanostructured W–Cu alloys prepared by mechanical alloying', *Nanostruct Mater*, **10**, 283–290.
Kim DG, Kim GS, Suk MJ, Oh ST and Kim YD (2004a), 'Effect of heating rate on microstructural homogeneity of sintered W–15wt%Cu nanocomposite fabricated from W–CuO powder mixture', *Scr Mater*, **51**, 677–681.

Kim DG, Kim GS, Oh ST and Kim YD (2004b), 'The initial stage of sintering for the W–Cu nanocomposite powder prepared from W–CuO mixture', *Mater Lett*, **58**, 578–581.

Kim JW, Chung HS, Shim JH, Ahn JP, Cho YW and Oh KH (2006), 'Synthesis and liquid phase sintering of TiN/TiB_2/Fe–Cr–Ni nanocomposite powder', *J Alloy Compd*, **422**, 62–66.

Knibloe JR, Wright RN, Sikka VK, Baldwin RH and Howell CR (1992), 'Elevated temperature behavior of Fe_3Al with chromium additions', *Mater Sci Eng*, **153**, 382–386.

Koch CC and Whittenberger JD (1996), 'Mechanical milling/alloying of intermetallics', *Intemetallics*, **4**, 339–355.

Kondoh K, Threrujirapapong T, Imai H, Umeda J and Fugetsu B (2009), 'Characteristics of powder metallurgy pure titanium matrix composite reinforced with multi-wall carbon nanotubes', *Compos Sci Technol*, **69**, 1077–1081.

Korác M, Andic Z, Tasic M and Kamberovic Z (2007), 'Sintering of Cu–Al_2O_3 powders produced by a thermomechanical route', *J Serbian Chem Soc*, **72**, 1115–25.

Lampke T, Wielage B, Pokhmurska H, Rupprecht C, Schuberth S, Drehmann R and Schreiber F (2011), 'Development of particle-reinforced nanostructured iron-based composite alloys for thermal spraying', *Surf Coat Technol*, **205**, 3671–3676.

Last HR and Garret RK (1996), 'Mechanical behavior and properties of mechanically alloyed aluminum alloys', *Metall Mater Trans*, **27**, 737–745.

Lee PW (1997), Powder metal technologies and applications, ASM International, Ohio.

Lee BS and Kang S (2001), 'Low-temperature processing of B_4C–Al composites via infiltration technique', *Mater Chem Phys*, **67**, 249–255.

Lee JS and Kim TH (1995), 'Densification and microstructure of the nanocomposite W-Cu powders', *Nanostruct Mater*, **6**, 691–694.

Lee YF and Lee SL (1999), 'Effects of Al additive on the mechanical and physical properties of silicon reinforced copper matrix composites', *Scr Mater*, **41**(7), 773–778.

Lee DW, Ha GH and Kim BK (2001), 'Synthesis of Cu–Al_2O_3 nano composite powder', *Scr Mater*, **44**, 2137–2140.

Li L and Lai M (1998), *Mechanical Alloying*, *Kluwer Academic Publishers*, Boston.

Li J, Ni X and Wang G (2007), 'Microstructure and magnetic properties of Co/Al_2O_3 nanocomposite powders', *J Alloys Compd*, **440**, 349–356.

Llorca-Isern N, Artieda-Guzmán C, Porras-Mateu N and Roca-Vallmajor A (2010), 'Structural and magnetic properties of nanocrystalline Cu–Fe–Co–Al_2O_3 composite powders processed by mechanical alloying', *Pulvimetalurgy World Congress Firenze*, Italy, volume **2**, 256.

Lu CJ and Li ZQ (2005), 'Structural evolution of the Ti–Si–C system during mechanical alloying', *J Alloy Compd*, **395**, 88–92.

Lü L, Lai MO and Wang HY (2000), 'Synthesis of titanium diboride TiB_2 and Ti–Al–B metal matrix composites', *J Mater Sci*, **35**, 241–248.

Lü L, Lai MO, Su Y, Teo HL and Feng CF (2001), '*In situ* TiB_2 reinforced Al alloy composites', *Scr Mater*, **45**, 1017–1023.

Maiti R and Chakraborty M (2008), 'Synthesis and characterization of molybdenum aluminide nanoparticles reinforced aluminium matrix composites', *J Alloys Compd*, **458**, 450–456.

Majumdar D, Kodas TT and Glicksman HD (1998), 'Generation of novel silver-silica powders by spray pyrolysis', *World Congress on Particle Technology*, 3, Brighton, UK, 1711–1719.

Matsumoto M, Kaneko K, Yasutomi Y, Ohara S, Fukui T and Ozawa Y (2002), 'Synthesis of TiO_2-Ag composite powder by spray pyrolysis', *J Ceram Soc Jpn*, **110**, 60–62.

Matsuura K, Obara Y and Kudoh M (2006), 'Fabrication of TiB_2 particle dispersed FeAl-based composites by self-propagating high-temperature synthesis', *ISIJ Int*, **46**, 871–874.

McCormick PG and Froes FH (1998), 'The fundamentals of mechanochemical processing', *JOM*, **50**(11), 61–65.

McCoy KP and Shaw KG (1994), 'Fabrication of carbide intermetallic composite powders by reaction synthesis', in *Specialty Materials and Composites. Advances in Powder Metallurgy & Particulate Materials*, Lall C (ed), Metal Powder Industries Federation, Michigan, 179–87.

Mendiratta MG, Ehlers SK and Lipsitt HA (1987), 'DO_3-B2-á phase relations in Fe–Al–Ti alloys', *Metall Trans*, **18**, 509–18.

Mishra RS, Bieler TR and Mukherjee AK (1992), 'On the superplastic behaviour of mechanically alloyed aluminium alloys', *Scr Metall Mater*, **26**, 1605–1608.

Montealegre I, Neubauer E, Angerer P, Danninger H and Torralba JM (2011), 'Influence of nano-reinforcements on the mechanical properties and microstructure of titanium matrix composites', *Compos Sci Technol*, **71**, 1154–1162.

Mortensen A (2007), *Concise Encyclopaedia of Composite Materials*, 2nd edition, Elsevier, Oxford.

Mortensen A, Cornie JA and Flemings MC (1988), 'Solidification processing of metal-matrix composites', *J Met*, **40**, 12–19.

Mousavi T, Karimzadeh F and Abbasi MH (2009), 'Mechanochemical assisted synthesis of NiTi intermetallic based nanocomposite reinforced by Al_2O_3', *J Alloys Compd*, **467**, 173–178.

Mukai T and Ishikawa K (1995), *J Jpn Soc Powder, Powder Metall*, **42**, 180–184.

Mulas G, Varga M, Bertoti I, Molnar A, Cocco G and Szepvolgyi J (1999), '$Cu_{40}Mg_{60}$ and Cu–MgO powders prepared by ball-milling: characterization and catalytic tests', *Mater Sci Eng*, **267**, 193–199.

Munir ZA (1988), 'Synthesis of high temperature materials by self-propagating combustion methods', *Bull Amer Ceram Soc*, **67**, 342–349.

Munir Z and Ealamloo-Grami M, (The Regents of the University of California) 1994. *Synthesis of Transition Metal Carbonitrides*, US patent application 5,314,656.1994-May-24.

Nardone VC and Prewo KW (1986), 'On the strength of discontinuous silicon carbide reinforced aluminum composites', *Scr Metall*, **20**, 43–48.

Neikov O, Naboychenko S, Mourachova I, Gopienko V, Frishberg I and Lotsko D (2009), *Handbook of Non-Ferrous Metal Powders: Technologies and Applications*, Elsevier, Amsterdam.

Nowosielski R (2007), 'Soft magnetic polymer–metal composites consisting of nanostructural Fe-basic powders', *J Achievements Mater Manufactur Eng*, **24**(1), 68–77.

Oleszak D (2001), 'Mechanically alloyed nanocrystalline NiAl–Al_2O_3 composite powders', in *Science of Metastable and Nanocrystalline Alloys: Structure, Properties and Modelling*, Dinesen AR, Eldrup M, Juul Jensen D, Linderoth S, Pedersen TB, Pryds NH, SchroederPedersen A and Wert JA (eds), Risoe National Laboratory, Roskilde, 3–7.

Pastor H (1988), 'Titanium-carbonitride-based hard alloys for cutting tools', *Mater Sci Eng*, **105–6**, 401–409.

Pérez-Bustamante R, Estrada-Guel I, Antúnez-Flores W, Miki-Yoshida M, Ferreira PJ

and Martínez-Sánchez R (2008), 'Novel Al-matrix nanocomposites reinforced with multi-walled carbon nanotubes', *J Alloys Compd*, **450**, 323–326.

Polkin IS and Borzov AB (1995), 'New materials produced by mechanical alloying', *Adv Perfor Mater*, **2**, 99–109.

Rafiei M, Enayati MH and Karimzadeh F (2009), 'Mechanochemical synthesis of $(Fe,Ti)_3Al–Al_2O_3$ nanocomposite', *J Alloys Comp*, **488**, 144–147.

Raghunathan S, Allen RJ, Persad C, Bourell DL, Eliezer Z and Marcus HL (1993), 'Tungsten and tungsten-based composites and alloys for high heat flux duty', *Specialty Materials and Composites. Advances in Powder Metallurgy & Particulate Materials*, in Lall C (ed), Metal Powder Industries Federation, Michigan, 175–187.

Ramaseshan R, Kakitsuji A, Seshadri SK, Nair NG, Mabuchi H, Tsuda H, Matsui T and Morii K (1999), 'Microstructure and some properties of $TiAl–Ti_2AlC$ composites produced by reactive processing', *Intermetallics*, **7**, 571–7.

Ravikiran A and Surappa MK (1997), 'Oscillations in coefficent of friction during dry sliding of A356 Al–30% wt SiCp MMC against steel', *Scr Mater*, **36**, 95–98.

Razavi-Hesabi Z, Simchi A and Seyed Reihani SM (2006), 'Structural evolution during mechanical milling of nanometric and micrometric Al_2O_3 reinforced Al matrix composite', *Mater Sci Eng*, **428**, 159–168.

Reddy BSB, Das K, Pabi SK and Das S (2007), 'Mechanical-thermal synthesis of Al-Ce/Al_2O_3 nanocomposite powders', *Mater Sci Eng A*, **445–6**, 341–6.

Ruiz-Navas EM, Fogagnolo JB, Velasco F, Ruiz-Prieto JM and Froyen L (2006), 'One step production of aluminium matrix composite powders by mechanical alloying', *Composites*, **37**, 2114–2120.

Sabooni S, Mousavi T and Karimzadeh F (2010), 'Mechanochemical assisted synthesis of $Cu(Mo)/Al_2O_3$ nanocomposite', *J Alloys Comp*, **497**, 95–99.

Sadeghian Z, Lotfia B, Enayatib MH and Beiss P (2011), 'Microstructural and mechanical evaluation of $Al–TiB_2$ nanostructured composite fabricated by mechanical alloying', *J Alloys Comp*, **509**, 7758–7763.

Sahoo PK, Kamal SSK, Premkumar M, Sreedhar B, Srivastava SK and Durai L (2011), 'Synthesis, characterization and densification of W\Cu nanocomposite powders', *Int J Refract Met Hard Mater*, **29**, 547–554.

Schaffer GB and McCormick PG (1989), 'Combustion synthesis by mechanical alloying', *Scr Metall*, **23**, 835–838.

Schaffer GB and McCormick PG (1990), 'Displacement reactions during mechanical alloying', *Metall Trans*, **21**(10), 2789–2794.

Schaffer GB and McCormick PG (1991), 'Anomalous combustion effects during mechanical alloying', *Metall Trans*, **22**(12), 3019–3024.

Schicker S, Garcia DE, Gorlov I, Janssen R and Claussen N (1999), 'Wet milling of $Fe/Al/Al_2O_3$ and $Fe_2O_3/Al/Al_2O_3$ powder mixtures', *J Am Ceram Soc*, **82**, 2607–12.

Sheibani S, Ataie A, Heshmati-Manesh S and Khayati GR (2007), 'Structural evolution in nano-crystalline Cu synthesized by high energy ball milling', *Mater Lett*, **61**, 3204–3207.

Sheibani S, Khakbiza M and Omidib M (2009), '*In situ* preparation of Cu–MnO nanocomposite powder through mechanochemical synthesis', *J Alloys Comp*, **477**, 683–687.

Shorowordi KM, Laoui T, Haseeb ASMA, Celis JP and Froyen L (2003), 'Microstructure and interface characteristics of B_4C, SiC and Al_2O_3 reinforced Al matrix composites: a comparative study', *J Mater Process Technol*, **142**, 738–743.

Suryanarayana C (2001), 'Mechanical alloying and milling', *Prog Mater Sci*, **46**, 1–184.

Takacs L (2002), 'Self-sustaining reactions induced by ball milling', *Prog Mater Sci*, **47**, 355–414.

Tang F, Wu XL, Ge SR, Ye JC, Zhu H, Hagiwara M and Schoenung JM (2008), 'Dry sliding friction and wear properties of B_4C particulate-reinforced Al-5083 matrix composites', *Wear*, **264**, 555–561.

Tee KL, Lü L and Lai MO (2001), '*In situ* stir cast Al–TiB_2 composite: processing and mechanical properties', *Mater Sci Technol*, **17**, 201–206.

Thian ES, Khor KA, Loh NH and Tor SB (2001), 'Processing of HA-coated Ti-6Al-4V by a ceramic slurry approach: an *in vitro* study', *Biomaterials*, **22**, 1225–32.

Tjong SC and Lau KC (2000), 'Abrasive wear behavior of TiB_2 particle-reinforced copper matrix composites', *Mater Sci Eng*, **282**, 183–186.

Tjong SC and Ma ZY (2000), 'Microstructural and mechanical characteristics of *in situ* metal matrix composites', *Mater Sci Eng*, **29**, 49–113.

Tjong SC, Wang GS and Mai YW (2005), 'High cycle fatigue response of *in-situ* Al-based composite containing TiB_2 and Al_2O_3 submicron particles', *Compos Sci Technol*, **65**, 1537–1546.

Torralba JM, da Costa CE, Cambronero LEG and Ruiz-Prieto JM (1997), 'PM aluminium composite reinforced with Ni_3Al', *Key Eng Mater*, **127–131**, 929–936.

Torres B, Lieblich M, Ibanez J and Garcia-Escorial A (2002), 'Mechanical properties of some PM aluminide and silicide reinforced 2124 aluminium matrix composites', *Scr Mater*, **47**(1), 45–49.

Van Meter ML, Kampe SL and Lawley A (1992), 'Dispersion Strengthened P/M Al-Mg Alloys' in *Advances in Powder Metallurgy and Particulate Materials*, Campus JM and German RM (eds), Metal Powder Industries Federation, Princeton, 285–301.

Varma HK, Kumar KP, Warrier KGK and Damodaran AD (1990), 'Silver-yttrium barium copper oxide composite derived from citrate gel', *Supercond Sci Technol*, **3**(2), 73–75.

Vijay R, Sundaresan R, Maiya MP and Srinivasa Murthy S (2006), 'Hydrogen storage properties of Mg–Cr_2O_3 nanocomposites: the role of catalyst distribution and grain size', *J Alloys Compd*, **424**, 289–293.

Walid MD (2008), 'Processing and characterization of CNT/Cu nanocomposites by powder technology', *Powder Metall Met Ceram*, **47**, 9–10.

Ward-Close CM, Minor R and Doorbar PJ (1996), 'Intermetallic-matrix composites – a review', *Intermetallics*, **4**, 217–29.

Welham NJ (1998), 'Mechanical activation of the formation of an alumina-titanium trialuminide composite', *Intermetallics*, **6**, 363–368.

Wu JM and Li ZZ (2000), 'Nanostructured composite obtained by mechanically driven reduction reaction of CuO and Al powder mixture', *J Alloys Compd*, **299**, 9–16.

Xi X, Xu X, Nie Z, He S, Wang W, Yi J and Tieyong Z (2010), 'Preparation of W–Cu nano-composite powder using a freeze-drying technique', *Int J Refract Met Hard Mater*, **28**, 301–304.

Xiong CS, Xiong YH, Zhu H and Sun TF (1995), 'Synthesis and structural studies of Cu–W alloys prepared by mechanical alloying', *Nanostruct Mater*, **5**, 425–432.

Xu X, Li Z, Zhang D and Chen Z (2010), '*In situ* synthesis of nanostructured carbon reinforcement in aluminum powders', *Mater Lett*, **64**, 1154–1156.

Yang J and Schaller R (2004), 'Mechanical spectroscopy of Mg reinforced with Al_2O_3 short fibres and C nanotubes', *Mater Sci Eng*, **370**, 512–515.

Ye JC, Han BQ and Schoenung JM (2006a), 'Mechanical behaviour of an Al–matrix composite reinforced with nanocrystalline Al-coated B_4C particulates', *Philos Mag Lett*, **86**, 721–732.

Ye JC, He JH and Schoenung JM (2006b), 'Cryomilling for the fabrication of a particulate B_4C reinforced Al nanocomposite: Part I. Effects of process conditions on structure', *Met Mater Trans*, **37**, 3099–3109.

Ye JC, Lee Z, Ahn B, He JH, Nutt SR and Schoenung JM (2006c), 'Cryomilling for the fabrication of a particulate B_4C reinforced Al nanocomposite: Part II. Mechanisms for microstructural evolution', *Met Mater Trans A*, **37**, 3111–3117.

Yeh CL and Chen YD (2005), 'Synthesis of niobium carbonitride by self-propagating combustion of Nb–C system in nitrogen', *Ceram Int*, **31**, 1031–9.

Yeh CL and Chen YD (2007), 'Combustion synthesis of vanadium carbonitride from V–C powder compacts under nitrogen pressure', *Ceram Int*, **33**, 365–371.

Yeh CL and Liu EW (2006), 'Preparation of tantalum carbonitride by self-propagating high-temperature synthesis of Ta–C system in nitrogen', *Ceram Int*, **32**, 653–658.

Yeh CL and Shen YG (2009), 'Formation of TiAl–Ti_2AlC *in situ* composites by combustion synthesis', *Intermetallics*, **17**, 169–173.

Ying DY and Zhang DL (2000), 'Processing of Cu–Al_2O_3 metal matrix nanocomposite materials by using high energy ball milling', *Mater Sci Eng*, **286**, 152–156.

Yoshimi K and Hanada S (1997), 'The strength properties of iron aluminides', *JOM*, **49**(8), 46–49.

Zeng Q, Baker I, McCreary V and Yan Z (2007), 'Soft ferromagnetism in nanostructured mechanical alloying FeCo-based powders', *J Magn Magn Mater*, **318**, 28–38.

Zhang DL (2004), 'Processing of advanced materials using high-energy mechanical milling', *Prog Mater Sci*, **49**, 537–560.

Zhang DL and Richmond JJ (1999), 'Microstructural evolution during combustion reaction between CuO and Al induced by high energy ball milling', *J Mater Sci*, **34**, 701–706.

Zhang X, Lu W, Zhang D and Wu R (1999), '*In situ* technique for synthesizing (TiB+TiC)/Ti composites', *Scr Mater*, **41**, 39–46.

Zhang DL, Cai ZH and Adam G (2004a), 'Mechanical milling of Al/TiO_2 composite powders', *JOM*, **56**, 53–56.

Zhang GJ, Ando M, Yang JF, Ohji T and Kanzaki S (2004b), 'Boron carbide and nitride as reactants for *in situ* synthesis of boride-containing ceramic composites', *J Eur Ceram Soc*, **24**, 171–178.

Zhang H, Chen MW, Ramesh KT, Ye J, Schoenung JM and Chin ESC (2006), 'Tensile behavior and dynamic failure of aluminum 6092/B_4C composites', *Mater Sci Eng*, **433**, 70–82.

Zhu SM, Tamura M, Sakamoto K and Iwasaki K (2000), 'Characterization of Fe_3Al-based intermetallic alloys fabricated by mechanical alloying and HIP consolidation', *Mater Sci Eng*, **292**, 83–89.

10
Porous metals: foams and sponges

R. GOODALL, The University of Sheffield, UK

DOI: 10.1533/9780857098900.2.273

Abstract: This chapter describes the processing and properties of metals containing significant fractions of porosity, processed using powders. The basic concepts used in porous materials research are introduced and the different types of processing techniques that have been explored are surveyed. The reported property data for different foams are collated and used to illustrate the range of properties that have been achieved and methods to predict the properties of porous metals from elementary knowledge about their structure are discussed. Finally, the outlook for porous metals research and some likely future directions of fruitful enquiry are suggested.

Key words: material properties, metal foams, processing.

10.1 Introduction

A distinct class of materials with their own properties and behaviours, porous metals (called metal foams or sponges) have been the subject of research for some time and are starting to be applied in engineering situations. This chapter looks at why these materials are so interesting, how they are processed, what properties they display and the underlying rules that they follow. The emphasis is on porous metals processed by a solid state powder route and the literature on these materials is reported. However, in general the same relationships between the porous structure and the base metal properties, and the overall foam behaviour are found in all foamed materials.

Porous metals are interesting for research and engineering for two principal reasons: they are able to achieve unusual properties in combination and these properties can be tailored to suit the needs of a particular application:

Property combinations: Porous metals can be thought of as composites and can display some of the properties of metals (such as high electrical and thermal conductivity, ductile failure at high stress, etc) with some of the properties of a porous structure (such as permeability to fluids, low density, etc). These can be combinations that are impossible to achieve with other materials; for example, a highly thermally conducting material that is permeable to fluids would be suitable as a heat exchanger.
Tailoring of properties: The properties of a porous metal depend on both the properties of the metal in dense (i.e. non-porous) form, and also on

the porous structure (essentially the amount, shape, size and distribution of porosity). As a result, small structural changes can be used to adjust the properties (within certain limits), allowing the precise properties required to be obtained. This could, for example, be of use in a protective application (against crushing or impact), where the strength could be adjusted to ensure maximum energy absorption, while ensuring that the protected component did not exceed the safe load or impulse.

10.1.1 Porous metals

Any metal with a fluid phase (liquid or, most usually, gas) distributed throughout it could be classified as a porous metal, although in practice the study of these materials is generally confined to those showing significant levels of porosity (greater than 50%) and where the second phase regions are uniformly distributed throughout the material (unlike the case of a cast part with a large internal pore, for example). In these structures, the regions of free space are called pores or cells and the solid phase is called the dense or parent metal, with the individual structural elements being termed struts, if they are thin relative to the pores, and being referred to as cell walls if they are larger. Figure 10.1 shows an example image of a porous structure with some of these features indicated.

Another important structural change can be discovered if it is imagined

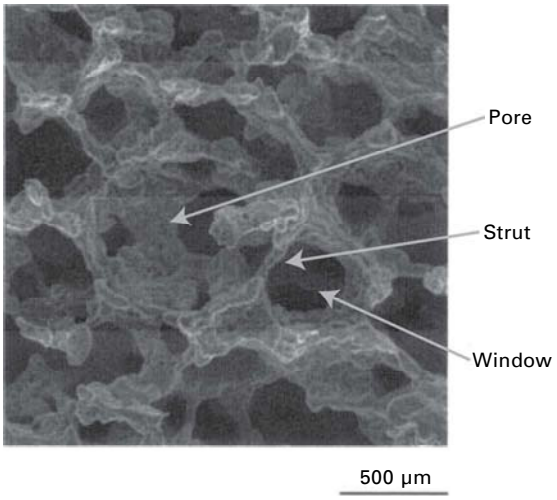

10.1 Example of a porous metal, indicating some of the typical features. The image (taken from Zhao and Sun, 2001) shows an aluminium foam processed by the space holder method. Foam micrograph reprinted from *Scripta Materialia*, Copyright (2001), with permission from Elsevier.

how the structure will change going from a metal with a low amount of porosity to one with much higher levels. With small amounts of a fluid phase, the pores will be isolated, existing as bubbles within the matrix. This is a closed cell structure and one that might be correctly called a metal foam. If we increase the amount of porosity, it is clear that at some point the pores will start to intersect and are likely to join, making a network that connects together and communicates with the external environment (this will occur at a volume fraction porosity of 0.64 (Arzt, 1982)). This is an open celled structure, and could be called a metal sponge, although the term metal foam is also applied.

10.1.2 Characteristics

In determining the properties of a porous metal, the two most important factors are the metal it is made from and the porous structure. The composition of the solid and any microstructure are easily determined by standard analysis techniques (e.g. energy dispersive X-ray spectrometry and optical microscopy), but the porous structure can be quite complex and difficult to quantify simply. The easiest identification to make is if the foam has open cells (which interconnect and are accessible by the outside environment) or closed cells (which are individually isolated and enclosed by metal, even if it is only a thin cell wall). Nevertheless, to interpret the properties it is normally necessary to quantify the structure and for this reason a number of parameters are commonly identified, Table 10.1.

In addition to these values, which would normally be given as the average for the whole specimen, the distribution of each of them will be important. In particular, for porous metals processed from powders, it may be found that the pore size distribution is bimodal. One peak may represent the size of the main pores, with a further peak at a size similar to the size of the powder particles, which represents residual porosity from incomplete sintering. If the

Table 10.1 Parameters frequently measured to characterise the structure of a porous metal

Parameter		Units	Measurement method
Volume fraction solid	Porosity	–	By measuring mass and volume, knowing density of base metal is required to calculate the porosity
	Density	kg m^{-3}	
Pore size (diameter)		m (mm)	Using image analysis on 2D sections (micrographs, optical or electron microscopy), for grain size/shape, using software or methods such as linear intercept (Higginson and Sellars, 2003). Measurements in 3D made using X-ray tomography (e.g. Tuncer *et al.*, 2011)
Pore aspect ratio		–	
Window size		m (mm)	

data is assimilated into a single average value, this underlying complexity can be missed.

10.1.3 Further information

Research has been carried out on metal foams since the 1960s and has been at a high level of intensity since around the 1980s. As a result there are a larger number of general reference works and reviews of the subject as a whole than will be covered in this chapter. Here the focus will be on metal foams and sponges processed using techniques based on powder metallurgy, but the wider subject can be accessed through books and review articles (Ashby *et al.*, 2000; Banhart, 2001; Dunand, 2004; Conde *et al.*, 2006; Colombo and Degischer, 2010; Goodall and Mortensen, 2013), and the proceedings of conferences such as the biennial MetFoam conference (Banhart *et al.*, 2003; Nakajima and Kanetake, 2005; Lefebvre *et al.*, 2007).

10.2 Powder processing: partial sintering and space holders

10.2.1 Partial sintering

When uniform powders are placed together, they will pack with space in between them which varies as a function of their coordination number (Arzt, 1982). A random packing of monosized spheres is usually taken to fill 64% of the available volume, although this will be more if the powder is pressed to form a compact. When sintered, the particles will bond and the pore fraction will be reduced. The simplest way to produce a porous metal is to interrupt this process at some point before full densification has been reached, Fig. 10.2. This was one of the first approaches used to produce porous metals from powder, for example with copper in the 1960s (Goodstein *et al.*, 1966) and some of the early methods are examined by Liu and Liang (2001). Sintering of powders is used commercially to produce porous metals by Schunk Sinter Metals (http://www.sintermetalltechnik.com). With larger pores, these can be used to control air flow as filters or silencers, and with smaller pores they can form self-lubricating bearings.

In more recent work, control of the final porosity over a relatively wide range (5–37%) has been achieved in titanium (Oh *et al.*, 2003), although the limit of the packing of particles (filling 64% of space) is once again roughly respected. Porous steel has been produced in this manner (Arockiasamy *et al.*, 2010) and titanium-based alloys (including NiTi with shape memory behaviour) have also been produced using hot pressing to accelerate bonding (Lagoudas and Vandygriff, 2002; Nomura *et al.*, 2005), although this may reduce the porosity in the final sample.

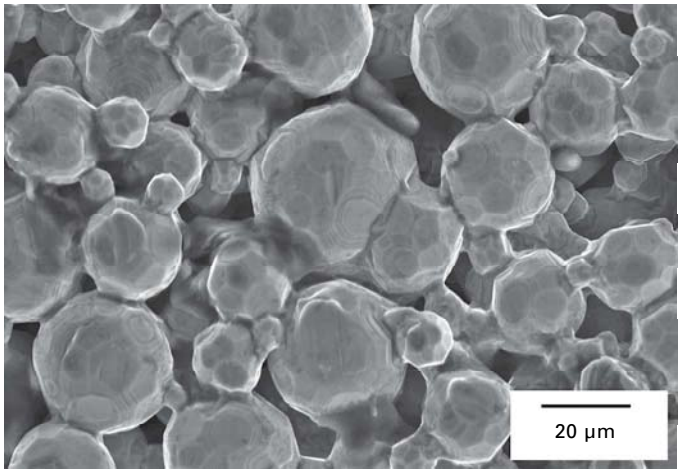

10.2 Porous titanium produced by partial sintering of gas atomised powder. Scanning Electron Microscope image courtesy of Mr Mark Taylor, the University of Sheffield.

With some metals, such as porous titanium, large particles (180–2000 µm diameter) have been used to increase the amount of porosity retained (Thieme *et al.*, 2001). As the driving force for sintering is less, liquid phase sintering was used to accelerate the formation of bonds. In this work, a more complex structure was made by combining together blocks of different structures at the green body stage, giving an overall part with a graded structure. Liquid phase sintering by niobium additions has also been used to accelerate consolidation in NiTi with NaCl space holders (Bansiddhi and Dunand, 2009).

The heat for the process need not always be provided externally. Where porous alloys or intermetallics are required (possibly to achieve a foam with a high melting point), it may be possible to produce them through reaction between different powders. These reactions can be exothermic and, because of the high surface area, have a tendency to enter positive feedback, releasing more heat and speeding up as the reaction progresses throughout the sample. This has been investigated as a specific technique, often termed self-propagating, high-temperature synthesis, SHS (Kobashi and Kanetake, 2002; Li *et al.*, 2002; Kim *et al.*, 2004; Biswas, 2005; Kanetake and Kobashi, 2006), typically used for NiTi and NiAl. Although based on a runaway reaction, meaning the process may seem difficult to control, with careful preparation and selection of the appropriate starting conditions (e.g powder size) and the inclusion of additional compounds that either enhance (e.g. B_4C) or suppress (e.g. TiC) the reaction, porous metals with controlled structures can be produced (Kobashi and Kanetake, 2002; Biswas, 2005; Kobashi *et al.*, 2006a, 2006b). It is even possible to include dense metal faceplates in the process to create sandwich panels directly (Nabavi and

Khaki, 2011). What causes the porosity to be developed in these alloys (which may be from around 10–85% (Kobashi and Kanetake, 2002)) is not fully understood, but may be due to the speed of the reaction limiting the time for porosity contained within the compact to be removed by evolution of the structure and because of the effect of hot gases generated during the process (Kanetake and Kobashi, 2006).

Even if there is no exothermic reaction, when powders of different elements or alloys are sintered together, the Kirkendall effect can act to increase porosity. The effect normally produces very fine scale porosity when the interdiffusion rates of the two metals are not equal and has been observed to occur at a sufficient level to generate a porous material with NiTi and Ni_3Al (He *et al.*, 2007; Dong *et al.*, 2009; Wen *et al.*, 2010; Liang *et al.*, 2011), but has also been used as a means of increasing porosity by adding to the pore fraction (Wang *et al.*, 1998) or by expanding a percolating network of particles (Ismail *et al.*, 2011).

Sintering of shapes other than powders has also been employed. While this includes exotic shapes such as hollow spheres, produced by coating expanded polystyrene spheres with metal powder and sintering (Nagel *et al.*, 1997; Uslu *et al.*, 1997; Lim *et al.*, 2002; Andersen *et al.*, 2000; Roy *et al.*, 2011), simpler shape changes will still show an effect. With a deviation from spherical particles, the percentage of space filled is generally reduced (Cumberland and Crawford, 1987; Yu and Standish, 1993), as these shapes do not pack as efficiently and the overall porosity of the powder compact can be increased by a substantial amount if extreme shapes such as fibres are used (Fedorchenko, 1979; Ducheyne *et al.*, 1978; Markaki *et al.*, 2003; Delannay, 2005; Clyne *et al.*, 2006; Tan *et al.*, 2006). With the lower number of particle to particle contacts in such systems, a route such as liquid phase sintering ensures good bond strength between fibres and enhances the properties of the material produced (Markaki *et al.*, 2003).

10.2.2 Space holders

Commonly, simply sintering powders does not produce materials with enough porosity, or a large enough pore size for many applications and workers in the field wish to enhance these and obtain some degree of control over the process. This is often done by including some other phase in the process, which occupies the space that will be required for the pores in the final sample. Although this can be a second phase which is in itself porous, forming what is called a *syntactic* foam (e.g. Xue and Zhao, 2011), more often it will be removed by some treatment at a later stage; this removable phase is called the *space holder*. The generic process is shown schematically in Fig. 10.3, where metal powder and space holder particles are blended, compacted and the space holder is then removed before sintering. The space

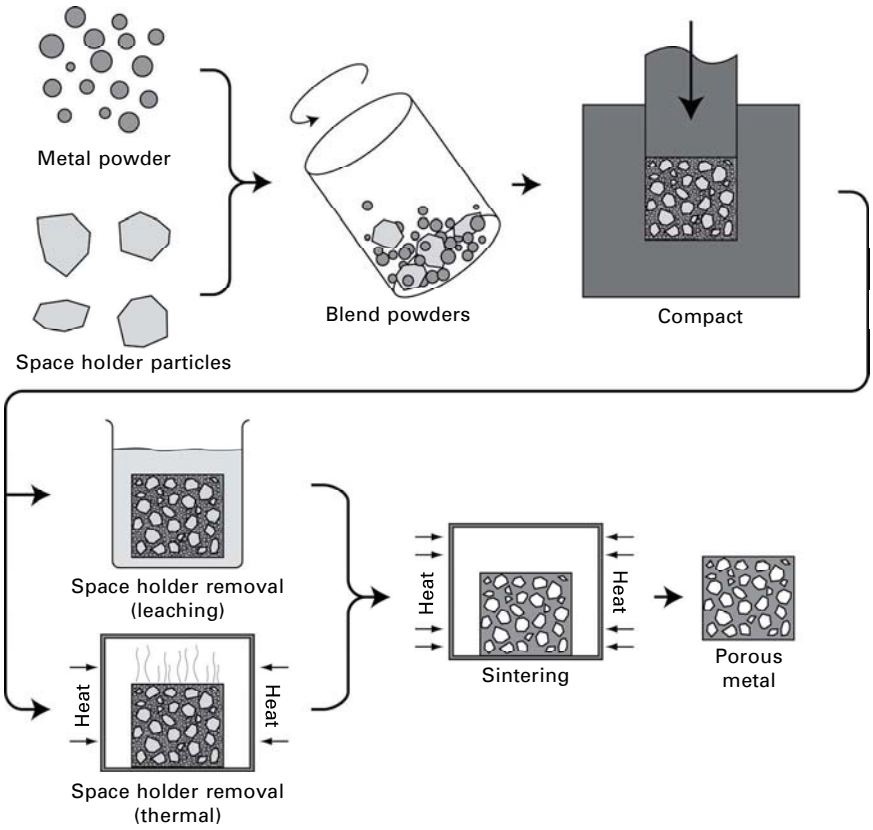

10.3 Schematic diagram of a space holder route for the production of porous metal.

holder also enhances green body strength (Laptev *et al.*, 2004, 2005), as does the degree of compaction, as would be expected. This can be sufficient that machining can be carried out on the green body, to avoid potentially challenging machining of the porous part (Laptev *et al.*, 2004).

Variants of the process have been used for all of the main metals and alloys from which foams and sponges are commonly made, including aluminium (Zhao and Sun, 2001; Wen *et al.*, 2003; Sun and Zhao, 2003; Zhao *et al.*, 2004; Jiang *et al.*, 2005b; Sun and Zhao, 2005a; Hakamada *et al.*, 2005a; Bin *et al.*, 2007), titanium (Bram *et al.*, 2000; Wen *et al.*, 2001; Rak *et al.*, 2003; Laptev *et al.*, 2004; Dunand, 2004; Rak and Walter, 2006; Esen and Bor, 2007; Ye and Dunand, 2010) and a variety of steels (Bram *et al.*, 2000; Bakan, 2006). As processes have been developed separately, different space holders tend to be preferred for different materials. For example, for aluminium foams, NaCl is frequently used, for titanium and its alloys, it may also be NaCl (where the metal is sintered with the space holder in the solid

state (Ye and Dunand, 2010)), carbamide (essentially urea pellets, used as fertilizer) (Tuncer *et al.*, 2011), magnesium particles (Esen and Bor, 2007, 2011) or a polymer binder phase.

Sintering–dissolution process

One of the first space holder methods developed to a significant extent (sometimes termed the sintering–dissolution process, SDP) used aluminium and NaCl (Zhao and Sun, 2001). Powders were blended together and compacted and the compact sintered below both the melting point of aluminium (660°C) and salt (801°C). To increase the rate, the temperature can be taken 10–20°C above the melting point of aluminium; at temperatures higher than this, the aluminium will begin to be excluded from the compact, as liquid aluminium does not wet salt (Zhao *et al.*, 2004). Finally, the space holder NaCl phase can be removed by leaching in water, leading to the formation of a foam of the type seen in Fig. 10.1. The removal of salt is normally successful, although for porosities below 60% some residual space holder may remain (Zhao and Sun, 2001), which is in agreement with models developed for dissolution from a multi-phase compact (Zhao, 2003). Addition of magnesium (Sun and Zhao, 2003, 2005a) may be made as a sintering aid, acting to reduce the oxide layer, although it has sometimes been found to be less effective than a combined addition of magnesium and tin (Zhao *et al.*, 2004). Where they work, these additions are helpful, as the pressure that can be applied without damaging the space holder particles (which are usually more fragile than the metals being sintered) prevents there being as high green densities as would be recommended with dense components in powder metallurgy (Zhao *et al.*, 2004). The SDP for aluminium is highly developed, with simulations of the compact being used to predict the spatial distribution of heat over time, the sintering time required (Sun and Zhao, 2005b) and modelling of the dissolution behaviour of a leachable space holder material being performed (Zhao, 2003; Sun and Zhao, 2005b).

Some workers have substituted a spark plasma sintering (SPS) step for conventional sintering in the NaCl space holder method (Wen *et al.*, 2003; Hakamada *et al.*, 2005a), including for NiTi (Fu *et al.*, 2006), where very fine grained metal powders (50 nm) were used. This produces a particularly fine grain sized microstructure, as the shortened processing time and time at elevated temperature experienced by the material means that grain growth cannot occur (Wen *et al.*, 2003). To further increase the porosity, SPS has been used with polymer spheres coated with a nickel alloy (Song and Kishimoto, 2006), although as the foams are closed celled (Hakamada *et al.*, 2005b), the polymer or its remnants can be trapped inside.

Sintering with other space holders

NaCl is by no means the only space holder used. Carbamide (urea) and ammonium hydrogen carbonate are frequently employed. These are not removed by dissolution as NaCl is, but can be removed by treatments at high temperature (either before sintering, or as an initial step in the sintering heat treatment). Methods using these space holders were developed at around the same time as the SDP, principally for producing higher melting point metals with porosity. The same procedures of blending (often using a solvent) and pressing powders, substituting ammonium hydrogen carbonate and carbamide for NaCl, have been used for titanium and magnesium foams (Bram *et al.*, 2000; Wen *et al.*, 2001, 2002a, 2002b, 2004; Zhuang *et al.*, 2008; Niu *et al.*, 2009; Nouri *et al.*, 2010; Tuncer *et al.*, 2011), superalloys (Bram *et al.*, 2000; Mi *et al.*, 2009), stainless steel (Gulsoy and German, 2008) and copper foams (Hakamada *et al.*, 2007), and examples have also been reported of polypropylene carbonate (PPC) (Hong *et al.*, 2008) and starch being used for titanium (Mansourighasri *et al.*, 2012). All of these are removed by a thermal treatment before sintering, which is effective in retaining the porous shape, even though they decompose at relatively low temperatures (around 200°C).

Carbamide is also a popular space holder for aluminium (Jiang *et al.*, 2005a) and has been used for stainless steels, not being removed thermally, but by water leaching (Bakan, 2006). Carbamide particles are available in different shapes, as either rough spheres or high aspect ratio flakes. The use of different forms of carbamide allows the pore shape to be controlled as this shape is preserved in the porous material (Bram *et al.*, 2000; Jiang *et al.*, 2005b).

Another important space holder is potassium carbonate, K_2CO_3 (Zhao *et al.*, 2005) and its use is sometimes called the lost carbonate process. This has the advantage that it is thermally decomposed, so an additional leaching treatment is not required. It also is not removed until high temperatures (891°C, when it melts and decomposes simultaneously (Zhao *et al.*, 2005)), meaning that it can contribute to structural integrity up to high temperatures. This has been used for higher melting point metals, such as copper (Zhao *et al.*, 2005; Thewsey and Zhao, 2008; El-Hadek and Kaytbay, 2008) and iron (Ma *et al.*, 2006).

Porous intermetallics and alloys

There is an interest in porous alloys and intermetallic materials for a range of applications, including high temperature use. Shape memory alloys of NiTi have been made by blending and cold pressing elemental powders on their own (Yuan *et al.*, 2004), or with NaCl (Zhao *et al.*, 2009), followed

by sintering where reaction between them takes place. The process has also been applied to a ferritic stainless steel containing Cr and Mo, using NaCl space holders (Scott and Dunand, 2010). With just elemental powders used, the pore size tends to be small (a few hundred micrometers) and the porosity low (around 30–40%); although these may be controlled by the use of a hot isostatic pressing (HIP) treatment (Yuan *et al.*, 2008). The inclusion of space holders permits high porosities, with a bimodal pore size distribution, where the larger pores are introduced by the salt particles, the smaller by the Kirkendall effect or residual porosity from the powder compact.

NiTi has also been processed from prealloyed powder, using NaCl (Bansiddhi and Dunand, 2008, 2009) or NaF as a space holder (Bansiddhi and Dunand, 2007). In both cases HIP was used to cause densification, although the high temperatures used necessitate either the use of a high melting point space holder (such as NaF, which is removed by a treatment in water of several weeks' duration (Bansiddhi and Dunand, 2007)) or by carrying out the process rapidly so that the space holder does not melt (as is done with NaCl (Bansiddhi and Dunand, 2008)). The advantages of the latter process stem mainly from the more easily obtained and handled space holder and improved process speed, and the reduced corrosion, cost and toxicity risks that result. The same process has been used with NaCl for another shape memory CuAlMn alloy (Gong *et al.*, 2011a, 2011b). As this is processed at high temperature (930°C), the salt does not have to be dissolved before the process is begun, as it will evaporate during the sintering process.

Metal injection moulding with space holders

Polymer particles have been used as space holders (Li and Lu, 2011) and organic binders may also be used to hold the powder in a specific shape to help with processing a specific component; this can play a dual role in preserving free space until a later stage of sintering (Rak and Walter, 2006). With this method, it is not possible to control pore size and shape externally, as the space holder has no rigid shape of its own, but this limitation is balanced by the advantage of not having to add a specific space holder phase, as the organic binder can be used to generate parts with complex shape (allowing net shaping or near net shaping of components) by methods like metal injection moulding (MIM).

Metal injection moulding (MIM) is another technique for forming powders into a shape for sintering and can often result in residual porosity (e.g. Guo *et al.*, 2009), suggesting that it may be exploited for porous metal production. The process can be used with elemental powders to produce a complex shape, which can then be processed further by a procedure such as SHS (Guoxin *et al.*, 2008), or sintered to allow reaction (Köhl *et al.*, 2009; Ismail *et al.*, 2011). MIM can also be used with elemental or pre-

alloyed powders (Bram *et al.*, 2011), using partial sintering to produce a porous material, or by including a space holder material in the mix (Köhl *et al.*, 2011). Examples have been demonstrated for Ti-6Al-4V with small (<50 μm) poly(methylmethacrylate) (PMMA) particles as space holders (Engin *et al.*, 2011), where the small size of the space holders avoid difficulties with material flow during injection, and for 316L stainless steel with slightly larger PMMA particles (around 75 μm) (Manonukul *et al.*, 2010). The advantage of PMMA is that it breaks down thermally and is easily removed without leaving a residue that could contaminate the metal parts or impair sintering, although the small pore size and early removal of PMMA in the sintering process mean that the pore fractions obtained are low. Alternatively, NaCl can be used as the space holder for titanium (Chen *et al.*, 2009; Bram *et al.*, 2011) and NiTi production (Köhl *et al.*, 2009; Bram *et al.*, 2011), which has been demonstrated for pore sizes of around 300–400 μm. This space holder material is removed by dissolution in water before heat treatment, which means that no specific treatments during the sintering are required and that the pores are all open.

Freeze casting

A different route from adding preformed space holders to a powder mix, or using a space holder that has no rigid shape, is to form space holder particles *in situ*. The freeze casting process, originally developed for ceramic powders, has been applied to titanium powder (Chino and Dunand, 2008; Fife *et al.*, 2009; Li and Dunand, 2011) and recently stainless steel (Driscoll *et al.*, 2011). In the process, a slurry is formed of water with powder in suspension (Chino and Dunand, 2008) and this is frozen in a directional manner. As the ice crystals form, they displace the powder particles, forming a space holder phase *in situ*, concentrating the powder particles in certain regions and removing liquid from around the particles. The powder is therefore brought into close contact, so that weak bonds may form. In the next stage, the space holder is removed by sublimation, leaving pores in the structure of powder particles, which a short sintering step can give the required cohesive strength. Due to directional solidification the ice crystals tend to become aligned along the direction of heat extraction and the pores are highly anisotropic (Chino and Dunand, 2008).

As the freezing is directional (and ice crystals tend to be highly planar (Fife *et al.*, 2009)) and the microstructure therefore not uniform, porous materials processed in this way can have highly anisotropic properties (Driscoll *et al.*, 2011). It is not usually possible to obtain metal powder particles as small as the ceramic powders used in freeze casting (which are often submicrometre in size), but the processing is improved by having the smallest particles possible (as they are more easily moved by the ice crystals

as they form (Chino and Dunand, 2008)), as is the final material (as smaller particles sinter more rapidly, forming stronger bonds) (Fife *et al.*, 2009).

Template methods

Other methods use a polymer foam as a template to define the porosity (in a sense, the polymer foam holds the space, although this is not done solely by occupying it as with other space holders). A different method that has been used for very low density nickel and stainless steel foams is by placing the powder particles in a slurry rather than a binder and coating an open cell carbon foam (which is itself formed from a polyurethane foam) (Queheillalt *et al.*, 2004). In this method the carbon foam is retained at the core of the struts in the foam. Titanium alloy (Ti-6Al-4V) has also been produced in foam form by using a polyurethane template dipped in slurry containing metal powder and a polymer binder, with the sintering step for the powder also removing the polymeric binder and foam (Li *et al.*, 2005). Perhaps more ambitious is the combination of the formation of the foam scaffold and inclusion of the metal powder in one process: the dispersal of large quantities of metal powder (titanium, iron and copper have been used) in one of the components of a foamable polymer system, such as polyurethane, the processing of the polymer, causing it to foam, and the subsequent heat treatment to remove the polymer and sinter the metal sufficiently to provide cohesive strength (Jee *et al.*, 2000; Guo *et al.*, 2000; Xie and Evans, 2004). Although the polymer foam is closed celled, the metal foams produced will be open celled (Jee *et al.*, 2000), with high fractions of porosity, typically over 90% (Jee *et al.*, 2000; Guo *et al.*, 2000). A related process uses a slurry of metal powder containing phosphoric acid (Angel *et al.*, 2005). The reaction between the powder and the acid liberates hydrogen, which foams the slurry forming a green body which can be sintered.

10.3 Powder processing: gas entrapment and additive layer manufacturing

10.3.1 Gas entrapment

To attempt to access different pore structures, workers have sought to use gas pressure to provide additional expansion of bodies formed from powder. This has some limitations, as for the effect of the gas pressure to be felt, the temperature needs to be high and the material needs to be in a highly deformable state (Kearns *et al.*, 1988) – in some cases, metals with superplastic properties have been employed (Dunand and Teisen, 1998) – making titanium a particularly suitable metal, although other materials,

notably NiTi with superelastic properties, have been produced (Oppenheimer *et al.*, 2004; Greiner *et al.*, 2005). Also, the effect of the gas will only be felt while the pores remain closed. As pores start to intersect each other and joining therefore becomes more likely at porosities between 50 and 64%, the upper limit of the porosity that is achieved by these methods tends to be around this point.

The most common version of the method sees a powder being compacted under an inert gas environment, such as argon, so that quantities of this gas become entrapped within the compact (Schwartz *et al.*, 1998). A similar goal may be achieved by cryogenic milling of the powder in the presence of argon (VanLeeuwen *et al.*, 2011), which results in very fine scale porosity. The compact is then sintered under vacuum, which causes the metal particles to bond, but at the same time expands the pores owing to the pressure of the trapped gas (Schwartz *et al.*, 1998; Dunand and Teisen, 1998; Davis *et al.*, 2001; Murray and Dunand, 2003, 2004; Murray *et al.*, 2003; Oppenheimer *et al.*, 2004; Greiner *et al.*, 2005). Figure 10.4 shows a schematic diagram of the process. Control of the process can control the foam produced. Applying a uniaxial stress during expansion can constrain the foam and cause the

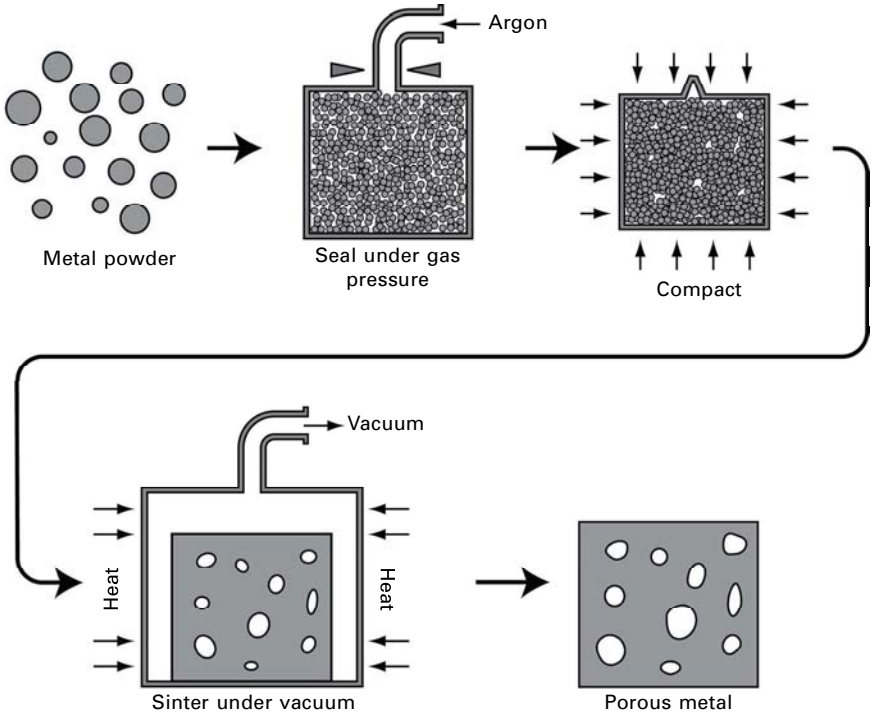

10.4 Schematic diagram of the gas entrapment process for porous metal creation.

pores to become aligned (Davis *et al.*, 2001), while repeated heating and cooling cycles can result in the membranes between the cells rupturing and the foam becoming much more open (Murray and Dunand, 2003). Workers have attempted to increase the porosity by including chemical agents that break down at high temperature to release gas, for example TiH_2 (Ricceri and Matteazzi, 2003) although success has been limited, at least in part by the high solubility in metal of the hydrogen gas released.

10.3.2 Additive layer manufacturing-based techniques

With current demands for efficiency in material and energy usage, new manufacturing techniques such as additive layer manufacturing (ALM) processes (also known as powder bed methods) are the subject of great current research interest. In this chapter it will not be attempted to give a full account of all these methods, but rather to focus on their use to produce porous metals.

For the majority of the materials discussed in the previous sections, the porosity contained within them is random in nature, being in pores of unpredictable size, shape and location (even if we can define global measures to characterise some of these properties, see earlier). The materials that can be made through ALM processes are very different in nature. The essential principle of the process translates a 3D image held in a computer into a metallic part, with very low levels of wastage or final machining required. This is carried out in specialised equipment, such as the systems sold commercially by Arcam AB (http://www.arcam.com/), EOS Electro Optical Systems (http://www.eos.info/en/home.html), Renishaw (http://www.renishaw.com) and others.

The processes have arisen from rapid prototyping, where a computer-aided design (CAD) model is created and formed into a solid part by adding layers (hence *additive layer manufacturing*, ALM). These methods were first applied to polymers, although some were adapted to produce metal parts; for example, 3D printing has been used to deposit shapes made from a slurry containing Ti-6Al-4V powder (Li *et al.*, 2006). This succeeded in making simple structures, with a minimum spatial resolution of around 500 μm.

Currently these rapid net shape manufacturing techniques are also available for metals. In one version, laser direct metal deposition (LDMD), metal powder is fed into a laser beam, which causes it to melt and be deposited on a substrate. By moving the powder injection and laser beam around the substrate, a 3D shape can be built up. Porous lattices have been achieved in Ti-6Al-4V and 316L stainless steel (Ahsan *et al.*, 2011), although the limited overhangs possible probably mean that the porosity will be limited to relatively low levels. A more widely used system for porous parts is shown schematically in Fig. 10.5. This uses a deposited layer of metal powder

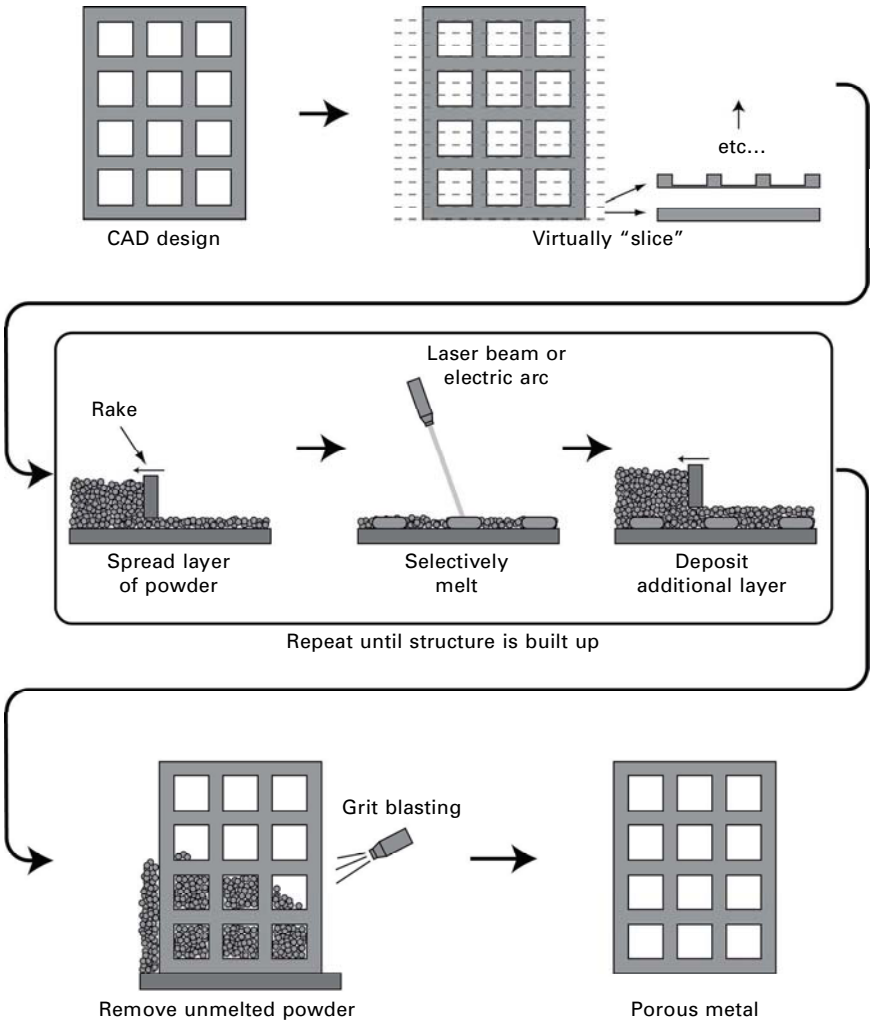

10.5 Schematic diagram representing the production of a metallic lattice using an ALM method.

(typically spherical particles are preferred owing to improved flowability). Once the layer has been spread across a build surface, a focussed heat source, such as a laser or electron beam is used to melt powder selectively in areas where the CAD model requires solid. In other areas it is left unheated. After treatment, another layer is deposited and the process is repeated until a 3D shape, encased and permeated by unmelted powder, is obtained. To produce a porous shape, this unmelted powder will have to be removed by grit blasting, for example. The powder can be recycled back into the process.

Systems where the metal powder is melted by an electron beam (often termed electron beam melting, EBM) have most commonly been used to make metallic lattices, often using titanium or Ti-6Al-4V, as these high value materials are common choices for the near net shaping offered by the machine. The most common choice of structure is a simple cubic lattice, or a lattice following the bond structure in diamond (Heinl *et al.*, 2007, 2008b; Cansizoglu *et al.*, 2008; Murr *et al.*, 2010a, 2010b; Li *et al.*, 2012). However, much more complex designs are possible, including lattices with re-entrant struts that are able to show negative Poissons ratios (auxetic behaviour) (Schwerdtfeger *et al.*, 2010). Porous shapes have also been made in a similar technique using a laser (selective laser melting, SLM), both in regular cubic-based lattices and structures replicating those of cancellous bone (Pattanayak *et al.*, 2011).

The main advantage of techniques like EBM is the great flexibility in the structures that can be produced, offering the possibility of having highly tailored structures. As well as regular lattices, random structures replicating regular foams (using tomography images of other foam types as the input) have been made (Murr *et al.*, 2010b, 2011; Ramirez *et al.*, 2011). The flexibility is such that the struts can be made both dense and hollow (Murr *et al.*, 2010b).

The nature of the processing will affect the material produced. The angle of struts relative to the build direction (the normal to the plane of the layers) can have an effect on the properties displayed by the lattice (Cansizoglu *et al.*, 2008) and the amount of energy input will affect the strut thickness and hence density (Heinl *et al.*, 2008a). In mechanical tests on the lattices it has been found that they have a relatively low fatigue resistance, partly due to the structure (as porous metals have low fatigue resistance generally and also because the microstructural condition of the Ti-6Al-4V used was not optimal for fatigue resistance (Li *et al.*, 2012)).

Because of interest from biomedical applications, lattices have also been produced from Co–Cr alloys (Murr *et al.*, 2011) and from copper for applications that require thermal or electrical flow (Ramirez *et al.*, 2011). For biomedical use the material condition should be suitable, as the alloys are well known and many researchers are looking at implantable parts made using such techniques (vanNoort, 2012), but the conductivity may be limited, as oxides, formed during the processing, were found throughout the copper lattices produced (Ramirez *et al.*, 2011).

10.4 Properties of porous metals

In the broadest sense, the properties displayed by a porous material will follow the same trends as seen in composites, with the properties of the whole being a blend of the properties of the individual constituents. An important

simplification can be made in that one of the limits is the properties of free space, which for most properties can be taken as zero.

10.4.1 Mechanical properties

Data reported in the literature for the Young's modulus and compressive strength (the most common properties measured) of porous metals processed from powder are summarised in Table 10.2 and the variation in relative Young's modulus (the Young's modulus of the foam divided by that of the metal from which it is made) with porosity is shown in Fig. 10.6 for different processing techniques and metals. It is clearly seen that there is a fall off in both of these properties as the porosity increases, with a very wide spread in the properties displayed. This is quite usual for foams (see the results summarised in Ashby *et al.* (2000), for example), owing to the random nature of the structure and the potentially severe effect of defects. With sintered powders, the potential for defects is even larger, enhancing the spread.

Although in foams generally the pore size does not affect the mechanical response (with some exceptions where the surface plays a significant role (Diologent *et al.*, 2009)), there is some evidence that larger pore size foams processed by powders have improved mechanical properties (Bin *et al.*, 2007), which was attributed to a change in the aspect ratio of the walls, although it is not clear why this may arise. In similar tests the same effect was found and in X-ray tomography investigations it was found that a larger pore size gives rise to larger struts (Tuncer *et al.*, 2011), although intriguingly, the consolidation within them is reduced, with more pore wall porosity, smaller interconnection size and a lower strut density. Nevertheless it appears that the strut size is the dominant effect.

Metal foams are often highlighted for applications where their energy absorbing qualities may be employed. Care needs to be taken with experimental investigations, as it has been found that the energy absorbed in a dynamic mode of loading for aluminium foams is less than that absorbed in static tests (Sun and Zhao, 2003). Observations on similar materials show that the plateau stress is increased at higher strain rates (Hakamada *et al.*, 2005a) and so the reduced energy absorption must be due to densification occurring at a lower strain. In NiTi by contrast, it has been found that the Young's modulus is higher in dynamic testing than in quasistatic testing, attributed to the superplastic behaviour of the base metal in this case (Greiner *et al.*, 2005). It has been found that NiTi has good energy absorbing and damping characteristics, attributed to the hysteresis behaviour of the dense metal (Köhl *et al.*, 2011). This has been employed to make dense materials for energy absorption, by infiltrating a porous NiTi network with magnesium (Li *et al.*, 2010). Investigation of the behaviour and mechanisms operating

Table 10.2 Literature data for the mechanical properties of porous metals processed from powders

Processing method	Metal	Pore size (μm)	Pore fraction	E (GPa)	σ_y (MPa)	Ref.
Partial sintering	Ti		0.04–0.36	7.8–88.8	–	(Oh *et al.*, 2003)
		200–1000	0.24–0.57	14.1–57.7	–	(Thieme *et al.*, 2001)
Self-propagating High-temperature Synthesis	NiTi	100–280	0.6	0.12–0.2	–	(Kim *et al.*, 2004)
Space holder	Ti	200–500	0.78	5.3	–	(Wen *et al.*, 2001)
		525	0.45–0.7	0.42–8.8	15–116	(Esen and Bor, 2007)
		100–500	0.45–0.52	1.7–2.8	99–132	(Hong *et al.*, 2008)
		200–500	0.8	2.9	–	(Wen *et al.*, 2002a)
		200–500	0.35–0.8	2.9–10.3	25–478	(Wen *et al.*, 2002b)
		100–300	0.64–0.79	1.9–3.7	–	(Mansourighasri *et al.*, 2012)
		355–500	0.42–0.51	23–39	–	(Ye and Dunand, 2010)
		50–300	0.42–0.72	0.28–3.03	17.5–316	(Chen *et al.*, 2009)
		140–1800	0.64	3.8–6.1	45–87	(Tuncer *et al.*, 2011)
	Al		0.51	–	2.8	(Jiang *et al.*, 2005a)
	Mg	200–500	0.5	0.35	–	(Wen *et al.*, 2001)
		70–400	0.35–0.55	0.7–1.8	11–17	(Wen *et al.*, 2004)
		200–400	0.36–0.43	3.6–18.1	15–31	(Zhuang *et al.*, 2008)
	Cu	300–425	0.02–0.78	1.26–14.5	3.5–258	(Hakamada *et al.*, 2007)
		120–500	0.5–0.85	8.1–33.7	–	(El-Hadek and Kaytbay, 2008)
	Stainless Steel 316L	750–1000	0.7	0.27–1.4	–	(Bakan, 2006)
	Stainless Steel	750–1000	0.4–0.6	46–55	832–1211	(Gulsoy and German, 2008)
MIM with space holders	Ti	10–41	0.27–0.56	0.8–2.2	653–1244	(Engin *et al.*, 2011)
		400	0.51	22.5	140	(Bram *et al.*, 2011)
Trapped gas expansion	Ti	200	0.22–0.41	39–60	120–200	(Davis *et al.*, 2001)
Powder on foam template	Ni alloy	8000	0.89–0.93	0.77–1.87	1.3–3.5	(Queheillalt *et al.*, 2004)
	Ti-6Al-4V	400–700	0.9	0.8	10.3	(Li *et al.*, 2005)

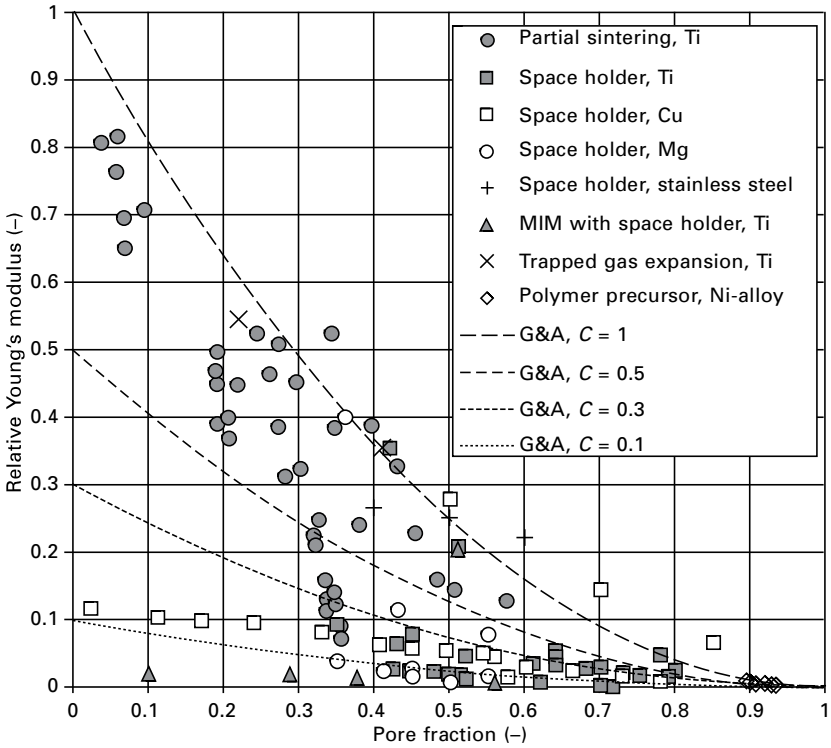

10.6 Literature data for the relative Young's modulus (E_{foam}/E_{metal}) of various porous metals produced from powder, plotted against pore fraction. Data for partial sintering with Ti are from Thieme *et al.* (2001) and Oh *et al.* (2003), for space holder with Ti from Wen *et al.* (2001, 2002a, 2002b), Esen and Bor (2007), Hong *et al.* (2008), Chen *et al.* (2009), Ye and Dunand (2010), Tuncer *et al.* (2011) and Mansourighasri *et al.* (2012), for space holder with Cu from Hakamada *et al.* (2007) and El-Hadek and Kaytbay (2008), for space holder with Mg from Wen *et al.* (2004) and Zhuang *et al.* (2008), for space holder with stainless steel from Bakan (2006) and Gulsoy and German (2008) for MIM with space holder from Engin *et al.* (2011) and Bram *et al.* (2011), for trapped gas expansion from Davis *et al.* (2001) and for polymer precursor from Queheillalt *et al.* (2004). Note that a wide variety of pore sizes are represented by the data. Also shown are the predictions of the Gibson–Ashby (G&A) model (Table 10.4) for open celled foams, with various values of the constant, *C*.

at different temperatures has shown that the trends in behaviour of the dense metal are conserved (Hakamada *et al.*, 2005a; Scott and Dunand, 2010). Foams processed from powders have also been investigated for creep (Scott and Dunand, 2010), which can be related to the dense metal properties by relatively accessible models (e.g. Hodge and Dunand, 2003; Mueller *et al.*, 2007).

10.4.2 Conduction properties

At temperatures within a few hundred degrees of ambient conditions, heat transport by radiation is low and at cell sizes below 4 mm, convection in the gas phase can be ignored (Skochdopole, 1961), leaving conduction through the solid phase the only significant mechanism of thermal transport. This being the case, parallels can be drawn between electrical and thermal conductivity and the same trends are observed. For most situations in most porous metals, the two properties can be assimilated into one although for some powder processed porous metals a difference has been found, attributed to defects in the structure (Thewsey and Zhao, 2008). For engineering use this is fortunate, as there have been relatively few measurements of either type of conductivity in powder processed metal foams. Some examples, in fact reporting values of electrical conductivity, are given in Table 10.3 and the variation in relative conductivity with porosity is shown in the graph in Fig. 10.7. As with mechanical behaviour, the trend is for the conductivity of a foam to be decreased as the porosity increases, with this reduction more rapid with the initial appearance of pores. Thermal conductivity follows similar trends and data for copper foams with different pore size and density have been reported (Thewsey and Zhao, 2008).

It has been found that the electrical conductivity of porous titanium processed by a space holder method decreases as pore size is reduced. This is, however, traced to differences in the pore shape (the aspect ratio) introduced when the pores are compacted in a uniaxial pressing step (Li and Lu, 2011). Differences in electrical conductivity with pore size have also been observed in copper and iron (Ma *et al.*, 2006). The conductivity is also higher for larger pores, which is suggested to be because of better bonding being achieved in the cell walls, which also have larger dimensions. This is, however, contrary to X-ray tomography results obtained on other types

Table 10.3 Literature data for the conduction properties of porous metals processed from powders. Where multiple data points are given, the minimum and maximum values are quoted in the table

Processing method	Metal	Pore size (μm)	Pore fraction	Conductivity (S m^{-1}) × 10^6	Ref.
	Cu	250–>1000	0.7–0.85	0.26–6.26	(Ma *et al.*, 2006)
		120–500	0.5–0.85	0.13–0.31	(El-Hadek and Kaytbay, 2008)
Space holder	Ti	150–400	0.1–0.67	0.33–1.41	(Li and Lu, 2011)
		136–403	0.31–0.64	0.13–0.69	(Li and Zhu, 2005)
	Fe	425–1500	0.68–0.76	0.95–1.45	(Ma *et al.*, 2006)
	Al	452–>2000	0.63–0.83	0.62–4.26	(Ma *et al.*, 2005)

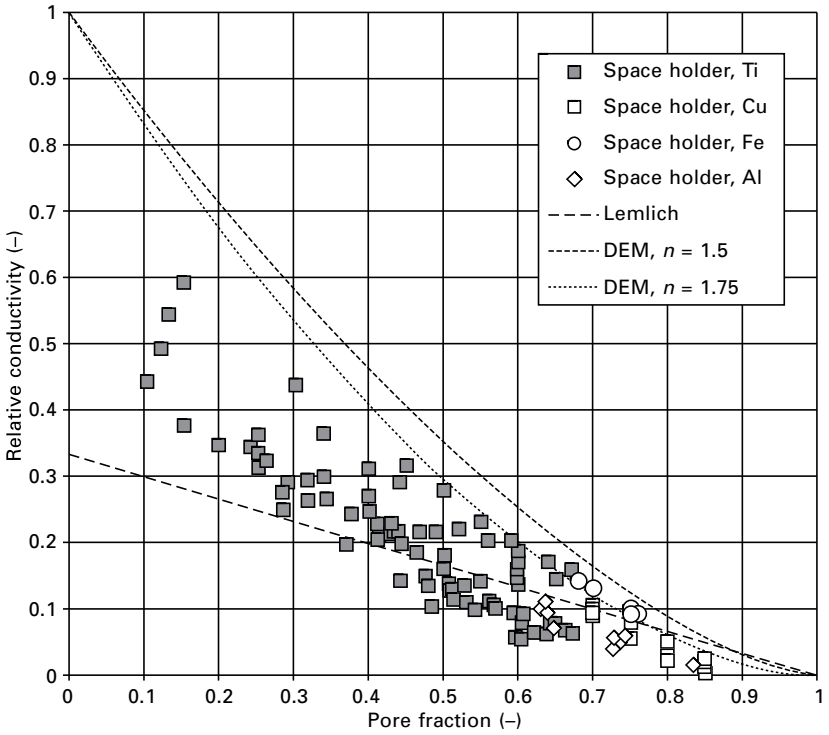

10.7 Literature data for the relative conductivity (S_{foam}/S_{metal}) of various porous metals produced from powder, with porosity. Data for space holder with Ti are from Li and Zhu (2005) and Li and Lu (2011), for Cu and Fe from Ma *et al.* (2006) and for Al from Ma *et al.* (2005). Also shown are the predictions of equations [10.1] and [10.2], the Lemlich and DEM models.

of porous metal processed from powder, where better consolidation is seen with smaller pores and higher pore densities, although larger struts are also produced, which appears to be the dominant effect for mechanical properties (Tuncer *et al.*, 2011).

In general, the conductivity of foams processed by powder methods is below that of other foams, as shown in Fig. 10.7. This is likely to be due to a greater content of impurities, such as entrained oxides, originating from the powder surfaces (Goodall *et al.*, 2006), a conclusion which is reinforced in the work of Li *et al.* (Li and Lu, 2011), who found the conductivity of dense commercial purity titanium processed by the same method as the porous metal in their work was 1.7×10^6 S m^{-1}, where the reference value for (commercial purity) CP Ti is 2.38×10^6 S m^{-1} (Lide, 2001), representing a relative conductivity of a little over 70% when the dense material is produced by that particular powder route.

10.4.3 Biological properties

Foams made from titanium, magnesium and NiTi are often suggested for use as biomaterial implants even if no biological testing is performed (Thieme *et al.*, 2001; Wen *et al.*, 2002a; Oh *et al.*, 2003; Dunand, 2004; Nomura *et al.*, 2005; Nouri *et al.*, 2010) and sufficiently high purities for use in the body have been achieved (Laptev *et al.*, 2004; Hong *et al.*, 2008). This is largely as the dense versions of these metals are currently used, or are leading candidates for actual implants, and the bioinertness is known.

Titanium foams have been pretreated to create a surface suitable for implants (Wen *et al.*, 2002b). Porous titanium has been exposed to simulated body fluid after surface treatments to provide a desirable surface for cell attachment (Hong *et al.*, 2008). While this gave a fine porous texture to the surface of the foam, which should perform well, no cell tests have yet been reported. Highly porous (90%) Ti-6Al-4V alloy has been subjected to cell culture tests, by seeding MC3T3-E1 osteoblast-like cells on samples of foam in cell culture media, with culture times of up to 3 days (Li *et al.*, 2005). It was found that cells attached to the material surface and spread and that there was evidence of extracellular matrix production.

Magnesium can degrade in the body environment, producing compounds that can be excreted through biological processes and is therefore attractive for degradable implants. In tests in a saline solution representing the body environment, breakdown of porous magnesium has been observed with, as expected, the dissolution rate being increased by increasing the porosity (Zhuang *et al.*, 2008).

Porous NiTi is particularly attractive for implants into bone, owing to the similarities in the stress–strain curve possible between the two materials (like bone, NiTi can display hysteresis within the superelastic region) (Bansiddhi *et al.*, 2008). Foams of NiTi have been produced and implanted into animal models (rabbits) (Kim *et al.*, 2004). In these tests, no inflammation was observed and after six weeks bone ingrowth occurred in all specimens examined. However, in the absence of a control test on other porous materials it is difficult to say how this behaviour ranks with other types. As more candidate porous biomaterials are produced from metal powders, a more comprehensive testing programme will be required.

10.5 Prediction of porous metal properties

10.5.1 Models for mechanical behaviour

The mechanical properties of foams are successfully modelled in many cases by simple relationships derived by considering a regular cubic structure (Fig. 10.8) which deforms by beam bending (Gibson and Ashby, 1997). Some of the simple predictions of this approach are given in Table 10.4, further

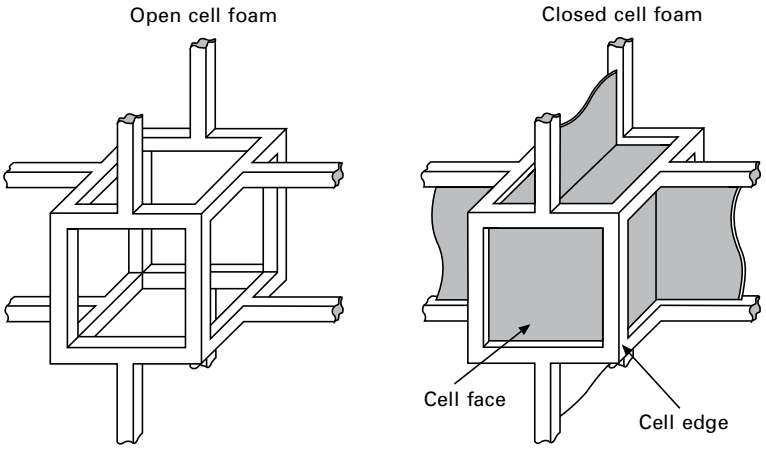

10.8 Regular structures considered by Gibson and Ashby (1997) in deriving their expressions for the properties of foams.

Table 10.4 Expressions for some foam properties derived by Gibson and Ashby (1997). In the table, ρ represents the density, *C* terms are constants and ϕ is the proportion of the solid in the cell edges as opposed to the faces, with other terms as defined in the table. The superscript * indicates that the property refers to the foam, the subscript s indicates that it refers to the dense metal

Mechanism	Open cell foam	Closed cell foam
Young's modulus, E	$\frac{E^*}{E_s} = C_1\left(\frac{\rho^*}{\rho_s}\right)^2$	$\frac{E^*}{E_s} = C_1\phi^2\left(\frac{\rho^*}{\rho_s}\right)^2 + C_1(1-\phi)\frac{\rho^*}{\rho_s}$
Yield strength, σ_y (compression)	$\frac{\sigma_y^*}{\sigma_{ys}} = C_2\left(\frac{\rho^*}{\rho_s}\right)^{3/2}$	$\frac{\sigma_y^*}{\sigma_{ys}} = C_2\left(\phi\frac{\rho^*}{\rho_s}\right)^{3/2} + C_2(1-\phi)\frac{\rho^*}{\rho_s}$
Fracture strength, σ_f (compression)	$\frac{\sigma_f^*}{\sigma_{fs}} = C_3\left(\frac{\rho^*}{\rho_s}\right)^{3/2}$	$\frac{\sigma_f^*}{\sigma_{fs}} = C_3\left(\phi\frac{\rho^*}{\rho_s}\right)^{3/2} + C_3(1-\phi)\frac{\rho^*}{\rho_s}$

results can be found in Gibson and Ashby (1997). The predictions of the equation for Young's modulus of open cell foams are shown compared to the data in Fig. 10.6.

The Gibson – Ashby model has frequently been used to understand the mechanical response of foams processed from metal powders, for example by Davis *et al.* (2001), Wen *et al.* (2002a), Hakamada *et al.* (2005, 2007) Jiang *et al.* (2005a), Esen and Bor (2007), Chino and Dunand (2008), Niu *et al.* (2009) and Bram *et al.* (2011). However, it does have certain limitations. While it broadly captures the trends, the constants in the equation vary with the precise foam structure and material, and hence have to be measured

for each set of experiments, acting like a fitting parameter. For example, many metal foams show mechanical properties that are below the simple Gibson–Ashby predictions (with $C = 1$) and require this constant to be reduced (sometimes this is called the 'knock-down' factor and frequently has a value around 0.3–0.5 (San-Marchi and Mortensen, 2001; Despois *et al.*, 2006)). The reason for this knock down is sometimes attributed to defects and attempts have been made to model their effects (Kepets *et al.*, 2007). For Fig. 10.6, it is clearly seen that some of the porous metals processed from powder, notably the partially sintered powders, follow the model with $C = 1$ reasonably well. Others, particularly some of the space holder examples, require the constant to be nearer 0.3 for a good match.

To go beyond the Gibson–Ashby approach, some workers have used models that may be more specific, but capture the behaviour of a particular foam type more precisely. Other relatively simple analytical models, based on Gibson–Ashby or similar approaches, have been used with some success in situations where they can capture the mechanisms operating in the microstructure (e.g. Li and Dunand, 2011). For sintered fibres, models have been developed for both the thermal behaviour and the stiffness (Clyne *et al.*, 2006), taking the bending of the fibre segment between bonds and accounting for the statistical distribution of these elements at different angles throughout the material. In sintered powders, calculations are sometimes made using the smallest amount of solid cross sectional area normal to the direction of the applied load; this will typically be the necks between the particles (Esen and Bor, 2011). Equations developed using this approach are called minimum surface area models and can work well when the density is high and there are no long ligaments of material that will deform by bending or twisting; this type of behaviour would be better captured by the Gibson–Ashby approach.

Other models have been examined and found to work in specific situations, including Eshelby's theory for isolated inclusions in a matrix (Greiner *et al.*, 2005), which evidently can be applied when the volume fraction porosity is low (around 20% in this case). Others have applied Mori–Tanaka models for the elastic properties of materials containing inclusions (El-Hadek and Kaytbay, 2008) with good correlations, and an extended version of these models indicates that a small amount of microporosity (> 5%), which is frequently present in samples produced from powder, reduces the anisotropy in properties seen when the pores are not uniform in shape and are aligned (as can also happen in materials produced from powders with space holders when a uniaxial pressing step is used) (Gong *et al.*, 2011b).

Another approach that has been shown to work well with foams processed from molten metal in various ways is the use of continuum mechanics approaches developed for composites (treating the porous material as a composite of metal and air) for elastic behaviour and a modified secant

modulus method (where the relationship between the elastic behaviour of the foam and the dense metal is used to gauge how the plastic behaviour of the foam will relate to that of the dense metal) for the plastic flow stress (Despois *et al.*, 2006). This has as yet not been tested against porous metals processed from powder.

10.5.2 Models for conduction

In work on electrical conductivity, it has been found that simple models can predict the variation in foam conductivity with density, if the conductivity of the solid is known (the evidence shows that the pore size and shape have little effect, although if the pores are not equiaxed there may be a departure from predictions) (Goodall *et al.*, 2006). The best performing models were those of Lemlich (1978), which was particularly effective for low density foams, with long thin struts and the differential effective medium (DEM) model (Torquato, 2002), which worked well for foams with closed or semi-enclosed pores. The equations for these models are:

$$\text{Lemlich:} \qquad \frac{K^*}{K_s} = \frac{(1 - V_p)}{3} \qquad [10.1]$$

$$\text{DEM:} \qquad \frac{K^*}{K_s} = (1 - V_p)^n \qquad [10.2]$$

where K is the conductivity, V_p is the volume fraction porosity and n is an exponent relating to pore shape. The superscript * indicates that the property refers to the foam, the subscript s indicates that it refers to the dense metal. In the DEM, if the pores are spherical, n takes a value 1.5. If the pores are non-spherical, the value will be >1.5. with 1.75 being a typical value for slightly ellipsoidal pores (Goodall *et al.*, 2006).

The predictions of these equations are shown on the graph in Fig. 10.7. Porous metals processed from powders fall below the conductivity predicted by the DEM model, which tends to better represent foams produced by other means with liquid metals as a starting point. The suggested explanation for this is that a powder metallurgical route is likely to include a certain amount of oxide from the surface of the powder, reducing the effective conductivity of the dense metal (Goodall *et al.*, 2006). The conductivity of powder metallurgical foams is somewhat closer to the Lemlich model at high porosities, although it climbs above this when the porosity falls to low values and the pores are isolated; this is unsurprising as the Lemlich model considers high porosity open celled structures with long straight struts.

10.5.3 Simulations

With the structure being such an important factor in determining the properties shown by a foam, and the fact that the structure has a complex, stochastic nature, research has included the use of simulations (such as finite element methods) on real and artificial foam structures to attempt to understand the behaviour. Finite element simulations of mechanical properties on a global and local scale have been performed for titanium foams processed by argon gas trapping (Shen *et al.*, 2006), using as inputs the results of simulations of the growth of pores in 3D. These structures are arrived at from real samples early in the process, where 2D sections are used to capture the distribution of the initially nucleated pores and as such should be superior to artificially generated porous structures. Overall the comparison to experimental stress–strain curves is good (Shen *et al.*, 2006). Finite element models of idealised lattices have also been used to study the effects of defects in the structure (Kepets *et al.*, 2007).

10.6 Future perspectives

Research in metal foams is still highly active, with groups in the UK, Germany, the USA, Japan and elsewhere using powder metallurgical techniques to produce samples, with the same goal of developing new materials and processes, and assisting the transition from research into applications. Recently this research has taken on developments in powder bed rapid manufacturing technologies and has started to produce more of the regular lattice structures that can be easily fabricated using these methods. It is likely that this trend will continue (particularly in view of the rapid developments being made in the processing technology), as an ordered structure is more highly predictable and the possibilities for tailoring the structure to an unprecedented degree of precision are attractive for optimisation of the materials for particular properties and applications. This is starting to include the concept of non-uniform lattices, where the structure varies with location in the component, allowing different behaviours to be prioritised in different parts.

Another factor that is likely to be an important future development is the creation of porous materials made from multiple materials. By using two or more materials, it is possible to engineer structures with unusual properties, such as the zero or negative thermal expansion coefficient structures proposed by Lakes (1996, 2007). The creation of systems with such behaviour on a scale small enough to be considered engineered materials, rather than structures, would open up a new range of exciting possibilities for materials scientists to work with. This will require new advances in the processing areas described here, along with the exploration of new techniques and, importantly, how they may be translated into industrial processes. A thorough

understanding of the processes behind the behaviour is also essential, so that the material design process can proceed with knowledge of the affect of the many available variables.

10.7 References

Ahsan, M. N., Paul, C. P., Kukreja, L. M. and Pinkerton, A. J. (2011) 'Porous structures fabrication by continuous and pulsed laser metal deposition for biomedical applications; modelling and experimental investigation'. *J. Mater. Process. Technol.*, **211**, 602–9.

Andersen, O., Waag, U., Schneider, L., Stephani, G. and Kieback, B. (2000) 'Novel metallic hollow sphere structures'. *Adv. Eng. Mat.*, **2**, 192–5.

Angel, S., Beck, W., Harksen, S. and Scholz, P. F. (2005) 'Functional and structural characterisitics of metallic foams produced by the slip reaction foam sintering (SRFS)-process'. *Mat. Sci. Forum*, **492–3**, 39–45.

Arockiasamy, A., Park, S. J. and German, R. M. (2010) 'Viscoelastic behaviour of porous sintered steels compact'. *Powder Metall.*, **53**, 107–11.

Arzt, E. (1982) 'The influence of an increasing particle coordination on the densification of spherical powders'. *Acta Metall.*, **30**, 1883–90.

Ashby, M. F., Evans, A. G., Fleck, N. A., Gibson, L. J., Hutchinson, J. W. and Wadley, H. N. G. (2000) *Metal Foams: A Design Guide*, Butterworth-Heinemann, Boston.

Bakan, H. I. (2006) A novel water leaching and sintering process for manufacturing highly porous stainless steel. *Scr. Mater.*, **55**, 203–206.

Banhart, J. (2001) Manufacture, characterisation and application of cellular metals and metal foams. *Prog. Mat. Sci.*, **46**, 599–632.

Banhart, J., Fleck, N. and Mortensen, A. (2003) Cellular metals: manufacture, properties, applications, *Proceedings Conference Metfoam 2003*, Berlin, 23–25 June 2003, Verlag MIT Publishing, Berlin, Germany.

Bansiddhi, A. and Dunand, D. C. (2007) Shape-memory NiTi foams produced by solid-state replication with NaF. *Intermetallics*, **15**, 1612–1622.

Bansiddhi, A. and Dunand, D. C. (2008) Shape-memory NiTi foams produced by replication of NaCl space-holders. *Acta Biomater.*, **4**, 1996–2007.

Bansiddhi, A. and Dunand, D. C. (2009) Shape-memory NiTi–Nb foams. *J. Mater. Res.*, **24**, 2107–2117.

Bansiddhi, A., Sargeant, T. D., Stupp, S. I. and Dunand, D. C. (2008) Porous NiTi for bone implants: a review. *Acta Biomater.*, **4**, 773–782.

Bin, J., Zejun, W. and Naiqin, Z. (2007) Effect of pore size and relative density on the mechanical properties of open cell aluminium foams. *Scr. Mater.*, **56**, 169–172.

Biswas, A. (2005) Porous NiTi by Thermal Explosion Mode of SHS: Processing, Mechanism and Generation of Single Phase Microstructure. *Acta Mater.*, **53**, 1415–1425.

Bram, M., Stiller, C., Buchkremer, H. P., Stover, D. and Baur, H. (2000) High-porosity titanium, stainless steel and superalloy parts. *Adv. Eng. Mat.*, **2**, 196–199.

Bram, M., Kohl, M., Buchkremer, H. P. and Stover, D. (2011) Mechanical properties of highly porous NiTi alloys. *J. Mater. Eng. Perform.*, **24**, 522–528.

Cansizoglu, O., Harrysson, O., Cormier, D., H. West and Mahale, T. (2008) 'Properties of Ti–6Al–4V non-stochastic lattice structures fabricated via electron beam melting'. *Mater. Sci. Eng. A*, **492**, 468–74.

Chen, L. J., Li, T., Li, Y. M., He, H. and Hu, Y. H. (2009) Porous titanium implants

fabricated by metal injection molding. *Trans. Nonferrous Met. Soc. China*, **19**, 1174–1179.

Chino, Y. and Dunand, D. C. (2008) Directionally freeze-cast titanium foam with aligned, elongated pores. *Acta Mater.*, **56**, 105–113.

Clyne, T. W., Golosnoy, I. O., Tan, J. C. and Markaki, A. E. (2006) Porous materials for thermal management under extreme conditions. *Phil. Trans. R. Soc. A*, **364**, 125–146.

Colombo, P. and Degischer, H. P. (2010) Highly porous metals and ceramics. *Mater. Sci. Technol.*, **26**, 1145–1158.

Conde, Y., Despois, J.-F., Goodall, R., Marmottant, A., Salvo, L., Marchi, C. S. and Mortensen, A. (2006) Replication processing of highly porous materials. *Adv. Eng. Mat.*, **8**, 795–803.

Cumberland, D. J. and Crawford, R. J. (1987) *The Packing of Particles*, Elsevier, Amsterdam.

Davis, N. G., Teisen, J., Schuh, C. and Dunand, D. C. (2001) Solid state foaming of titanium by superplastic expansion of argon-filled pores. *J. Mater. Res.*, **16**, 1508–1519.

Delannay, F. (2005) Elastic model of an entangled network of interconnected fibres accounting for negative Poisson ratio behaviour and random triangulation. *Int. J. Solids Struct.*, **42**, 2265.

Despois, J.-F., Mueller, R. and Mortensen, A. (2006) Uniaxial deformation of microcellular metals. *Acta Mater.*, **54**, 4129–4142.

Diologent, F., Goodall, R. and Mortensen, A. (2009) Surface oxide in replicated microcellular aluminium and its influence on the plasticity size effect. *Acta Mater.*, **57**, 286–94.

Dong, H. X., Jiang, Y., He, Y. H., Song, M., Zou, J., Xu, N. P., Huang, B. Y., Liu, C. T. and Liaw, P. K. (2009) *J. Alloys Comp.*, **484**, 907.

Driscoll, D., Weisenstein, A. J. and Sofie, S. W. (2011) 'Electrical and flexural anisotropy in freeze tape cast stainless steel porous substrates'. *Mater. Lett.*, **65**, 3433–5.

Ducheyne, P., Aernoudt, E. and De_Meester, P. (1978) The mechanical behaviour of porous austenitic stainless steel fibre structures. *J. Mater. Sci.*, **13**, 2650–2658.

Dunand, D. C. (2004) Processing of titanium foams. *Adv. Eng. Mat.*, **6**, 369–376.

Dunand, D. C. and Teisen, J. (1998) Superplastic foaming of titanium and Ti-6Al-4V. *Porous and Cellular Materials for Structural Applications*. In Schwartz, D. S., Shih, D. H., Evans, A. G. and Wadley, H. G. (eds) San Francisco, CA, USA, Materials Research Society Symposium Proceedings, Vol. 521, Warrendale PA, USA.

El-Hadek, M. A. and Kaytbay, S. (2008) Mechanical and physical characterization of copper foam. *Int. J. Mech. Mater. Des.*, **4**, 63–69.

Engin, G., Aydemir, B. and Gülsoy, H. Ö. (2011) Injection molding of micro-porous titanium alloy with space holder technique. *Rare Metals*, **30**, 565–571.

Esen, Z. and Bor, S. (2007) Processing of titanium foams using magnesium spacer particles. *Scr. Mater.*, **56**, 341–344.

Esen, Z. and Bor, S. (2011) Characterization of Ti–6Al–4V alloy foams synthesized by space holder technique. *Mater. Sci. Eng. A*, 528, 3200–3209.

Fedorchenko, I. M. (1979) Progress in work in the field of high-porosity materials from powders and fibers. *Soviet Powder Metall. Met. Ceram.*, **18**, 615–622.

Fife, J. L., Li, J. C., Dunand, D. C. and Voorhees, P. W. (2009) Morphological analysis of pores in directionally freeze-cast titanium foams. *J. Mater. Res.*, **24**, 117–124.

Fu, Y. Q., Gu, Y. W., Shearwood, C., Luo, J. K., Flewitt, A. J. and Milne, W. I. (2006) Spark plasma sintering of TiNi nano-powders for biological application. *Nanotechology*, **17**, 5293–5298.

Gibson, L. J. and Ashby, M. F. (1997) *Cellular Solids*, Cambridge University Press, Cambridge.

Gong, S., Li, Z., Xu, G. Y., Liu, N., Zhao, Y. Y. and Liang, S. Q. (2011a) 'Fabrication, microstructure and property of cellular CuAlMn shape memory alloys produced by sintering–evaporation process'. *J. Alloys Comp.*, **509**, 2924–8.

Gong, S., Li, Z. and Zhao, Y. Y. (2011b) An extended Mori–Tanaka model for the elastic moduli of porous materials of finite size. *Acta Mater.*, **59**, 6820–6830.

Goodall, R. and Mortensen, A. (2013) Porous Metals. In *Physical Metallurgy*, 5th Edition. Laughlin, D. and Hono, K. (eds), Netherlands Elsevier, Amsterdam.

Goodall, R., Weber, L. and Mortensen, A. (2006) The electrical conductivity of microcellular metals. *J. Appl. Phys.*, **100**, 044912.

Goodstein, D. L., Mccormick, W. D. and Dash, J. G. (1966) Sintered copper sponges for use at low temperature. *Cryogenics*, **6**, 167–168.

Greiner, C., Oppenheimer, S. M. and Dunand, D. C. (2005) High strength, low stiffness, porous NiTi with superelastic properties. *Acta Biomaterialia*, **1**, 705–716.

Gulsoy, H. O. and German, R. M. (2008) Sintered foams from precipitation hardened stainless steel powder. *Powder Metall.*, **51**, 350–353.

Guo, Z. X., Jee, C. S. Y., Ozguven, N. and Evans, J. R. G. (2000) Novel polymer-metal based method for open cell metal foams production. *Mat. Sci. Tech.*, **16**, 776–780.

Guo, S., Duan, B., He, X. and Qu, X. (2009) Powder injection molding of pure Titanium. *Rare Metals*, **28**, 261–265.

Guoxin, H., Lixiang, Z., Yunliang, F. and Yanhong, L. (2008) Fabrication of high porous NiTi shape memory alloy by metal injection molding. *J. Mater. Process. Technol.*, **206**, 395–399.

Hakamada, M., Nomura, T., Yamada, Y., Chino, Y., Hosokawa, H., Nakajima, T., Chen, Y., Kusuda, H. and Mabuchi, M. (2005a) 'Compressive properties at elevated temperatures of porous aluminium processed by the spacer method'. *J. Mater. Res.*, **20**, 3385–90.

Hakamada, M., Yamada, Y., Nomura, T., Kusuda, H., Chen, Y. and Mabuchi, M. (2005b) Effect of sintering temperature on compressive properties of porous aluminum produced by spark plasma sintering. *Mater. Trans.*, **46**, 186–188.

Hakamada, M., Asao, Y., Kuromura, T., Chen, Y., Kusuda, H. and Mabuchi, M. (2007) Density dependence of the compressive properties of porous copper over a wide denisty range. *Acta Mater.*, **55**, 2291–2299.

He, Y., Jiang, Y., Xu, N., Zou, J., Huang, B., Liu, C. T. and Law, P. K. (2007) Fabrication of Ti-Al micro/nanometer-sized porous alloys through the Kirkendall effect. *Adv. Mater.*, **19**, 2102–2106.

Heinl, P., Rottmair, A., Körner, C. and Singer, R. F. (2007) Cellular titanium by selective electron beam melting. *Adv. Eng. Mater.*, **9**, 360–364.

Heinl, P., Körner, C. and Singer, R. F. (2008a) Selective electron beam melting of cellular titanium. *Adv. Eng. Mater.*, **10**, 882–888.

Heinl, P., Muller, L., Korner, C., Singer, R. F. and Muller, F. A. (2008b) Cellular Ti–6Al–4V structures with interconnected macro porosity for bone implants fabricated by selective electron beam melting. *Acta Biomater.*, **4**, 1536–1544.

Higginson, R. and Sellars, M. (2003) *Quantitative Metallography*, Maney, London.

Hodge, A. M. and Dunand, D. C. (2003) Measuring and modelling of creep in open-cell NiAl foams. *Met. Mater. Trans. A*, **34**, 2353–2363.

Hong, T. F., Guo, Z. X. and Yang, R. (2008) Fabrication of porous titanium scaffold materials by a fugitive filler method. *J. Mater. Sci: Mater. Med.*, **19**, 3489–3495.

Ismail, M. H., Goodall, R., Davies, H. A. and Todd, I. (2011) Porous NiTi alloy by metal injection moulding/sintering of elemental powders: Effect of sintering temperature. *Mater. Lett.*, **70**, 142–145.

Jee, C. S. Y., Ozguven, N., Guo, Z. X. and Evans, J. R. G. (2000) Preparation of high porosity metal foams. *Met. Mater. Trans. B*, **31**, 1345–1352.

Jiang, B., Zhao, N. Q., Shi, C. S., Du, X. W., Li, J. J. and Man, H. C. (2005a) 'A novel method for making open cell aluminium foams by powder sintering process'. *Mater. Lett.*, **59**, 3333–6.

Jiang, B., Zhao, N. Q., Shi, C. S. and Li, J. J. (2005b) Processing of open cell aluminium foams with tailored porous morphology. *Scr. Mater.*, **53**, 781–785.

Kanetake, N. and Kobashi, M. (2006) Innovative processing of porous and cellular materials by chemical reaction. *Scr. Mater.*, **54**, 521–525.

Kearns, M. W., Blenkinsop, P. A., Barber, A. C. and Farthing, T. W. (1988) Manufacture of a novel porous metal. *Int. J. Powder Metall.*, **24**, 59–64.

Kepets, M., Lu, T. J. and Dowling, A. P. (2007) Modeling of the role of defects in sintered FeCrAlY foams. *Acta Mech. Sin*, **23**, 511–529.

Kim, J. S., Kang, J. H., Kang, S. B., Yoon, K. S. and Kwon, Y. S. (2004) Porous TiNi biomaterial by self-propagating high-temperature synthesis. *Adv. Eng. Mat.*, **6**, 403–406.

Kobashi, M. and Kanetake, N. (2002) Processing of intermetallic foam by combustion reaction. *Adv. Eng. Mat.*, **4**, 745–747.

Kobashi, M., Kuze, K. and Kanetake, N. (2006a) Cell structure control of porous titanium composite synthesised by combustion reaction. *Adv. Eng. Mat.*, **8**, 836–840.

Kobashi, M., Wang, R. X., Inagaki, Y. and Kanetake, N. (2006b) Effects of processing parameters on pore morphology of combusion synthesised Al-Ni foams. *Mater. Trans.*, **47**, 2172–2177.

Köhl, M., Habijan, T., Bram, M., Buchkremer, H. P., Stover, D. and Koller, M. (2009) Powder metallurgical near-net-shape fabrication of porous NiTi shape memory alloys for use as long-term implants by the combination of the metal injection molding process with the space-holder technique. *Adv. Eng. Mater.*, **11**, 959–968.

Köhl, M., Bram, M., Moser, A., Buchkremer, H. P., Beck, T. and Stöver, D. (2011) Characterization of porous, net-shaped NiTi alloy regarding its damping and energy-absorbing capacity. *Mater. Sci. Eng. A*, **528**, 2454–2462.

Lagoudas, D. C. and Vandygriff, E. L. (2002) 'Processing and characterization of NiTi porous SMA by elevated pressure sintering. *J. Intell. Mater. Syst. Struct.*, **13**, 837–850.

Lakes, R. (1996) Cellular solid structures with unbounded thermal expansion. *J. Mater. Sci. Lett.*, **15**, 475–477.

Lakes, R. (2007) Cellular solids with tunable positive or negative thermal expansion of unbounded magnitude. *Appl. Phys. Lett.*, **90**, 221905.

Laptev, A., Bram, M., Buchkremer, H. P. and Stover, D. (2004) Study of production route for titanium parts combining very high porosity and complex shapes. *Powder Metall.*, **47**, 85–92.

Laptev, A., Vyal, O., Bram, M., Buchkremer, H. P. and Stover, D. (2005) Green strength of powder compacts provided for production of highly porous titanium parts. *Powder Metall.*, **48**, 358–364.

Lefebvre, L. P., Banhart, J. and Dunand, D. C. (2007) 'Porous metals and metallic foams', *Proceedings Conference Metfoam 2007*. Montreal, Sept. 5–7, 2007, DESTech Publications, Lancaster, PA.

Lemlich, R. (1978) A theory for the limiting conductivity of polyhedral foam at low density. *J. Colloid Interface Sci.*, **64**, 107–110.

Li, J. C. and Dunand, D. C. (2011) 'Mechanical properties of directionally freeze-cast titanium foams'. *Acta Mater.*, **59**, 146–58.

Li, B. Q. and Lu, X. (2011) The effect of pore structure on the electrical conductivity of Ti. *Trans. Porous Media*, **87**, 179–189.

Li, C.-F. and Zhu, Z.-G. (2005) Apparent electrical conductivity of porous titanium prepared by the powder metallurgy method. *Chinese Phys. Lett.*, **22**, 2647–2650.

Li, Y. H., Rong, L. J. and Li, Y. Y. (2002) Compressive property of porous NiTi alloy synthesized by combustion synthesis. *J. Alloys Comp*, **345**, 271–274.

Li, J. P., Li, S. H., Blitterswijk, C. A. V. and Groot, K. D. (2005) A novel porous Ti6Al4V: Characterization and cell attachment. *J. Biomed. Mater. Res. A*, **73**, 223–233.

Li, J. P., Wijn, J. R. D., Blitterswijk, C. A. V. and Groot, K. D. (2006) Porous Ti6Al4V scaffold directly fabricating by rapid prototyping: preparation and *in vitro* experiment. *Biomaterials*, **27**, 1223–1235.

Li, D. S., Zhang, X. P., Xiong, Z. P. and Mai, Y. W. (2010) Lightweight NiTi shape memory alloy based composites with high damping capacity and high strength. *J. Alloys. Comp.*, **490**, L15–L19.

Li, S. J., Murr, L. E., Cheng, X. Y., Zhang, Z. B., Hao, Y. L., Yang, R., Medina, F. and Wicker, R. B. (2012) Compression fatigue behavior of Ti–6Al–4V mesh arrays fabricated by electron beam melting. *Acta Mater*, **60**, 793–802.

Liang, W., Jiang, Y., Hongxing, D., He, Y., Xu, N., Zou, J., Huang, B. and Liu, C. T. (2011) The corrosion behavior of porous Ni3Al intermetallic materials in strong alkali solution. *Intermetallics*, **19**, 1759–1765.

Lide, D. R. (2001) *CRC Handbook of Chemistry and Physics*, CRC Press, Boca Raton, FL.

Lim, T. J., Smith, B. and Mcdowell, D. L. (2002) Behaviour of a random hollow sphere metal foam. *Acta Mater.*, **50**, 2867–2879.

Liu, P. S. and Liang, K. M. (2001) Functional materials of porous metals made by P/M, electroplating and some other techniques. *J. Mater. Sci.*, **36**, 5059–5072.

Ma, X., Peyton, A. and Zhao, Y. (2005) Measurement of the electrical conductivity of open-celled aluminium foam using non-contact eddy current techniques. *NDTandE Int.*, **38**, 359–367.

Ma, X., Peyton, A. J. and Zhao, Y. Y. (2006) Eddy current measurements of electrical conductivity and magnetic permeability of porous metals. *NDTandE Int.*, **39**, 562–568.

Manonukul, A., Muenya, N., Léaux, F. and Amaranan, S. (2010) 'Effects of replacing metal powder with powder space holder on metal foam produced by metal injection moulding'. *J. Mater. Process. Technol.*, **210**, 529–35.

Mansourighasri, A., Muhamad, N. and Sulong, A. B. (2012) Processing titanium foams using tapioca starch as a space holder. *J. Mater. Process. Technol.*, **121**, 83–89.

Markaki, A. E., Gergely, V., Cockburn, A. and Clyne, T. W. (2003) Production of a highly porous material by liquid phase sintering of short ferritic stainless steel fibres and a preliminary study of its mechanical behaviour. *Compos. Sci. Technol.*, **63**, 2345–2351.

Mi, G. F., Li, H. Y., Liu, X. Y. and Wang, K. F. (2009) Preparation, Structure and Mechanical Properties of Nickel Based Porous Spherical Superalloy. *J. Iron Steel Res., Int.*, **16**, 92–96.

Mueller, R., Soubielle, S., Goodall, R., Diologent, F. and Mortensen, A. (2007) On the steady state creep of microcellular metals. *Scr. Mater.*, **57**, 33–6.

Murr, L. E., Gaytan, S. M., Medina, F., Lopez, H., Martinez, E., Machado, B. I., Hernandez, D. H., Martinez, L., Lopez, M. I., Wicker, R. B. and Bracke, J. (2010a) Next-generation biomedical implants using additive manufacturing of complex, cellular and functional mesh arrays. *Phil. Trans. R. Soc. A*, **368**, 1999–2032.

Murr, L. E., Gaytan, S. M., Medina, F., Martinez, E., Martinez, J. L., Hernandez, D. H., Machado, B. I., Ramirez, D. A. and Wicker, R. B. (2010b) Characterization of Ti–6Al–4V open cellular foams fabricated by additive manufacturing using electron beam melting. *Mater. Sci. Eng. A*, **527**, 1861–1868.

Murr, L. E., Amato, K. N., Li, S. J., Tian, Y. X., Cheng, X. Y., Gaytan, S. M., Martinez, E., Shindo, P. W., Medina, F. and Wicker, R. B. (2011) Microstructure and mechanical properties of open-cellular biomaterials prototypes for total knee replacement implants fabricated by electron beam melting. *J. Mech. Behav. Biomed. Mater.*, **4**, 1396–1411.

Murray, N. G. D. and Dunand, D. C. (2003) 'Microstructure evolution during solid-state foaming of titanium'. *Comp. Sci. Tech.*, **63**, 2311–16.

Murray, N. G. D. and Dunand, D. C. (2004) Effect of thermal history on the superplastic expansion of argon-filled pores in titanium: Part I Kinetics and microstructure. *Acta Mater.*, **52**, 2269–2278.

Murray, N. G. D., Schuh, C. A. and Dunand, D. C. (2003) Solid-state foaming of titanium by hydrogen-induced internal-stress superplasticity. *Scr. Mater.*, **49**, 879–883.

Nabavi, A. and Khaki, J. V. (2011) Manufacturing of aluminum foam sandwich panels: comparison of a novel method with two different conventional methods. *J. Sandwich Struct. Mater.*, **13**, 177–187.

Nagel, A. R., Uslu, C., Lee, K. J., Cochran, J. K. and Sanders, T. H. (1997) Steel closed cell foams from direct oxide reduction. In *Synthesis/Processing of Lightweight Metallic Materials II*. Ward-Close, C. M., Froes, F. H., Chellman, D. J. and Cho, S. S. (eds) The Minerals, Metals and Materials Soc., Warrendale, PA, USA.

Nakajima, H. and Kanetake, N. (2005) Porous metals and metal foaming technology, *Proceedings Conference MetFoam* 2005 Kyoto, Japan, Sept. 21-23rd 2005, Japan Institute of Metals, Sendai, Japan.

Niu, W., Bai, C., Qiu, G., Wang, Q., Wen, L., Chen, D. and Dong, L. (2009) Preparation and characterization of porous titanium using space-holder technique. *Rare Metals*, **28**, 338–342.

Nomura, N., Kohama, T., Oh, I. H., Hanada, S., Chiba, A., Kanehira, M. and Sasaki, K. (2005) Mechanical properties of porous Ti–15Mo–5Zr–3Al compacts prepared by powder sintering. *Mater. Sci. Eng. C*, **25**, 330–335.

Nouri, A., Hodgson, P. D. and Wen, C. E. (2010) Effect of process control agent on the porous structure and mechanical properties of a biomedical Ti–Sn–Nb alloy produced by powder metallurgy. *Acta Biomater.*, **6**, 1630–1639.

Oh, I. K., Nomura, N., Masahashi, N. and Hanada, S. (2003) Mechanical properties of porous titanium compacts prepared by powder sintering. *Scr. Mater.*, **49**, 1197–1202.

Oppenheimer, S. M., O'Dwyer, J. G. and Dunand, D. C. (2004) 'Porous, superelastic NiTi produced by powder metallurgy'. *TMS Lett.*, **1**, 93–4.

Pattanayak, D. K., Fukuda, A., Matsushita, T., Takemoto, M., Fujibayashi, S., Sasaki, K., Nishida, N., Nakamura, T. and Kokubo, T. (2011) Bioactive Ti metal analogous to human cancellous bone: Fabrication by selective laser melting and chemical. *Acta Biomater.*, **7**, 1398–1406.

Queheillalt, D. T., Katsumura, Y. and Wadley, H. N. G. (2004) Synthesis of stochastic open cell Ni-based foams. *Scr. Mater.*, **50**, 313–317.

Rak, Z. S. and Walter, J. (2006) Porous titanium foil by tape casting technique. *J. Mater. Proc. Tech.*, **175**, 358–363.

Rak, Z., Berkeveld, L. D. and Snijders, G. (2003) *Method for producing a porous titanium material article*. International Patent WO 03/092933A1.

Ramirez, D. A., Murr, L. E., Li, S. J., Tian, Y. X., Martinez, E., Martinez, J. L., Machado, B. I., Gaytan, S. M., Medina, F. and Wicker, R. B. (2011) Open-cellular copper structures fabricated by additive manufacturing using electron beam melting. *Mater. Sci. Eng. A*, **528**, 5379–5386.

Ricceri, R. and Matteazzi, P. (2003) PM processing of cellular titanium. *Int. J. Powder Metall.*, **39**, 53–61.

Roy, S., Wanner, A., Beck, T., Studnitzky, T. and Stephani, G. (2011) Mechanical properties of cellular solids produced from hollow stainless steel spheres. *J. Mater. Sci.*, **46**, 5519–5526.

San-Marchi, C. and Mortensen, A. (2001) Deformation of open-cell aluminium foam. *Acta Mater.*, **49**, 3959–3969.

Schwartz, D. S., Shih, D. S., Lederich, R. J., Martin, R. L. and Deuser, D. A. (1998) Development and scale-up of the low density core process for Ti-64. In *Porous and Cellular Materials for Structural Applications*. Schwartz, D. S., Shih, D. H., Evans, A. G. and Wadley, H. G. (eds) San Francisco, CA, USA, Materials Research Society Symposium Proceedings Vol. 521, Warrendale PA, USA.

Schwerdtfeger, J., Heinl, P., Singer, R. F. and Körner, C. (2010) Auxetic cellular structures through selective electron-beam melting. *Phys. Status Solidi*, **247**, 269–272.

Scott, J. A. and Dunand, D. C. (2010) 'Processing and mechanical properties of porous Fe–26Cr–1Mo for solid oxide fuel cell interconnects'. *Acta Mater.*, **58**, 6125–33.

Shen, H., Oppenheimer, S. M., Dunand, D. C. and Brinson, L. C. (2006) Numerical modelling of pore size and distribution in foamed titanium. *Mech. Mater.*, **38**, 933–944.

Skochdopole, R. E. (1961) The thermal conductivity of foamed plastics. *Chem. Eng. Prog.*, **57**, 55–59.

Song, Z. and Kishimoto, S. (2006) The cell size effect of closed cellular materials fabricated by pulse current assisted hot isostatic pressing on the compressive behaviour. *Scr. Mater.*, **54**, 1531–1535.

Sun, D. X. and Zhao, Y. Y. (2003) Static and dynamic energy absorption of Al foams produced by the sintering and dissolution process. *Metall. Mater. Trans. B*, **34**, 69–74.

Sun, D. X. and Zhao, Y. Y. (2005a) Phase changes in sintering of Al/Mg/NaCl compacts of manufacturing Al foams by the sintering and dissolution process. *Mat. Lett.*, **59**, 6–10.

Sun, D. X. and Zhao, Y. Y. (2005b) Simulation of thermal diffusivity of Al/NaCl powder compacts in producing Al foams by the sintering and dissolution process. *J. Mater. Process Tech.*, **169**, 83–88.

Tan, J. C., Elliott, J. A. and Clyne, T. W. (2006) Analysis of tomography images of bonded fibre networks to measure distributions of fibre segment length and fibre orientation. *Adv. Eng. Mater.*, **8**, 495–500.

Thewsey, D. J. and Zhao, Y. Y. (2008) Thermal conductivity of porous copper manufactured by the lost carbonate sintering process. *Phys. Status Solid A*, **205**, 1126–1131.

Thieme, M., Wieters, K. P., Bergner, F., Scharnweber, D., Worch, H., Ndop, J., Kim, T. J. and Grill, W. (2001) Titanium powder sintering for preparation of a porous functionally graded material destined for orthopaedic implants. *J. Mater. Sci.: Mater. Med.*, **12**, 225–231.

Torquato, S. (2002) *Random Heterogeneous Media*, Springer, New York.

Tuncer, N., Arslan, G., Maire, E. and Salvo, L. (2011) Investigation of spacer size effect on architecture and mechanical properties of porous titanium. *Mater. Sci. Eng. A*, **530**, 633–642.

Uslu, C., Lee, K. J., Sanders, T. H. and Cochran, J. K. (1997) 'Ti-6Al-4V hollow sphere foams'. In *Synthesis/Processing of Lightweight Metallic Materials II*. Ward-Close, C. M., Froes, F. H., Chellman, D. J. and Cho, S. S. (eds) The Minerals, Metals and Materials Soc., Warrendale, PA, USA.

Vanleeuwen, B. K., Darling, K. A., Koch, C. C. and Scattergood, R. O. (2011) Novel technique for the synthesis of ultra-fine porosity metal foam via the inclusion of condensed argon through cryogenic mechanical alloying. *Mater. Sci. Eng. A*, **528**, 2192–2195.

Vannoort, R. (2012) The future of dental devices is digital. *Dental Mater.*, **28**, 3–12.

Wang, N., Starke, E. A. and Wadley, H. N. G. (1998) Porous Al alloys by local melting and diffusion of metal powders. In *Porous and Cellular Materials for Structural Applications*. Schwartz, D. S., Shih, D. H., Evans, A. G. and Wadley, H. G. (eds) San Francisco, CA, USA, Materials Research Society Symposium Proceedings Vol. 521, Warrendale PA, USA.

Wen, C. E., Mabuchi, M., Yamada, Y., Shimojima, K., Chino, Y. and Asahina, T. (2001) Processing of biocompatible porous Ti and Mg. *Scr. Mater.*, **45**, 1147–1153.

Wen, C. E., Mabuchi, M., Yamada, Y., Shimojima, K., Chino, Y., Hosokawa, H. and Asahina, T. (2003) Processing of fine-grained aluminium foam by spark plasma sintering. *J. Mat. Sci. Lett.*, **22**, 1407–1409.

Wen, C. E., Yamada, Y., Shimojima, K., Chino, Y., Asahina, T. and Mabuchi, M. (2002a) Processing and mechanical properties of autogenous titanium implant materials. *J. Mater. Sci.: Mater. Med.*, **13**, 397–401.

Wen, C. E., Yamada, Y., Shimojima, K., Chino, Y., Hosokawa, H. and Mabuchi, M. (2002b) Novel titanium foam for bone tissue engineering. *J. Mater. Res.*, **17**, 2633–2639.

Wen, C. E., Yamada, Y., Shimojima, K., Chino, Y., Hosokawa, H. and Mabuchi, M. (2004) Compressibility of porous magnesium foam: dependency on porosity and pore size. *Mater. Lett.*, **58**, 357–360.

Wen, C. E., Xiong, J. Y., Li, Y. C. and Hodgson, P. D. (2010) 'Porous shape memory scaffolds for biomedical applications: a review', *Phys. Scr.*, T139, 014070.

Xie, S. and Evans, J. R. G. (2004) High porosity copper foam. *J. Mat. Sci.*, **39**, 5877–5880.

Xue, X. B. and Zhao, Y. Y. (2011) 'Ti matrix syntactic foam fabricated by powder metallurgy: particle breakage and elastic modulus'. *JOM*, **63**, 43–7.

Ye, B. and Dunand, D. C. (2010) Titanium foams produced by solid-state replication of NaCl powders. *Mater. Sci. Eng. A*, **528**, 691–697.

Yu, A. B. and Standish, N. (1993) Characterisation of non-spherical particles from their packing behaviour. *Powder Technol.*, **74**, 205–213.

Yuan, B., Chung, C. Y. and Zhu, M. (2004) Microstructure and matrensitic transformation behaviour of porous NiTi shape memory alloy prepared by hot isostatic pressing processing. *Mat. Sci. Eng. A*, **382**, 181–187.

Yuan, B., Zhu, M., Gao, Y., Li, X. and Chung, C. Y. (2008) Forming and control of pores by capsule-free hot isostatic pressing in NiTi shape memory alloys. *Smart. Mater. Struct.*, **17**, 025013.

Zhao, Y. Y. (2003) Stochastic modelling of removability of NaCl in sintering and dissolution process to produce Al foams. *J. Porous Mater*, **10**, 105–111.

Zhao, Y. Y. and Sun, D. X. (2001) A novel sintering-dissolution process for manufacturing Al foams. *Scr. Mater.*, **44**, 105–110.

Zhao, Y. Y., Han, F. and Fung, T. (2004) Optimisation of compaction and liquid-state sintering in sintering and dissolution process for manufacturing Al foams. *Mat. Sci. Eng. A*, **364**, 117–125.

Zhao, Y. Y., Fung, T., Zhang, L. P. and Zhang, F. L. (2005) Lost carbonate sintering process for manufacturing metal foams. *Scr. Mater.*, **52**, 295–298.

Zhao, X., Sun, H., Lan, L., Huang, J., Zhang, H. and Wang, Y. (2009) Pore structures of high-porosity NiTi alloys made from elemental powders with NaCl temporary space-holders. *Mater. Lett.*, **63**, 2402–2404.

Zhuang, H., Han, Y. and Feng, A. (2008) Preparation, mechanical properties and in vitro biodegradation of porous magnesium scaffolds. *Mater. Sci. Eng. C*, **28**, 1462–1466.

11

Evolution of microstructure in ferrous and non-ferrous materials

H. DANNINGER, C. GIERL-MAYER and S. STROBL, Vienna University of Technology, Austria

DOI: 10.1533/9780857098900.2.308

Abstract: The most prominent features of powder metallurgy (PM) materials are their fine and regular microstructure and in many cases their porosity. Here, it is shown how the porosity changes with manufacturing parameters in sintered materials and how preparation has to be done to avoid artefacts. The matrix microstructures, with regard to the alloying technique and resulting element distribution, and the microstructural development during sintering of powder injection moulded products are described. The fine homogeneous microstructure is a typical feature of fully dense PM materials as shown for tool steels and hard metals. The pronounced effect of doping elements on microstructural stability is presented for PM refractory metals.

Key words: homogeneity, phases, porosity, powder metallurgy microstructures, sintering.

11.1 Introduction

Powder metallurgy (PM) products have a different manufacturing route from standard metallic components and this has a strong impact on the microstructure and resulting properties. The fact that in PM processing, none or, at best, only a small fraction of liquid phase is present – in contrast to ingot metallurgy which starts from fully liquid materials – results in usually finer and much more homogeneous microstructures; by the powder route, immiscible components such as W and Cu or Al and Al_2O_3 can be combined. However, this tendency to lack of segregation also means that PM materials are more sensitive to impurities, particles from slag, ceramic linings and dust which are not removed by gravity segregation, as in the case of classical ingot metallurgy, but remain within the powder. Therefore, cleanliness is an essential precondition in PM manufacturing and this is evident when entering a PM factory in comparison to a foundry.

The huge variety of starting powders available and alloying variants for PM multicomponent systems means that even for a given overall composition a multitude of different microstructures can be obtained. In many PM products, porosity is a further microstructural component feature, in part as an inevitable, but frequently unwelcome consequence of the manufacturing

process; in part, however, porosity is the *raison d'etre* for PM materials as, for example, in self-lubricating bearings or sintered filters. In particular the presence of the porosity also has a strong impact on the metallographic preparation of PM materials; specific care has to be taken to depict the porosity metallographically realistically since both unintentional closing and enlarging of the pores is easily done during preparation, as will be discussed below.

11.2 Metallographic preparation techniques for powder metallurgy products

In general, the metallographic preparation techniques used for the preparation of conventional metals can also be applied to powder metallurgy products; there are however several differences and peculiarities that have to be considered. The main difference from cast and wrought products is once more the porosity of many PM materials. In contrast to pores present in particular in cast products, the pores in PM materials – except in filters – are fine and mostly very regularly distributed (Figs 11.1 and 11.2). In metallographic preparation, there is a pronounced risk of artefacts, the pores being partially or completely closed during grinding and polishing.[1,2] This risk is the more pronounced the higher the ductility of such materials. Very easily sintered plain iron can appear fully dense after metallographic preparation (Fig. 11.3(a)) although density measurement through water displacement (Archimedes) method shows that there is considerable porosity. Frequently the presence of pores can be recognized by the emergence of wormlike lines in the seemingly dense material. One remedy for this problem is the use of mainly abrasively acting media; extended polishing with 3 µm diamond grit is preferable here compared to SiC, Al_2O_3 or Cr_2O_3. Diamond polishing is also recommended if X-ray diffraction (XRD) is to be done on the sections since in particular the softer polishing media also result in compressive residual stresses that adversely affect the precision of the XRD measurement.

The second way to reveal the pores precisely is by combining polishing with etching (Fig. 11.3(b)). By appropriate combining of both, a realistic image of the pores can be obtained, the metal layers covering the pores that have been generated by polishing being etched off. This is of particular importance if the properties of a sintered material – mechanical, magnetic or electrical – are to be related to the pore geometry, which happens frequently. However, there is also a risk of overetching, that is opening the pores too much. To obtain a correct image of the pores, a commonly used measure is to compare the porosity obtained by water displacement with that obtained from the sections by quantitative metallography; if both are in good agreement it can be assumed that the section has been prepared correctly.[2]

A third method is impregnation of the pores – after 6 µm diamond polishing

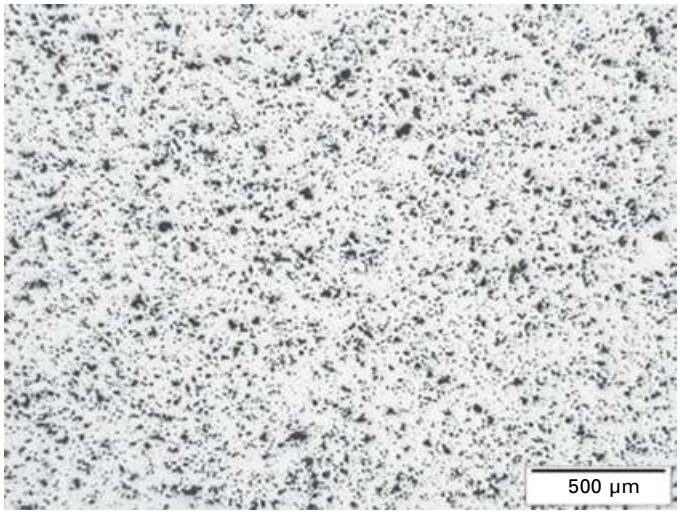

(a)

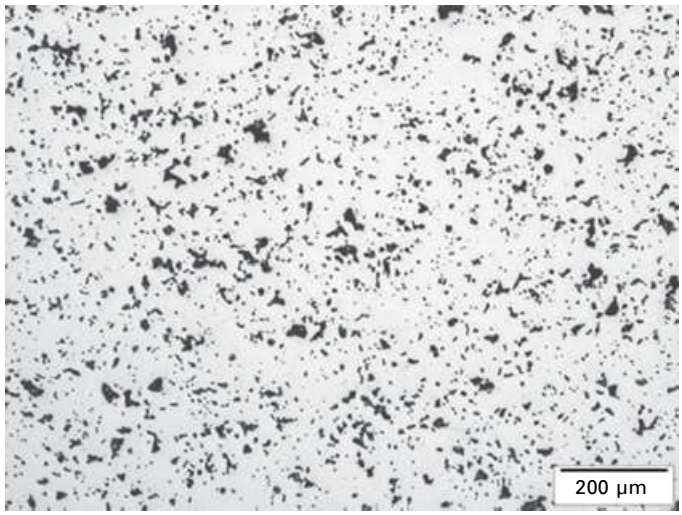

(b)

11.1 Porosity in sintered steel Fe–1.5% Cr–0.2% Mo–0.5% C (compacted at 700 MPa, sintered 60 min at 1280°C): (a) overview, (b) higher magnification.

– with low-viscosity resins that are cured afterwards, either thermally or catalytically, by the presence of metal surfaces and the absence of air. If this is done properly, pore closing can be effectively prevented.

Another feature of many PM products that affects the metallographic preparation is the widely varying hardness of the microstructural constituents. In many types of sintered steels, chemically heterogeneous microstructures

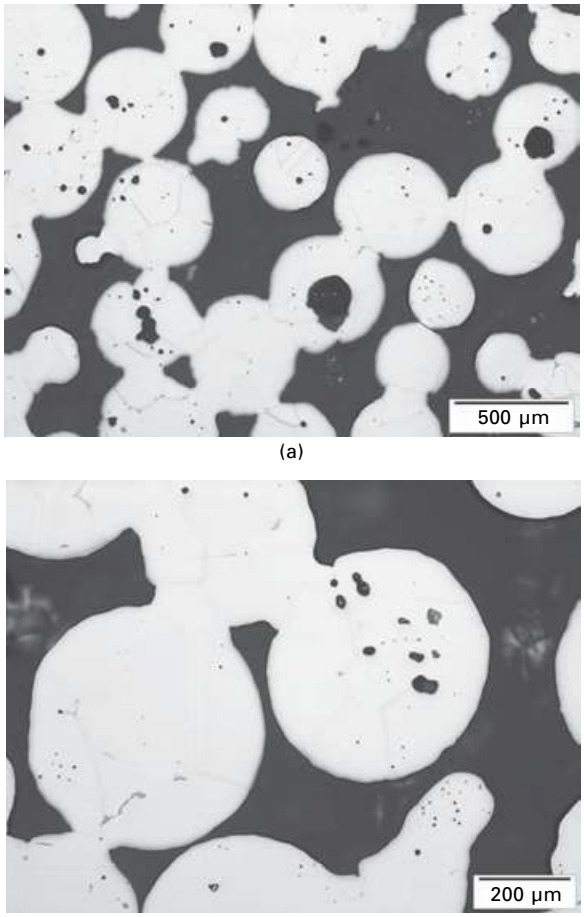

11.2 Porosity in sintered bronze filter (pre-alloyed powder Cu–11Sn, sintered for 60 min at 810°C in H_2): (a) overview, (b) detail.

are observed and, as a consequence, ferrite and retained austenite are present, as well as martensite,[3–7] and the transition may be within a few micrometres. In hard metals, metallic Co and WC form the microstructure, the size of the phases being frequently << 1 µm.[8] This means that polishing techniques have to be applied that prevent preferential removal of the softer phase; once more, using diamond grit for polishing is recommended.

When etching, the presence of open porosity may be a nuisance since the etchant enters the pores and then gradually tends to exude, resulting in overetched stains around the pores. This is particularly common with heat treated, martensitic or bainitic steels (Fig. 11.4). Here, once more impregnation of the section with low-viscosity resins is an effective measure for sealing

(a)

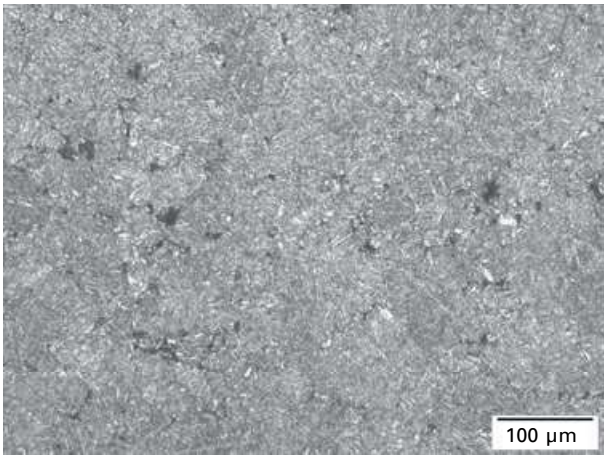

(b)

11.3 Sintered steel Fe–1.8% Cr–0.5% C (sintered 60 min at 1250°C in N_2): (a) pores partially closed by polishing, (b) same as (3a), Nital etched.

the pores. Sometimes swabbing produces better results compared with immersion.

Overetching may, however, be useful for multiphase materials. If one of the phases can be selectively removed, better insight into the three-dimensional structure may be obtained. This is shown in Fig. 11.5 for tungsten heavy alloys:[9] while in the plane section the distribution of the phases can only be estimated, after etching away the tungsten phase a much more clear image of the structure can be gained, in particular with respect to the connectivity of the W phase.

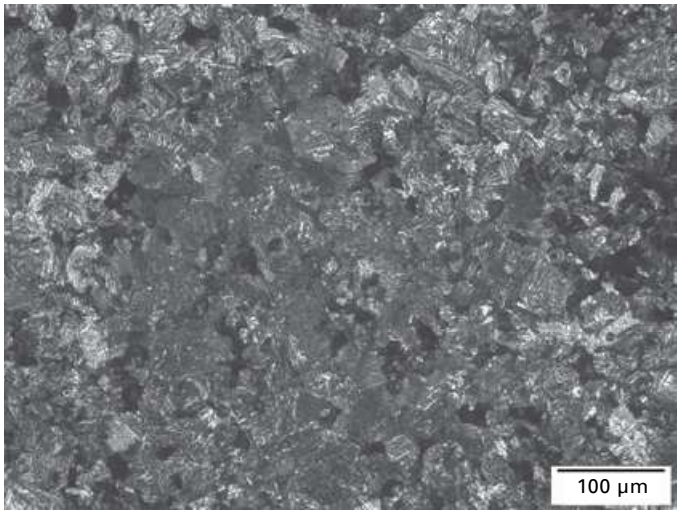

(a)

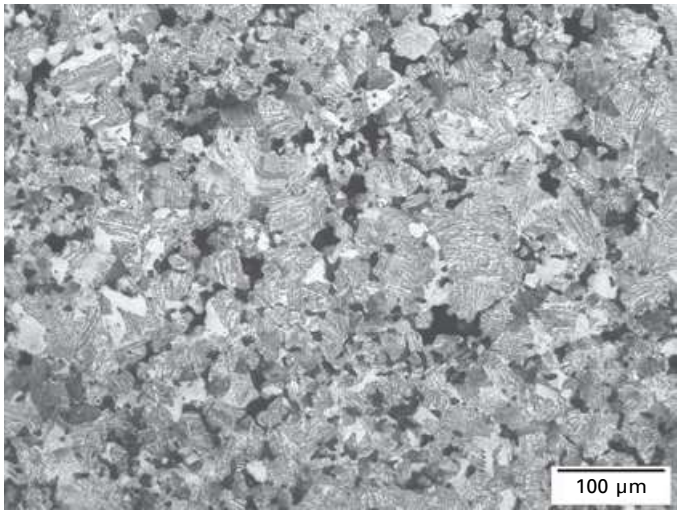

(b)

11.4 Image of (a) overetched (Nital etched, 60 s) and (b) properly etched (Nital etched, 12 s) sintered steel (Fe–0.85% Mo–0.7% C, sintered 1 h at 1150°C in N_2).

11.2.1 Fractographic techniques

The fracture modes encountered in PM materials are basically the same as those in ingot metallurgy materials; these are ductile rupture, transgranular (cleavage) fracture and intergranular failure, examples being shown in Fig. 11.6. However, both the wide range of compositions and the combination of widely different constituents results in a large variety of appearance.

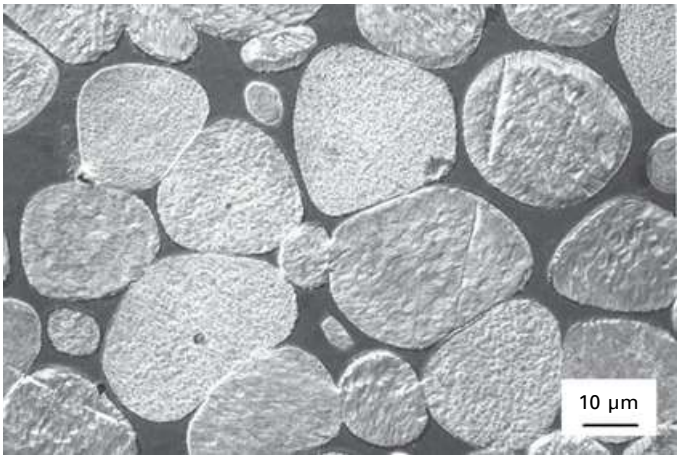

(a)

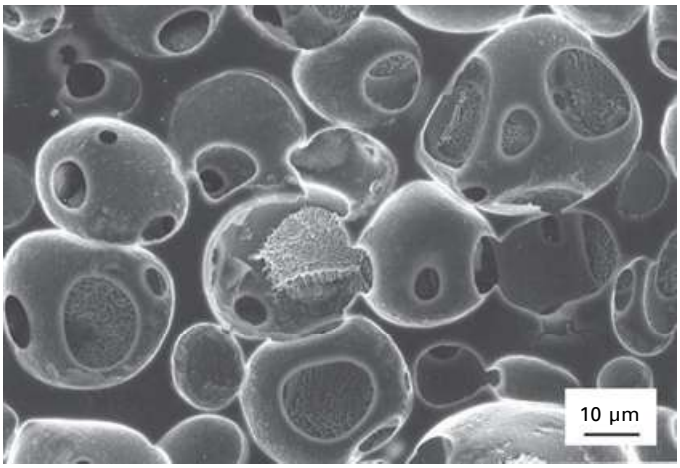

(b)

11.5 Tungsten heavy alloy W–6.7% Ni–3.3% Fe, liquid phase sintered at 1475°C: (a) metallographic section, (b) section, long time etched with saturated $Cu(NH_3).SO_4$ solution.

For multiphase materials, which are very common in PM, the interfaces are of crucial importance for the mechanical behaviour; low interfacial strength is usually linked to inadequate mechanical properties, as shown for W–Ni–Fe heavy alloys in Fig. 11.7: in the brittle materials the Ni–Fe–W binder is easily separated from the W spheres while in the ductile one excellent adherence is observed.[9]

Furthermore, the presence of pores may strongly affect the fracture mode. Here, in particular, the presence of interconnected pores plays a major role, since this type of porosity implies isolated sintering contacts or

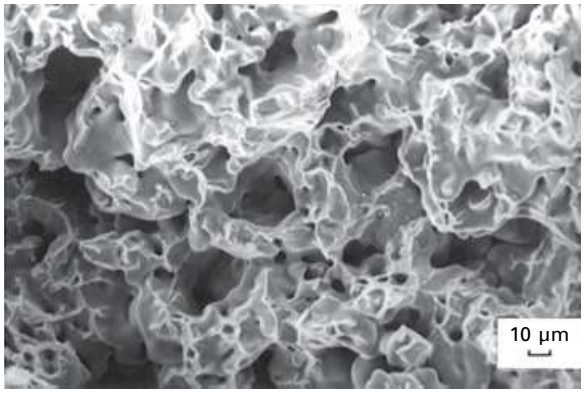

(a)

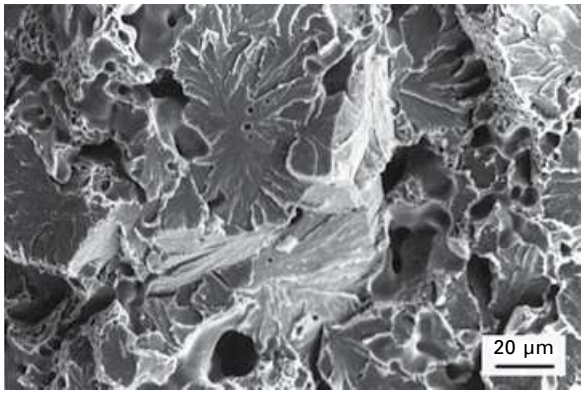

(b)

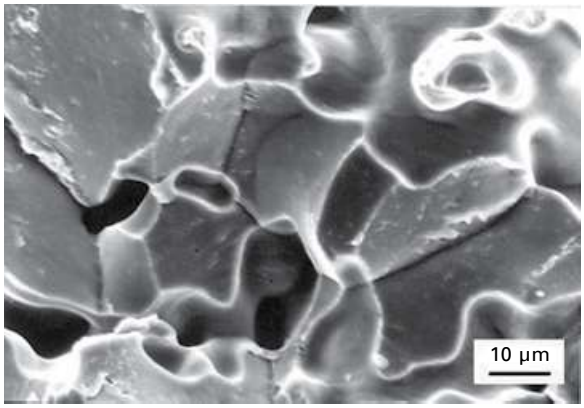

(c)

11.6 Different fracture modes in ferrous PM materials: (a) ductile rupture of Fe–3% Cu, (b) mixed cleavage–ductile rupture in sintered Fe–Mo–C, (c) intergranular failure in Fe–Mo–C–P.

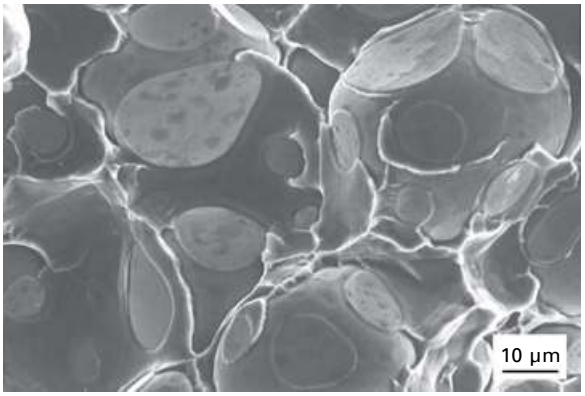

(a)

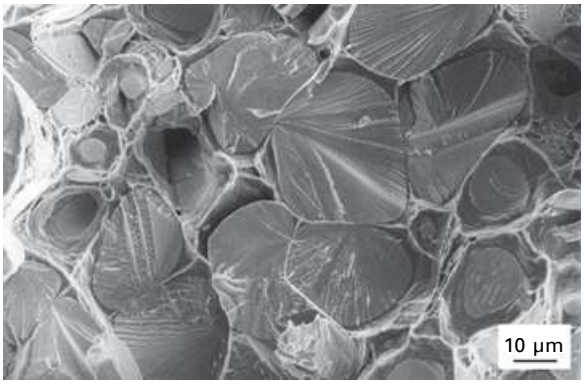

(b)

11.7 W heavy alloys with low and high interfacial strength and resulting widely different ductility.[9] (a) low interfacial strength, brittle, (b) high interfacial strength, ductile.

'necks'. It has been shown quite early[10,11] that such isolated necks exhibit a different behaviour compared to bulk material. For fully dense (Armco) or high density sintered plain iron, fracturing at 77K, at the temperature of liquid nitrogen for example, results in pronounced cleavage, as shown in Fig. 11.8(a). If however sintered iron with a porosity of 12–15%, which is fully interconnected, is tested at the same temperature, ductile rupture of the individual necks occurs despite the low temperature (Fig. 11.8(b)). Slesar[10, 11] explained this by the absence of dislocation pile-up effects in the very small cross sections of the necks, dislocation sliding also being possible at low temperatures.

Since in porous sintered materials, for example sintered steels or Al alloys, in reality the sintering contacts are of relevance for the properties and not the pores – pores do not bear any load nor conduct heat or electricity – measuring the dimensions of the contacts is an important task. Since the pore structure,

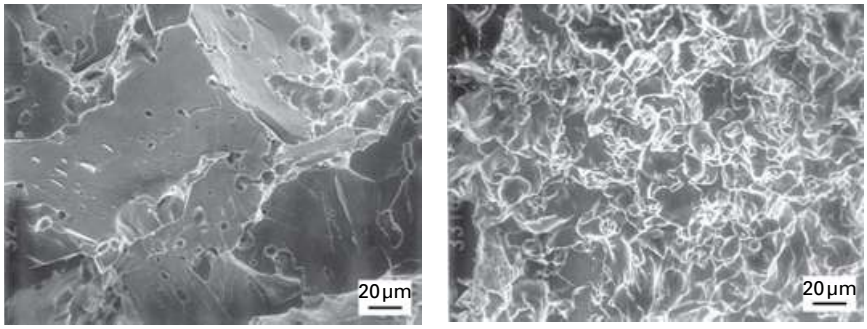

(a) (b)

11.8 Fracture surfaces of sintered plain iron with different porosity, broken at 77K. Total porosity, (a) 3.8%, (b) 13.3%.

at least for interconnected porosity, is a three-dimensional pore network, metallographic techniques, which depict only a two-dimensional section, are not very helpful. Fractographic approaches are more suitable; from fractographs the 'effective load-bearing cross section' A_c (or its opposite, the 'plane porosity P'_x) can be measured by quantitative image analysis.[11,12] Of course an image that is taken about 90° to the general plane of the fracture surface will not yield the real area of contacts that have fractured in an angle to this plane but only a projection of this area into the plane. However, this projection of the real contact area gives the correct figure when correlating the load-bearing cross section to properties that are measured by loading perpendicular to the plane, that is tensile or push-pull fatigue loading.

In any case it should be considered that it is usually the size of the sintered, undestroyed, contact that is of interest. Therefore fracture surfaces that have been generated with significant deformation before fracture tend to yield erroneous results for the load-bearing cross section A_c. The same holds if failure occurs predominantly through the particle cores and not through the sintering necks, as in the case of pronounced cleavage. While plastic deformation tends to result in too low values for A_c, cleavage results in too high values. Therefore, the way that fracture surfaces are generated is of crucial importance. With many materials, impact loading at 77K is a suitable way to generate low-deformation impact fracture, although with some risk of cleavage. Fatigue fracture surfaces are usually the best choice, in particular for failure after high cycle fatigue loading, that is closely above the fatigue endurance strength, since the slow crack growth results in preferential propagation through the weakest areas, the contacts, without any marked plastic deformation.

If such fracture surfaces are obtained, the area of the broken necks can be measured on fractographic images using image analyzing software packages. Fully automatic software is frequently difficult to use since the contrast

between the broken necks and the internal pore surfaces may be too low to detect reliably in automatic systems. If the failed necks exhibit a finely rugged structure, as for example with some heat treated sintered steels, the grey scale gradient can be used,[13] since the internal pore surfaces are rather uniformly grey, with only slight gradients. Fracture surfaces thus evaluated are shown in Fig. 11.9; in Fig. 11.9(b) which relates to Fig. 11.9(a) and in Fig. 11.9(d) which relates to Fig. 11.9(c) the detected area of the failed neck is shown in white. If however the contrast between broken neck and pore is visible only to the operator but not to the system, semi-automatic systems have to be used (e.g. Dlapka *et al.*[14]), an approach that at least alleviates the contrasting problem but tends to bring about a considerable 'operator effect'.

Recently it has been stated that the load-bearing cross section can also be obtained from quantitative metallography data,[15] *that is from sections*, but it has still to be checked how reliable this approach is over a wide range of porosity and materials. Of course the sensitivity to metallographic preparation is also very pronounced here.

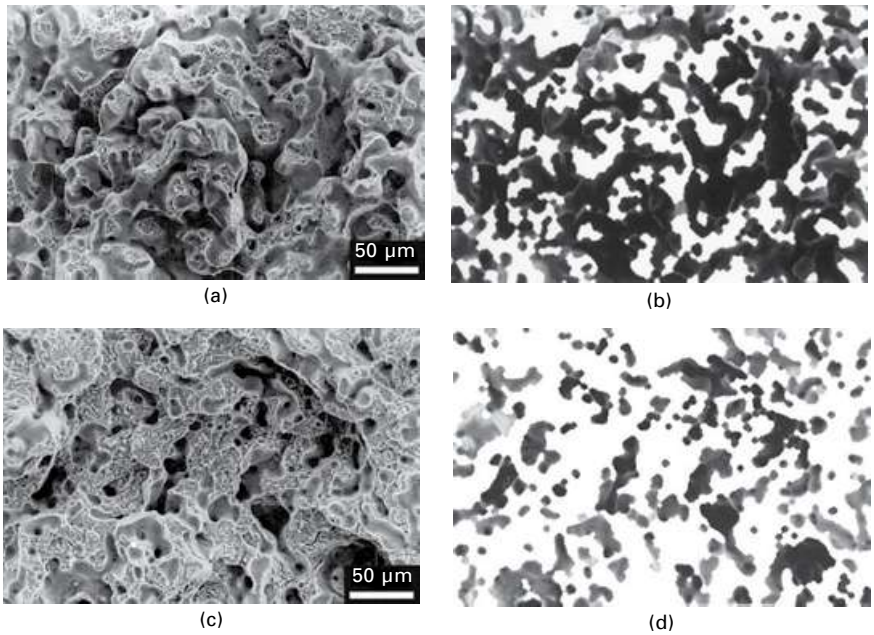

11.9 Fracture surfaces of sintered steel Fe–1.5% Mo–0.7% C, quenched and tempered, and impact tested at 77K:[13] (a) total porosity 12.3%, (b) as (a), broken contacts marked white, (c) total porosity 6.2%, (d) as (c), broken contacts marked white.

11.3 Microstructures of ferrous powder metallurgy materials

11.3.1 Sintered steels: evolution of pore structure

In sintered steels, the porosity depends on one hand on the compacting pressure, which, combined with the compactibility of the starting powder mix, defines the total porosity, and on the other hand on the sintering process which defines the pore morphology, usually represented by shape factors (e.g. Blanco *et al.*[16]) and, within a certain porosity range, the connectivity as well. Typical images of sintered steels with different total porosity but sintered in the same way are shown in Fig. 11.10; images of steels with the same porosity but differently sintered are shown in Fig. 11.11.

As stated above, in the porosity range common for sintered steel parts, the pores are virtually interconnected and open to the surface, as they are in the initial state, for example, in a dewaxed green compact. At higher density levels, however, the pore channels linking the triple junctions tend to become smaller and smaller, and if intense sintering is applied, these channels are closed and the triple junctions remain as isolated pores. The transformation from interconnected to isolated pores is difficult to record, in principle only low deformation fracture studies as described above being suited to reveal this process. Since, however, interconnected porosity can be regarded to be roughly equivalent to open porosity and isolated porosity to closed porosity, measuring the closed porosity through He pycnometry is a reasonably good approach to determine the isolated porosity (although it must be considered that there may be closed pores that are interconnected). Furthermore, for numerous secondary operations it is the open porosity that counts, for example for gas carburizing or electroplating.

He pycnometry studies[14] have shown that the transition from open to closed porosity is mainly a function of the density, that is the total porosity, but in addition both the sintering parameters and the steel composition play a major role. Higher sintering temperature and a longer time results in pore closing at lower density levels and, equally, Cr prealloyed sintered steels show earlier pore closing than Mo prealloyed ones (Fig. 11.12).

So far it has been assumed that all pores present are left over from the green compact and have just had their morphology changed by the sintering process. However, there is also formation of new pores during sintering, the so-called secondary porosity (Fig. 11.13). These pores are generated from alloy element particles if transient liquid phase is formed during sintering.[17] The particles melt, either by congruent melting (as in the case of Cu) or by eutectic reaction with the matrix[18] and the liquid is rapidly distributed in the steel matrix by capillary forces, the driving force being the fast formation of solid solution, in other words it is an entropy-driven process. Depending on the way these pores are generated, their size is correlated to that of the

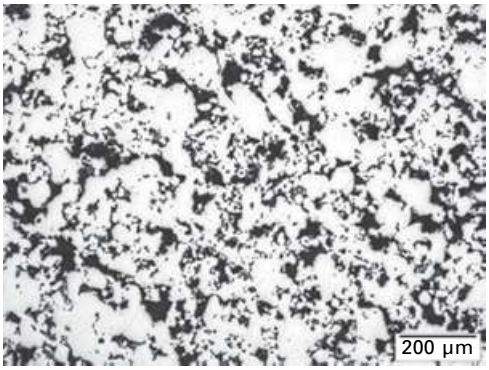

(a)

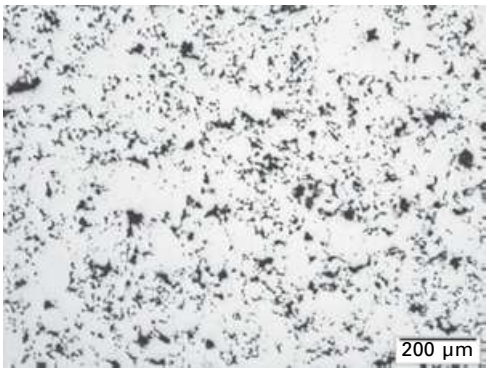

(b)

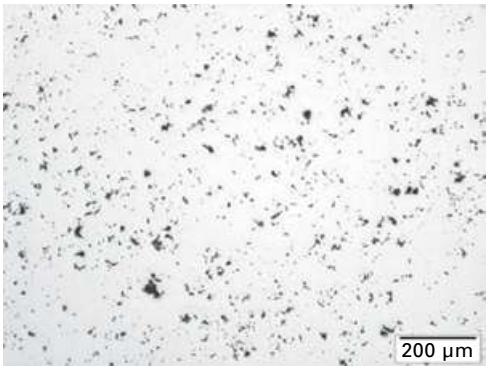

(c)

11.10 Metallographic sections of sintered steel Fe–0.85% Mo–0.3% C with varying porosity, sintered 30 min 1120°C, unetched: (a) 25% total porosity, (b) 9% total porosity, (c) 5% total porosity.

initial alloy element particle in different ways: for congruent melting, the size of the pore is virtually the same as that of the original particle, while for eutectic melting, as for example for Mo particles in an Fe-C matrix, the

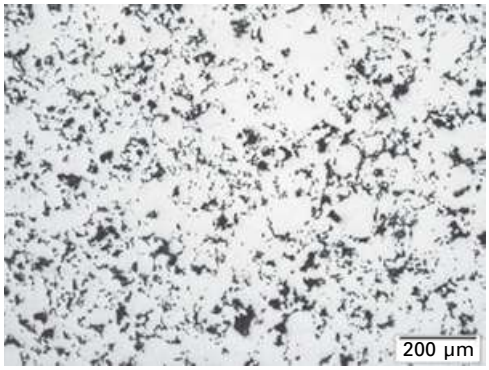

(a)

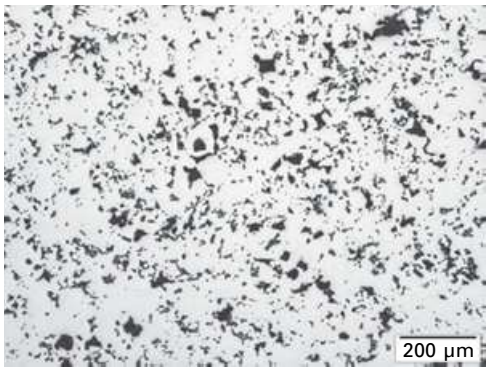

(b)

11.11 Sintered steel Fe–0.85% Mo–0.3% C with 15% porosity, unetched: (a) sintered 30 min 1120°C, (b) sintered 60 min 1280°C.

pore may be double the size of the original particle, since most of the melt consists of matrix material. These secondary pores may have an adverse effect on the properties, in particular on the fatigue endurance strength, since they act as crack initiation sites.[19,20] Therefore, both careful selection of the alloy powder grade as well as proper mixing, to avoid formation of alloy particle agglomerates, are required.

11.3.2 Sintered steels: austenite grain size

Compared to wrought steels, sintered steels are 'heat treated' (= sintered) at very high temperatures. Compared to the standard austenitizing temperature of a structural steel, the common sintering temperatures are extremely high. Therefore, excessive austenite grain growth would be expected, which is, however, not the case (see Fig. 11.14).

The reason for this is the pinning effect of the pores. As has been shown by Dlapka *et al.*,[21] that even fairly low volume fractions of pores effectively

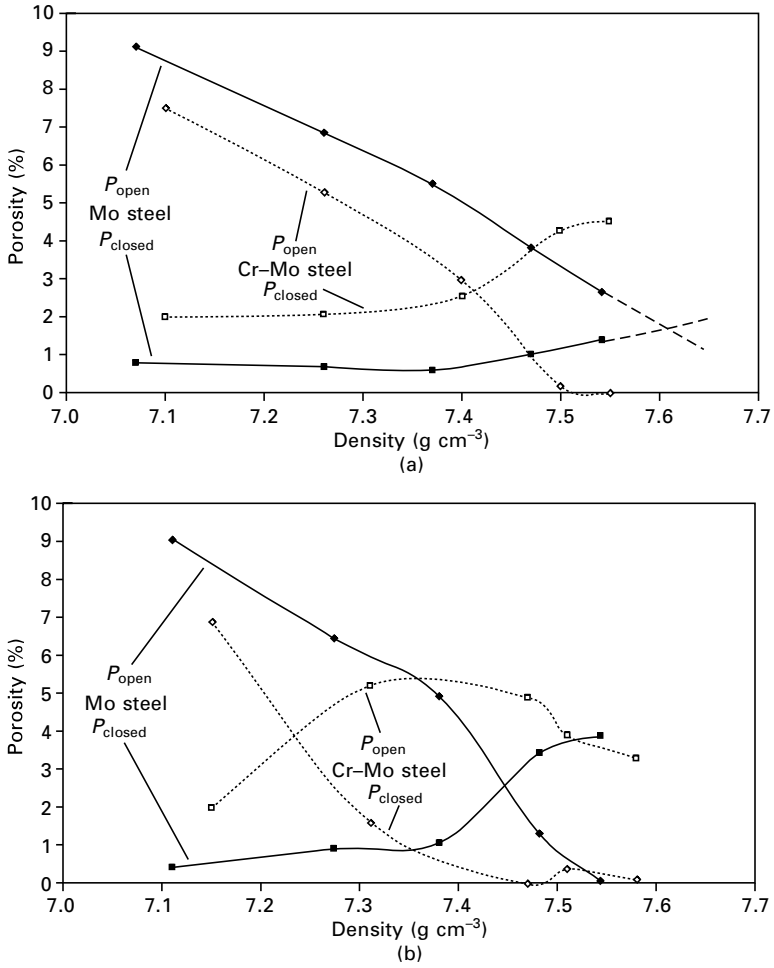

11.12 Open and closed porosity of different sintered steels as a function of the density and the sintering parameters.[14] (a) Sintered at 1120°C, (b) sintered at 1250°C.

prevent grain growth during sintering as well as during heat treatment, meaning that sintered steels are insensitive to overheating. The maximum austenite grain size is the size of the original powder particles. Only in the case of very high relative density, >7.6 g cm^{-3}, combined with intense sintering, has significant grain growth been recorded; under normal conditions, austenite grain growth can be safely neglected with sintered steels.

11.3.3 Sintered steels: carbon dissolution

As with wrought steels, with sintered steels the most common alloy element is carbon. It is usually introduced by admixing fine natural graphite grades,

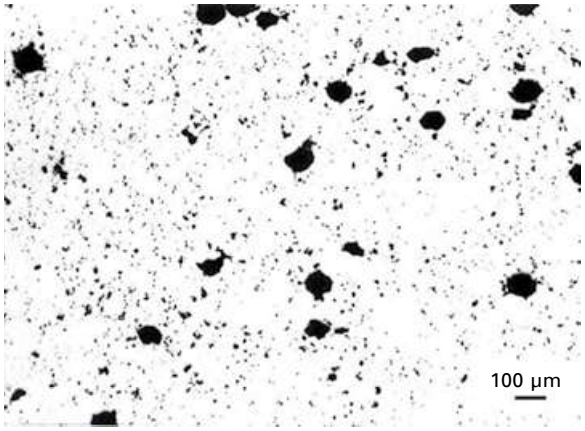

11.13 Secondary porosity in different sintered steels prepared from mixed powders: (a) Fe–3% Cu, unetched, (b) Fe–1.5% Mo–0.7% C, Nital etched.

the graphite being dissolved during sintering. It has been observed that this dissolution does not occur immediately when the eutectoid temperature is attained but that considerable overheating is necessary; in plain carbon steels prepared from atomized iron powder, the graphite is dissolved in the temperature range 900–1000°C, as indicated both by metallographic analysis, considering the amount of pearlite formed, see Fig. 11.15 (from Momeni[22], and analysis of the free carbon (Fig. 11.16). The traditional notion is that natural graphite grades are more readily dissolved in iron than artificial ones; however, today very suitable artificial grades are commercially available.[23,24]

11.3.4 Sintered steels: effect of alloying techniques

One of the main parameters affecting the microstructure of sintered alloy steels is the alloying technique (see also Chapter 7). This is something unknown

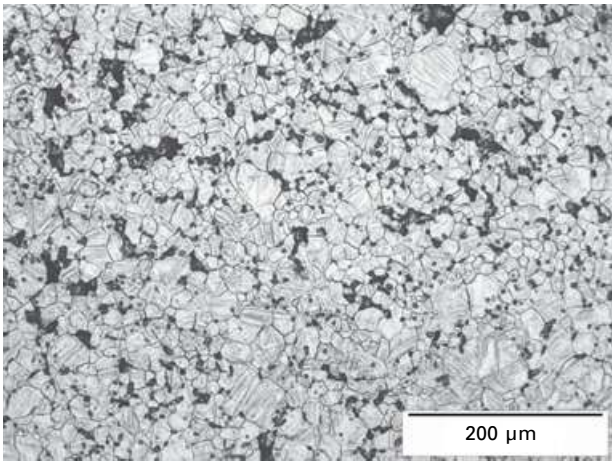

(a)

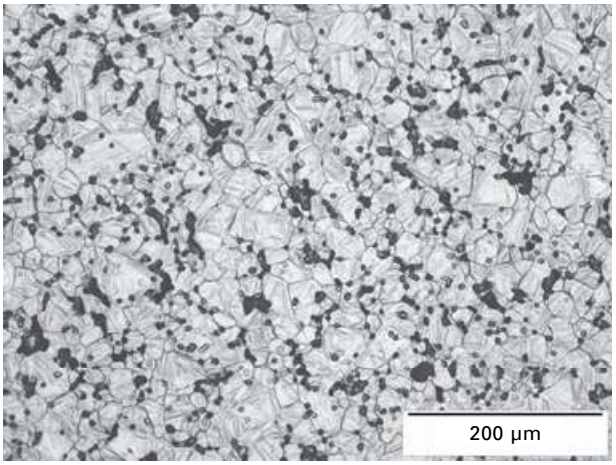

(b)

11.14 Sections of Cr prealloy steel, sinter hardened at different temperatures and simultaneously thermally etched: (a) 1120°C, (b) 1250°C.

with wrought steels, but for sintered steels the same nominal composition may result in completely different microstructures, depending on the starting powder used, in particular if chemically homogeneous (prealloyed) or heterogeneous (mixed or diffusion bonded) grades are employed. In Fig. 11.17 different types of sintered steels are shown: the quite regular upper bainitic structure of an Mo prealloy steel is visible compared to a similar steel produced from a mixed powder; in the mixed powder, after sintering at moderate temperature a mixed microstructure is formed containing pearlite, bainite and some martensite, depending on the local Mo content. Undissolved Mo

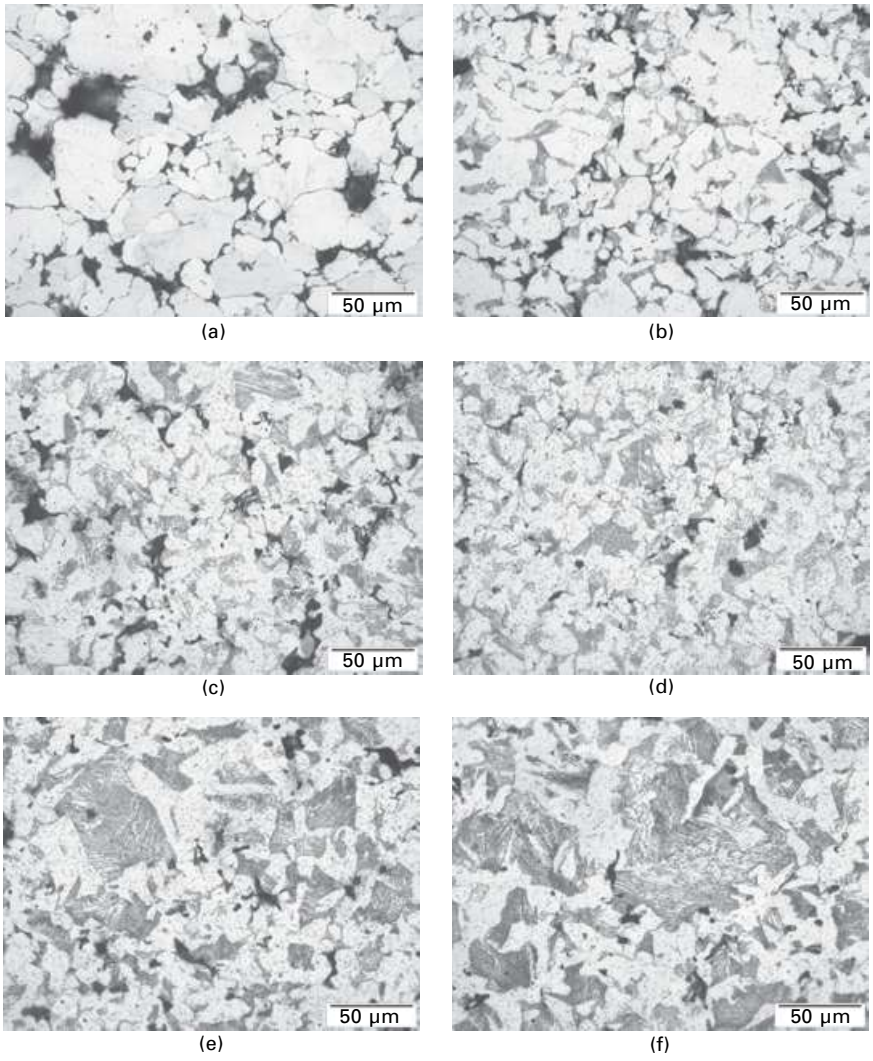

11.15 Fe–0–5% C after sintering for 60 min at different temperatures:[22] (a) 700°C, (b) 800°C, (c) 900°C, (d) 1000°C, (e) 1100°C, (f) 1200°C.

is also visible which has, however, been transformed into carbide. Typically, a prealloyed steel will exhibit virtually the same microstructure regardless of the sintering temperature while changing the sintering temperature may have a dramatic effect on the microstructure of a mixed or diffusion bonded steel, as visible when comparing Figs. 11.17(b) and 11.17(d).

Diffusion bonded Ni–Cu–Mo steels result in the typical 'Distaloy' microstructure (after the trade name of a major manufacturer), as shown

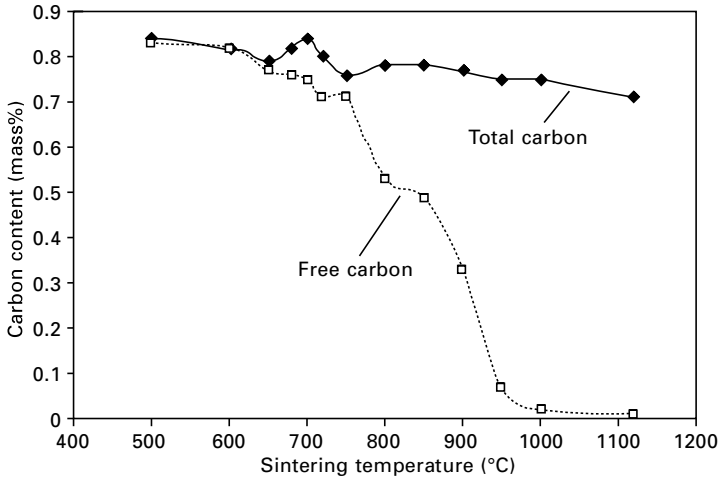

11.16 Free graphite in Fe–0.8% C as a function of the sintering temperature. Starting materials are water atomized iron powder and natural graphite.[23]

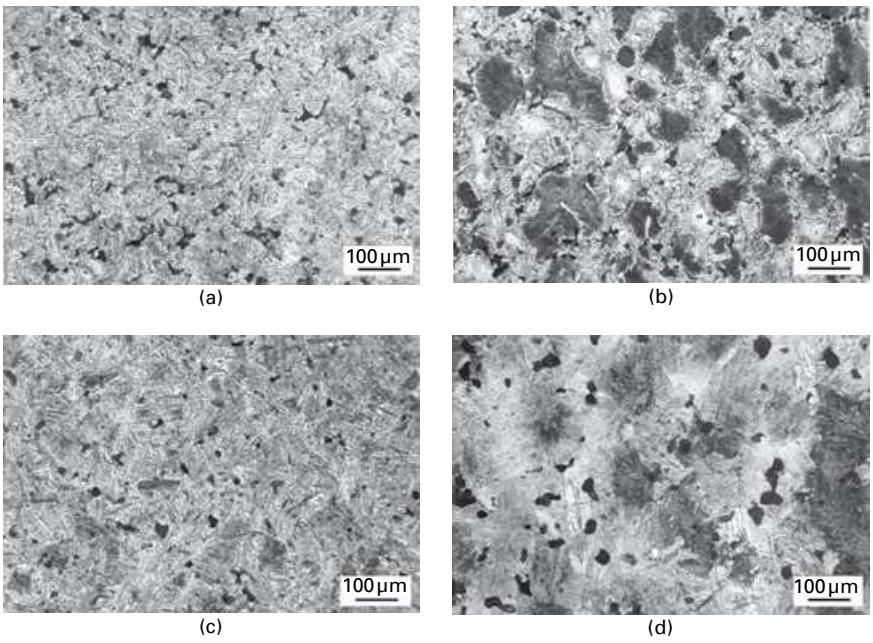

11.17 Fe–1.5% Mo–0.7% C, prealloyed vs. mixed, sintered 1200°C vs. 1320°C: (a) prealloyed, 1200°C, (b) mixed, 1200°C, (c) prealloyed, 1320°C, (d) mixed, 1320°C.

in Fig. 11.18(a). Here, widely varying microstructural constituents such as ferrite, pearlite, bainite, martensite and retained austenite are found closely adjacent to one another, as a consequence of the heterogeneous distribution of the alloy elements.[25] *There are however also 'hybrid' variants, which* combine prealloying and diffusion bonding; most commonly they are based on Mo prealloyed steel grades and contain Ni or Cu or both as diffusion bonded alloy elements. Such steel grades are widely used as sinter hardening grades; typical microstructures are shown in Fig. 11.18(b).

An attractive way to produce sintered steels with regular heterogeneous microstructure is by coating. Iron or steel powders can be coated with

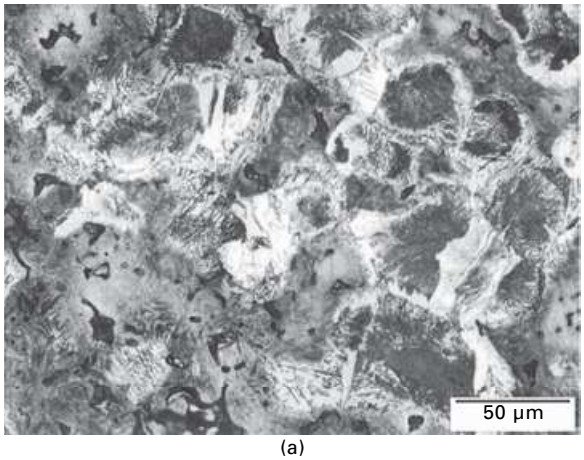

(a)

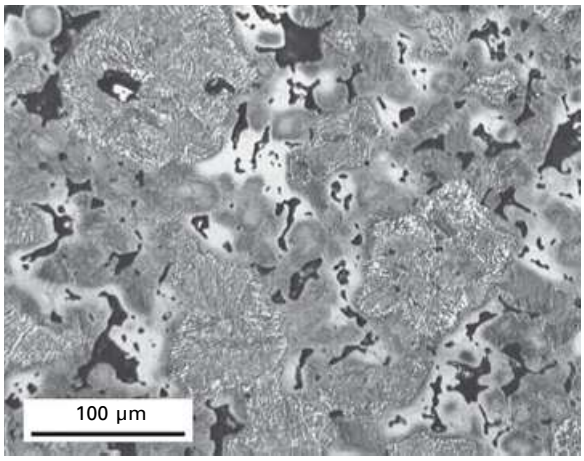

(b)

11.18 Microstructure of different diffusion alloyed and hybrid alloyed (prealloy + diffusion bonding) sintered steels (photos: Höganäs AB): (a) diffusion bonded Ni–Cu–Mo alloy steel, (b) hybrid alloy steel (Fe–Mo)–Ni–Cu.

Cu by cementation (Fig. 11.19(a)); such alloying results in more regular microstructure,[26] *in particular* less free Cu (Fig. 11.19(b) and (c)). Coating with other elements, such as Ni, is more difficult and must be done, for example, by electroplating, since the common electroless 'Ni' deposits contain significant amounts of P and thus cannot be regarded as real Ni layers.[27] Ni electroplated iron powder can be processed to steels with 'micrograd ient' structure, that is a fairly regular but heterogeneous distribution of Ni, with resulting graded transition between the microstructural constituents (Fig. 11.19(d)).

11.3.5 Sintered steels: effect of heat treatment

Sintered steels can be heat treated in the same way as wrought steels when considering their special features. The open pores cause problems when quenching in an oil or salt bath, being filled with the quench media, and during

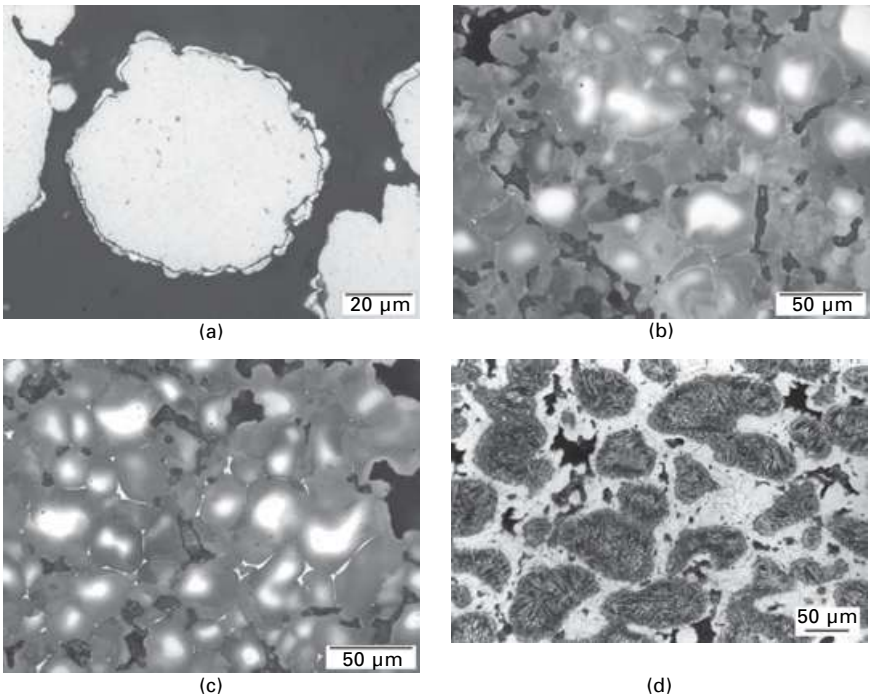

11.19 Microstructures of sintered steels manufactured from coated starting powders: (a) Cu coated Fe powder (Fe–8% Cu), (b) Cu alloy steel (Fe–8% Cu) from coated powder (dark areas: Fe–Cu solid solution; white: unalloyed iron), (c) Cu alloy steel (Fe–8% Cu) from mixed powders, bright grain boundary phase: free copper (d) sintered steel prepared from Ni coated Fe powder (dark areas: pearlite/bainite; light areas: martensite and retained austenite).

gas carburizing or nitriding, resulting in a tendency to 'through treatment', that is carburizing or nitriding of the cores. On the other hand, overheating is not a problem owing to the grain growth inhibiting effect of the pores.

Sintered steel parts are frequently sinter hardened, by blowing cold gas onto them immediately upon leaving the sintering zone of the furnace. If the alloy composition is suitably selected, fully martensitic microstructures are obtained, as shown in Fig. 11.20. Since the cooling rates obtained with sinter

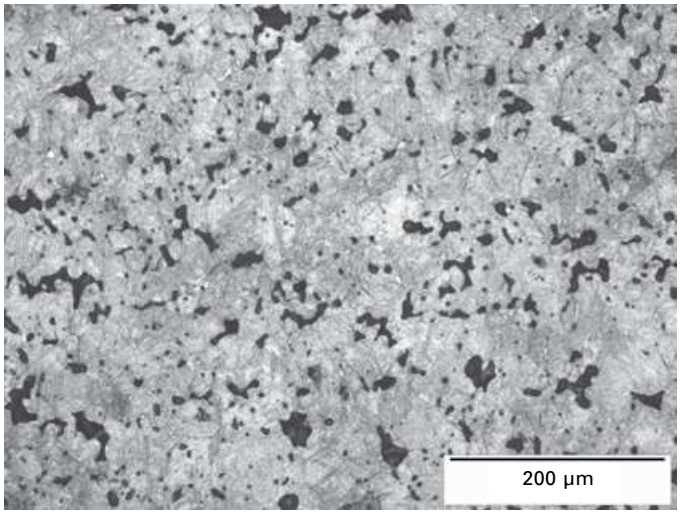

(a)

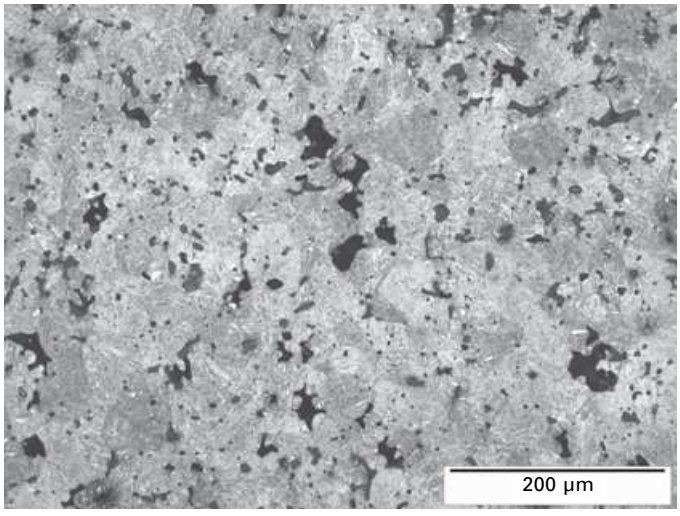

(b)

11.20 Microstructures of sinter hardened Cr–Mo prealloyed steels:[28] (a) as gas quenched, (b) gas quenched and tempered at 180°C.

hardening are barely >3 K s^{-1}, air hardening behaviour is required, which means sufficient amounts of Cr, Mo, Ni and Cu, with the combination of Mo+Cu or Cr+Cu being particularly effective. Tempering or at least stress relieving is usually done after sinter hardening. Generally, sinter hardening is more economical than separate heat treatment and also results in cleaner parts without oil; the penalty is the higher alloy element content necessary.

Quench and temper treatments are frequently done as induction hardening of the surface and subsurface zone, which is the standard procedure, for example for sprockets: In Fig. 11.21, for a typical sintered steel, the hardened martensitic surface zone is shown compared to the non-hardened ferritic–pearlitic core. Rapid austenitizing is followed by emulsion quenching, which

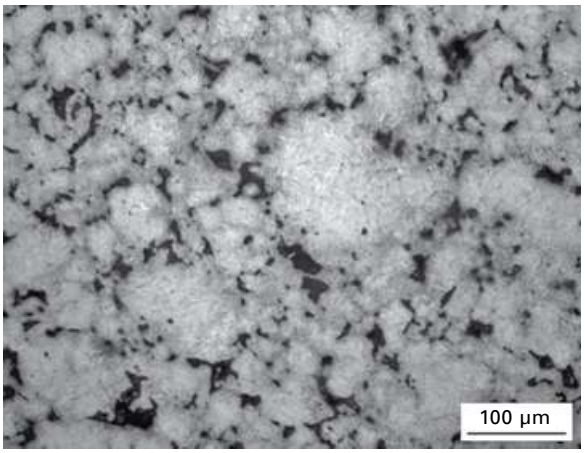

(a)

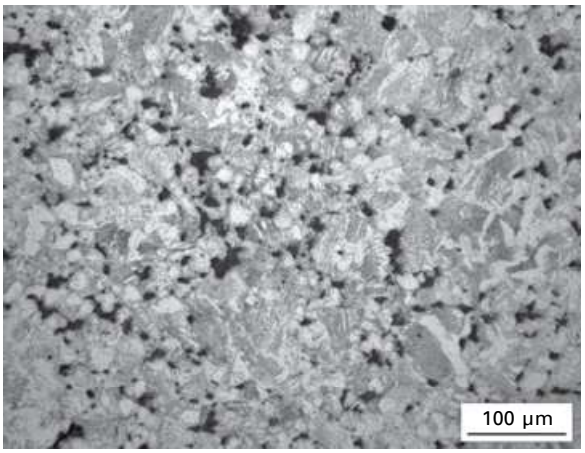

(b)

11.21 Induction hardened sprockets from Cu alloyed sintered steel: (a) induction hardened surface zone, (b) base material.

results in hard surfaces and reasonably tough cores, although the process has to be done properly to avoid quench cracks.

The most popular way of obtaining hard surfaces and tough cores is, however, thermochemical treatment by carburizing, carbonitriding or nitriding. In case of parts with homogeneous porosity, the problem of through carburizing can at least be alleviated by adapting the parameters; for surface densified parts, it is however extremely difficult to obtain well carburized densified areas without overcarburizing the non-densified surfaces. Here, either plasma carburizing or low pressure carburizing combined with high pressure gas quenching are alternatives, in particular LP carburizing has been shown to be suited to surface densified PM gears.[29] Since both processes use oxygen-free carbon carriers – CH_4 and C_2H_2 or C_3H_8, respectively – they are also applicable for Cr alloyed sintered steels and do not suffer from the oxidation problems encountered with gas carburizing using $CO–H_2$ mixes. Microstructures of carburized parts are shown in Fig. 11.22.

For nitriding, standard gas nitriding tends to result in through nitriding, with pronounced expansion; therefore, plasma nitriding is the method of choice here, which limits the nitriding effect on the surface. Mo prealloyed steels are particularly well suited here, and more recently Cr and Cr–Mo prealloyed steels have also been used.[30] In general, chemically homogeneous prealloyed steel grades are better suited to thermochemical treatments than heterogeneous ones prepared from mixed or diffusion bonded powders.

11.3.6 Sintered steels: microstructures of joints

As explained in Chapter 7, joining PM parts to each other or to wrought steel parts is a very common procedure, but the processes applied differ from those used in standard steel metallurgy. Fusion welding is done mainly through laser or electron beam welding, with a very narrow joint (see Fig. 11.23(a) and (b)), to avoid pore agglomeration and the formation of large voids. Otherwise, projection welding is the preferred process, once more offering a very limited weld zone. Frequently this is done as capacitor discharge welding, for which a typical joint is shown in Fig. 11.24.

Brazing PM parts is usually done during sintering, as sinter brazing. Here the effect of open pores that tend to wick rapidly the liquid filler has to be considered, leaving an empty gap in the joint. Therefore, reactive fillers have to be used that solidify in contact with iron through peritectic reactions,[31] thus blocking the pores and keeping the filler in the joint. Typically, Ni–Cu–Mn base fillers are used, which leave a highly hardenable joint, as indicated in Fig. 11.25(a). Recently[32] it has been shown that plain Fe–C fillers with a eutectic composition work well if the sintering temperature is sufficiently high; the advantage is that the composition is very similar to that of the

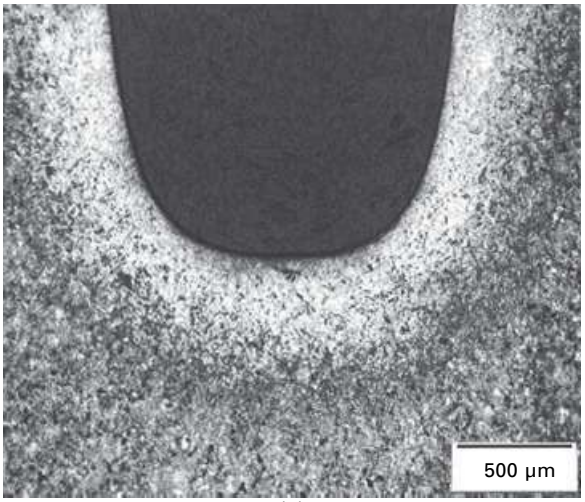

(a)

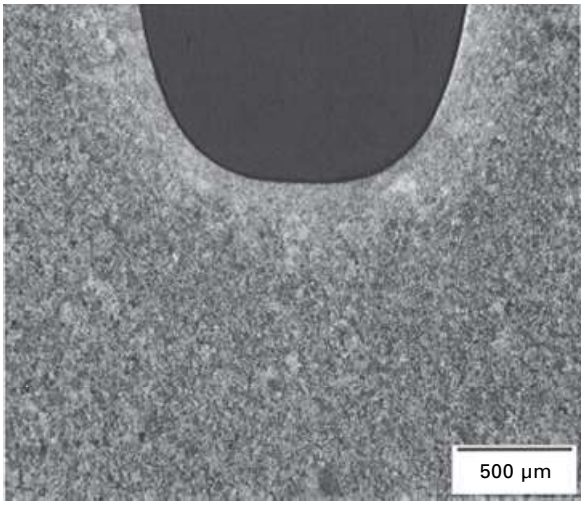

(b)

11.22 Microstructures of surface densified sintered steel gears, differently carburized: (a) low pressure carburized, (b) standard gas carburized.

parts to be joined and thus the mechanical and electrochemical behaviour is similar (Fig. 11.25(b)).

'Sinter bonding', a diffusion bonding that uses the different dimensional behaviour, for example of Fe–Cu and Fe–C during sintering, is also very common in PM parts production. If, in a concentric joint, the inner part swells and the outer one shrinks, a solid metallic bond is generated through diffusion processes that give excellent strength without any additional manufacturing steps being necessary.

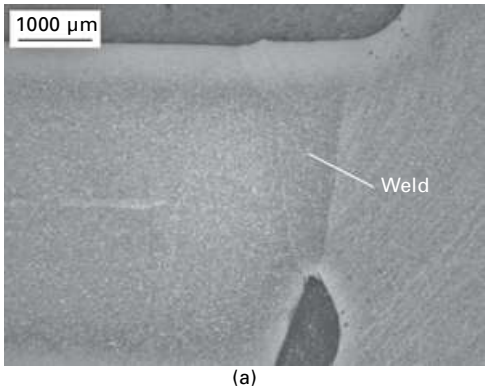

(a)

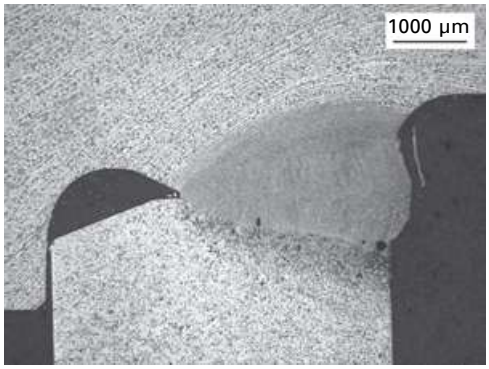

(b)

11.23 Joint between sintered steel and wrought steel parts generated by special fusion welding techniques (photos: MIBA): (a) laser welding, (b) electron beam welding.

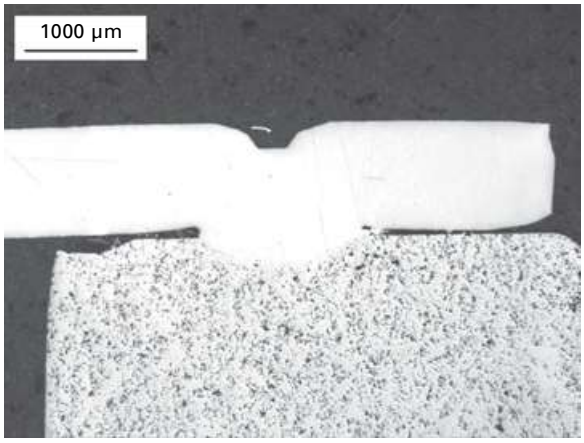

11.24 Joint between sintered steel and wrought steel parts generated by capacitor discharge welding (photo: MIBA).

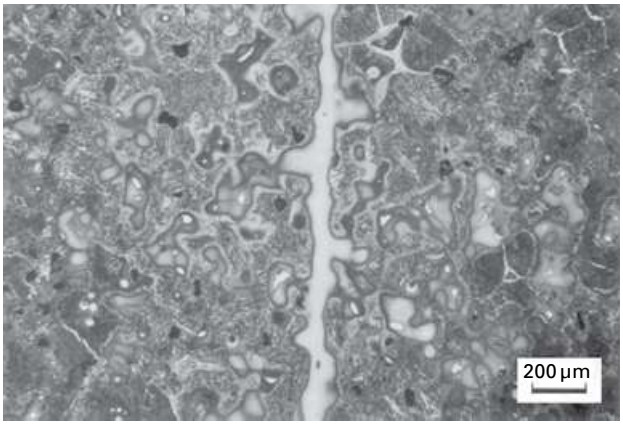

(a)

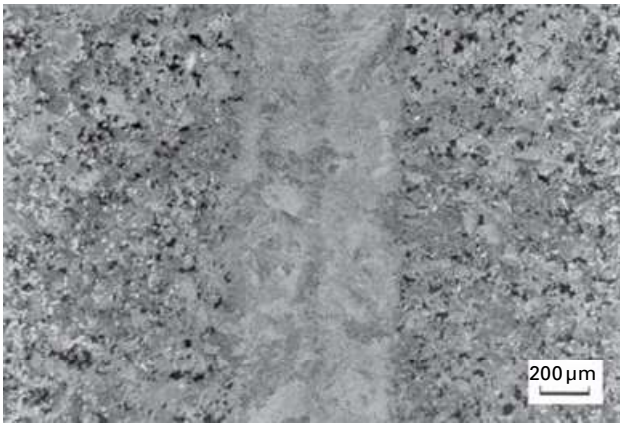

(b)

11.25 Sintered steel parts sinter brazed with reactive fillers: (a) Ni–Cu–Mn–Fe–B fillller, (b) near-eutectic Fe–C filler.

11.3.7 Metal injection moulding (MIM) ferrous materials

The most characteristic feature of metal injection moulding (MIM) parts is the pronounced change in the porosity during sintering. While a debinded MIM part usually has a porosity in the range of >40%, after sintering the porosity is virtually always <5% and frequently close to zero. Furthermore, the pore connectivity changes: in a 'brown' (debinded) part the porosity is fully interconnected, to enable removal of the 'backbone' binder component in the first stage of sintering. Subsequently, the pores not only decrease in size but also become isolated, forming more or less spherical voids, that is during sintering the structure changes from a 'sponge-type', with open and interconnected porosity, to a 'swiss cheese' one, with isolated and well rounded pores. This change in the structure is easily visible from

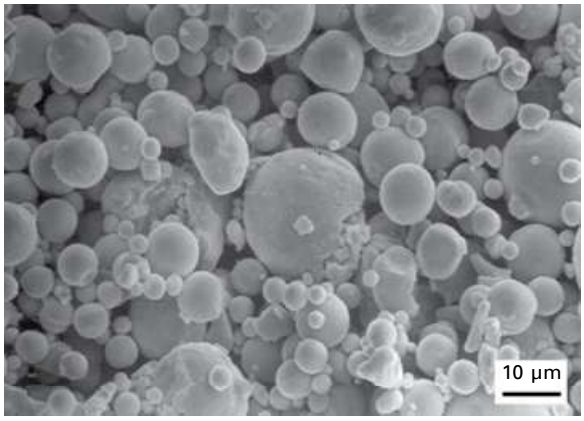

(a)

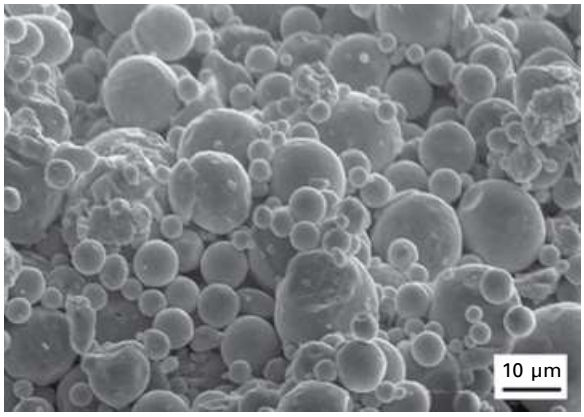

(b)

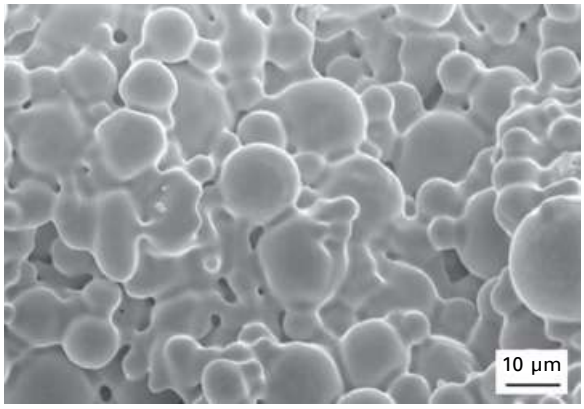

(c)

11.26 Stainless steel MIM specimens in different manufacturing states, from powder to virtually dense product (photos: Fraunhofer-IFAM Bremen): (a) gas atomized MIM powder, (b) thermally debinded compact, (c) sintered 5 min at 1180°C, (d) sintered 5 min at 1340°C, (e) sintered 1 h at 1300°C, (f) sintered 1 h at 1350°C.

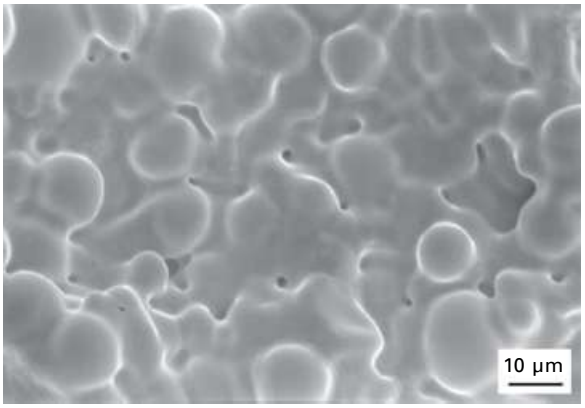

(d)

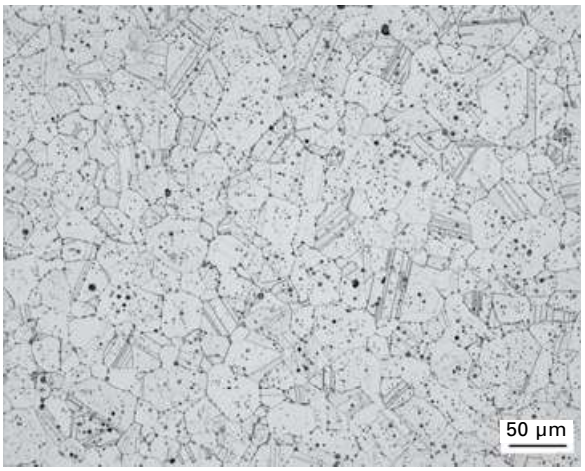

(e)

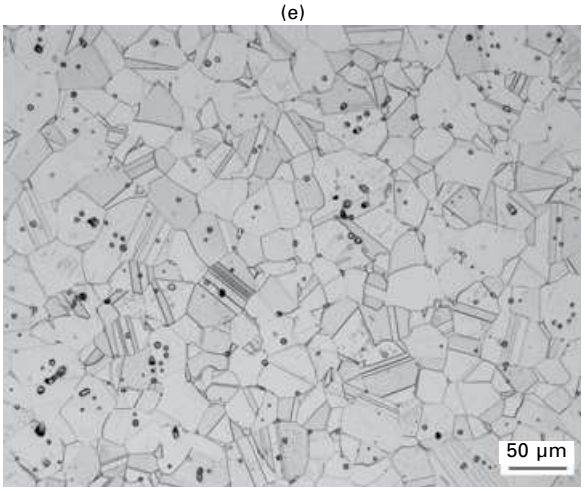

(f)

11.26 Continued

Fig. 11.26(a)–(f), depicting the different manufacturing state of a stainless steel part, from the powder to an almost fully dense material with only a few small pores.

11.3.8 Microstructures of powder metallurgy tool steels

As stated in Chapter 7, one of the major advantages of powder metallurgy tool steels compared to ingot metallurgy (IM) ones is the fine and isotropic microstructure attainable via the powder metallurgy route. This holds for virtually all grades of tool steels: cold and hot work tool steels, high speed steels and injection moulding grades. This means that compared to IM steels which exhibit a pronounced microstructural orientation, caused by the hot working necessary to disintegrate the brittle eutectic networks, the PM grades have the same microstructure in all directions and the same properties, which is very helpful for the designer of a tool.

In Fig. 11.27, the microstructure of an ingot metallurgy cold work tool steel (1.2379/AISI D2) is shown perpendicular and parallel to the tooling direction; the pronounced anisotropy is clearly visible. In Fig. 11.28, a powder metallurgy grade is shown; here, there is a finer and much more regular microstructure. It is also evident that the carbides are more rounded. The same holds for high speed steels (HSS); here the fine and rounded carbides dominate. This rounded shape may slightly lower the cutting performance compared to the coarse, angular carbides in IM HSS, but the toughness, hot and cold workability and also the grindability are very much improved.

In PM HSS, the composition is qualitatively the same as in IM HSS, and the carbide types are therefore also identical, mostly MC and M_6C. However, the content of carbide-forming elements may be markedly higher, up to >15%, and the carbide content is also higher accordingly. The finer microstructure of the PM steels can accommodate the high carbide contents without compromising the toughness, which would not be possible with IM steels. For cold work tool steels, PM steels are primarily VC based, that is the microstructure is dominated by MC carbides and not by M_7C_3 as in the case of IM steels. This gives very high wear resistance, in particular to abrasion, combined with attractive toughness.

As stated in Chapter 7, another approach for producing tool steels through powders is pressing and sintering, using water atomized powders. Here maintaining the optimum sintering temperature is of crucial importance; the optimum temperature between undersintering, with resulting porosity, and oversintering, which causes grain growth, has to be safely met.

The press-and-sinter route offers the advantage of additional hard phase reinforcement. This was already found in the 1930s when the so-called 'ferro-TiC', in fact steel-TiC composites, were invented. These materials are

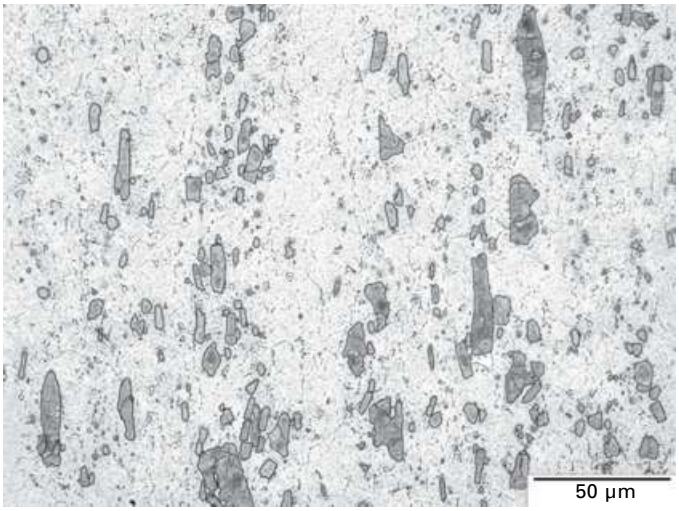

(a)

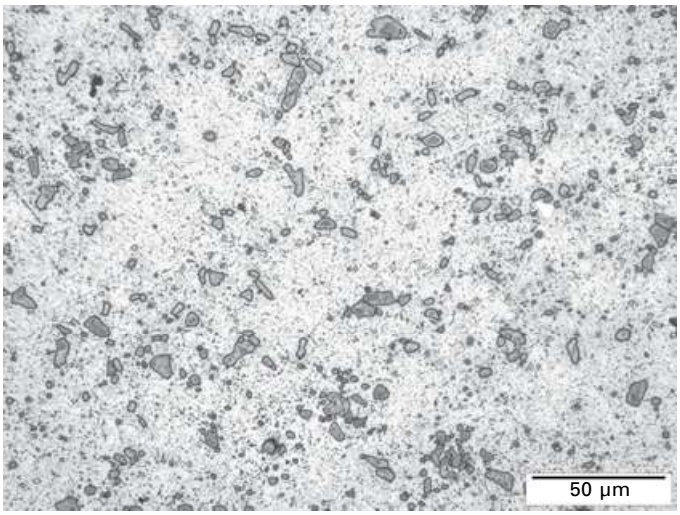

(b)

11.27 Wrought cold work tool steel (AISI D2 / 1.2379), longitudinal and cross sections:[33] (a) longitudinal section, (b) cross section.

commercially available today under the brand name 'Ferro-Titanit' (DEW) and, by choosing the right matrix material, can be tailored to different property profiles, the chance to combine high abrasion resistance with equally high corrosion resistance being particularly attractive, for example in polymer processing.

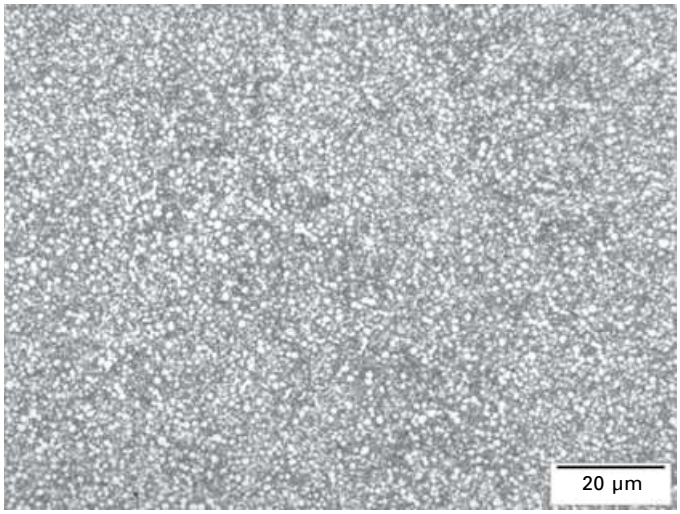

(a)

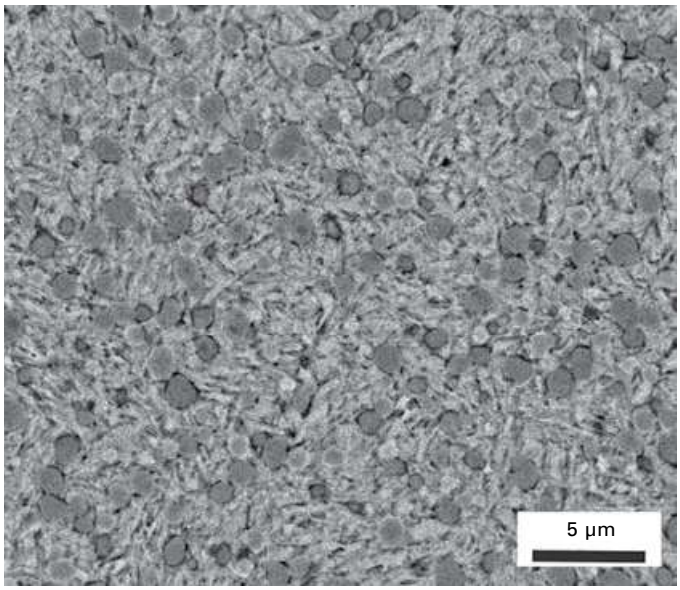

(b)

11.28 PM cold work tool steel Böhler K390:[33] (a) light optical image, (b) SEM image.

11.4 Non-ferrous materials

11.4.1 Cu-based sintered materials

From the microstructural viewpoint, Cu-based sintered materials follow similar lines to Fe-based ones. The pores present in the green compact

('primary pores') are mostly retained during sintering and tend to inhibit grain growth. Secondary pores may be generated in compacts from mixed powder grades in the presence of low-melting alloy elements, typically Sn, if too coarse Sn powders are used or if agglomerates are formed during mixing. In particular when sintering bronze from prealloyed powders, for example for filter purposes, the different diffusion coefficients of Cu and Sn in the Cu lattice cause enrichment of Sn in the sintering contacts, which can be identified by a lighter colour there compared to the standard yellow bronze colour (see Fig. 11.29).

(a)

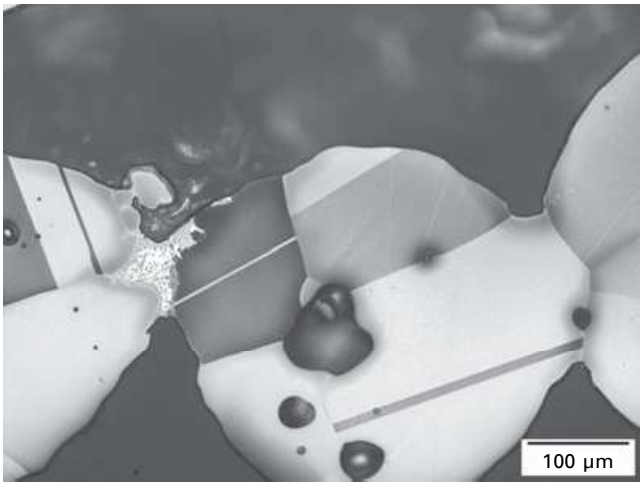

(b)

11.29 Gravity sintered bronze filter (prealloyed powder Cu–11Sn, sintered at 800°C, 30 min, H_2): (a) gravity sintered bronze filter, optical image, (b) as (a), microstructure.

Brass is much more tricky to sinter than bronze owing to the high vapour pressure of Zn – the boiling point of Zn is in the range of the usual sintering temperatures – and therefore measures have to be taken to avoid excessive Zn loss, such as sintering in semi-closed containers; using prealloyed powders is also helpful here. In case of proper sintering, regular microstructures can be obtained, however with a considerable effect of the sintering temperature, as evident from Fig. 11.30.

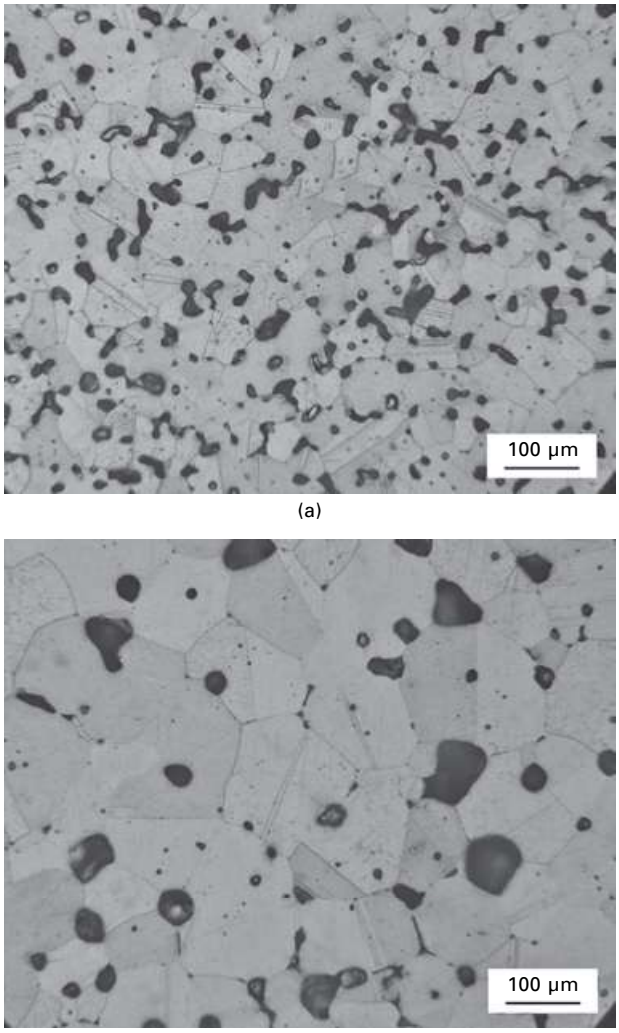

11.30 Microstructures of brass sintered at different temperatures:[34] (a) 910°C, (b) 950°C.

For electrical contact materials, for example in medium voltage interrupters, Cu–Cr is an attractive option; owing to the mutual insolubility, this is a typical two-phase pseudoalloy, Cr particles being embedded in a continuous Cu matrix (Fig. 11.31).

11.4.2 Powder metallurgy light alloys

Powder metallurgy light alloys can be structured into two groups: pressed and sintered parts and fully dense high performance materials, which are available mainly as semi-finished products.

For Al-based precision parts the main difference from other pressed and sintered materials is the presence of stable oxide layers covering the Al particles. These skins prevent sintering and have to be penetrated during the sintering process, which is done by liquid phase sintering in pure N_2,[35–40] usually combined with chemical attack by a strongly reducing metal, typically Mg. Therefore, Al sintered alloys contain elements that form a liquid phase in the range of the typical sintering temperatures (550–620°C), either by eutectic reaction with Al, as in the case of Cu,[36] or by formation of a supersolidus liquid phase, as with Al-Si-*x*-*y* alloys,[38] the latter sintering process resulting in considerable shrinkage while the former is stable dimensionally if properly done. Addition of trace elements such as Sn is also reported to assist sintering.[41]

In the former case, the as-sintered microstructure exhibits Al–Cu phases; after heat treatment, usually a T6 treatment with solutionizing, quenching and artificial ageing, these phases have disappeared, being transformed into

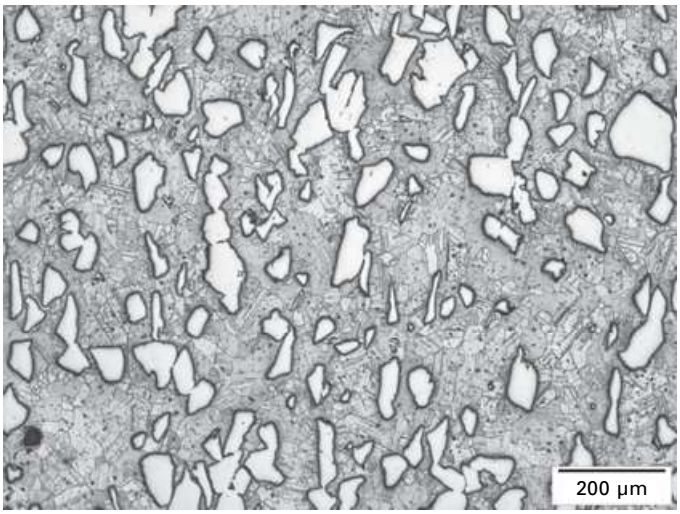

11.31 Microstructure of sintered Cu–Cr contact material.

nanosize precipitates, which results in a fairly homogeneous microstructure. The fragments of the oxide skins remain in the material; usually they are too small to be found in metallographic sections, but they act as microdefects, resulting in dimple formation and lowering the ductility. In fracture surfaces, these oxide fragments are occasionally visible (Fig. 11.32).

The microstructures of hypereutectic Al–Si alloys, in contrast, look quite different: these materials are produced from a mix of plain Al powder and a high-Si masteralloy which forms the supersolidus liquid phase, and this is discernible in the sintered microstructure. This 'hetero-supersolidus sintering' is done at temperatures at which still heterogeneous microstructures are obtained (Fig. 11.33(a)); the dark grey areas are Si phases which give the material attractive wear resistance, while the low porosity, as a consequence of the pronounced shrinkage, results in improved mechanical properties. Sintering at higher temperatures results in homogeneous but markedly coarser microstructures (Fig. 11.33(b)) and inferior mechanical properties. More recently, Al–Zn–Mg–Cu alloys have been prepared following this special 'hetero-supersolidus sintering' route.

Fully dense Al PM products may be compared to PM tool steels: they are expensive but offer superior performance. The main benefits offered by the PM route here are on the one hand the combination of immiscible components, for composite materials such as Al–SiC or Al–Al_2O_3 (Fig. 11.34: extruded Al–Al_2O_3 powder mix) or for dispersion strengthened materials that contain insoluble nanosize phases which strengthen the material in a similar way as precipitates but up to much higher temperatures. The second benefit is the very high cooling rate obtained with particulate materials: very fine and in part supersaturated structures can be obtained, as shown in Fig. 11.35 for Al–Si alloys produced by PM compared to standard IM. For the

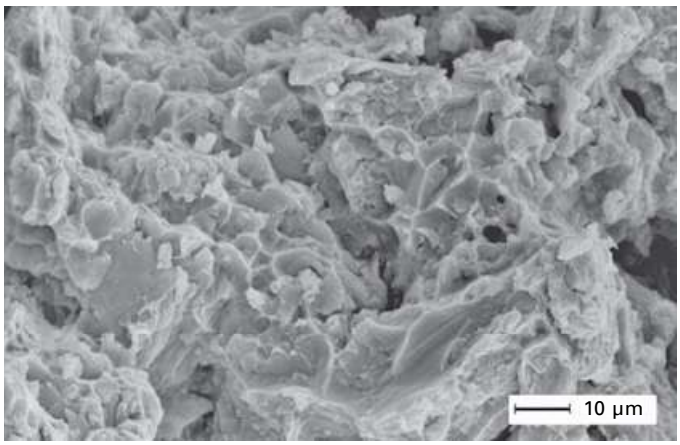

11.32 Fracture surface of sintered Al–Cu–Mg–Si (AA 2014).

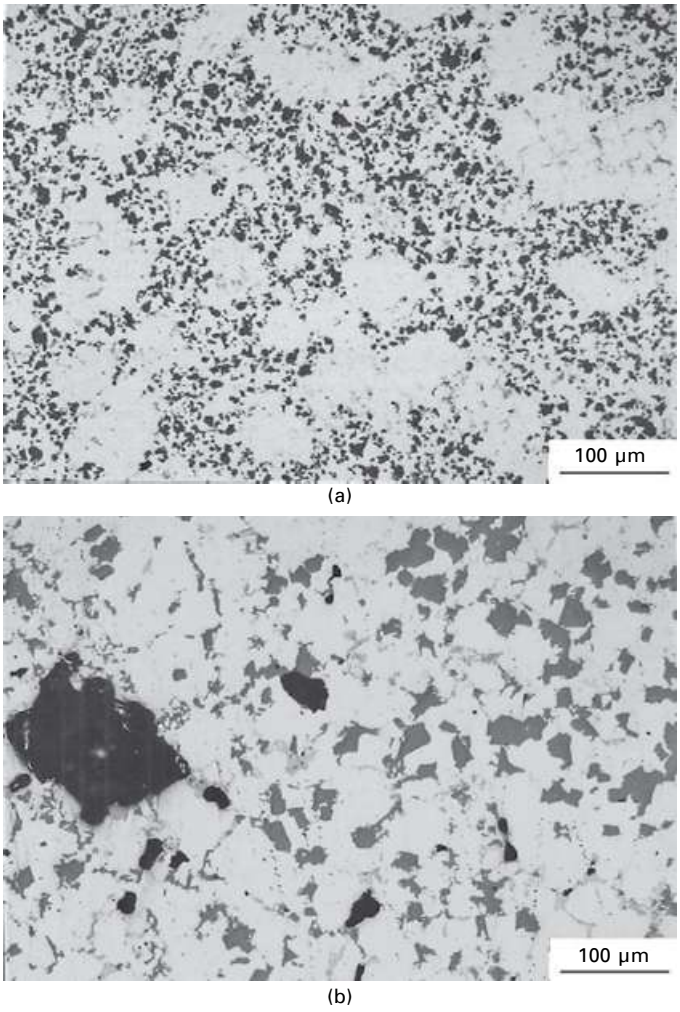

11.33 Hypereutectic Al–Si–Mg–Cu sintered at optimum temperature, 555°C (a) and oversintered, 580°C (b) (photos: Ecka Granulate GmbH).

so-called 'RS' (rapidly solidified) materials, the PM route is the most viable way; here, alloy elements that are insoluble in solid Al are introduced, for example by atomization of a suitable melt, and during processing ultrafine Al–Fe phases are precipitated which have a strengthening effect but with much lower tendency to overageing at higher temperatures than Al–Cu or Zn–Mg based precipitates. Therefore, high strength and creep resistance up to >300°C can be obtained.

PM Ti alloys are produced predominantly by the powder injection moulding route, for example for medical applications; the main features given for

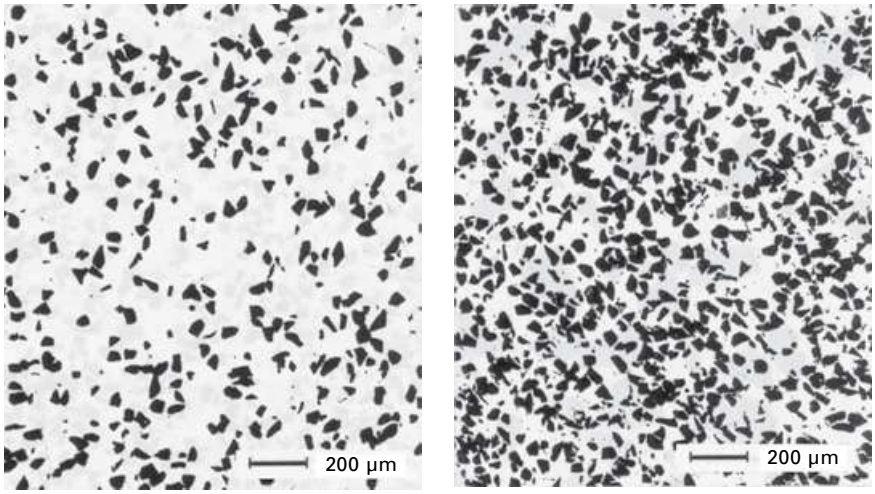

(a) (b)

11.34 Microstructures of Al–Al_2O_3 prepared by extrusion of powder compacts: (a) Al – 20 wt% (14.7 vol%) Al_2O_3, (b) Al – 40 wt% (31.5 vol%) Al_2O_3.

MIM steel products also hold here.[42] Typical microstructures are shown in Fig. 11.36; once more the very fine and regular microstructure and the low porosity are evident.

11.4.3 Powder metallurgy refractory metals

Refractory metals have been among the first products of 'modern' powder metallurgy,[43] starting with the metal filament lamp invented by Carl Auer von Welsbach, who used osmium, and the commercialized tungsten filament lamp developed in industrial scale by Coolidge.[44] From the microstructural viewpoint, important aspects are on one hand the importance of attaining high, at best full, density, which is achieved by high temperature sintering with subsequent hot working, and on the other hand the tendency of refractory metals to grain coarsening at the very high service temperatures common for these metals, which results in embrittlement.

The problem of embrittlement has been solved in different ways: for W filaments, the so-called 'non-sag' grades are used in which formation of coarse, elongated grains with high creep resistance is enforced by rows of K bubbles formed at service temperature parallel to the wire axis.[43] Stabilization of the grain structure or forcing grain growth to proceed in a defined direction can also be attained by dispersoids. For W, ThO_2 has been a common additive, for example in welding electrodes; today, Th is regarded as unfavourable and other stable oxides such as La_2O_5 are introduced that give

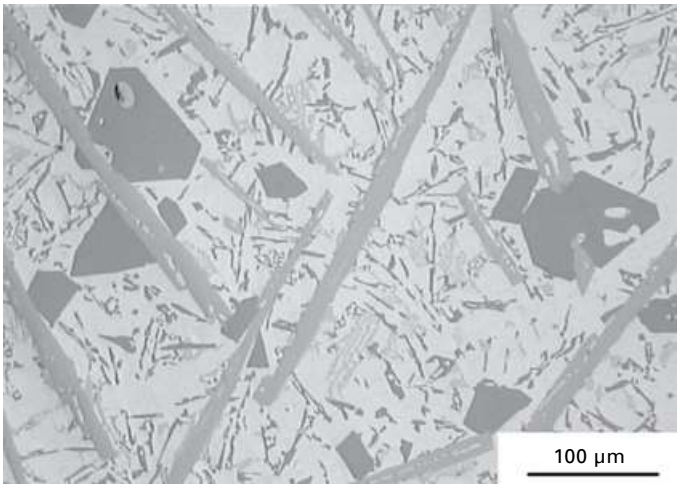

(a)

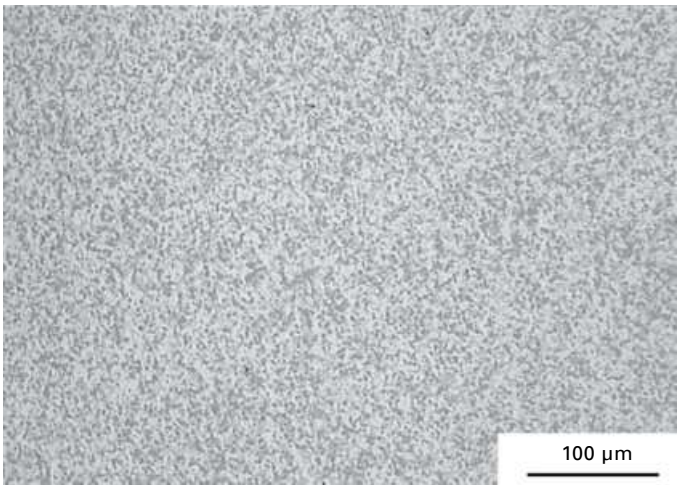

(b)

11.35 Hypereutectic Al–Si alloy, differently manufactured (photos: Powder Light Metals GmbH): (a) prepared by die casting, (b) prepared by PM/melt spinning.

fine microstructures (compare Fig. 11.37(a) and (b)). For tungsten, alloying with Re is an effective, though expensive, way to improve the mechanical properties (Fig. 11.37(c)).

For Mo, stabilization by fine carbides of Ti and Zr has proved to be effective, the respective grades are termed 'TZM'; here also, rare earth element oxides are used as dispersoids, for example for lighting purposes. Microstructures are shown in Fig. 11.37(d)–(f). In Fig. 11.37(g) and (h),

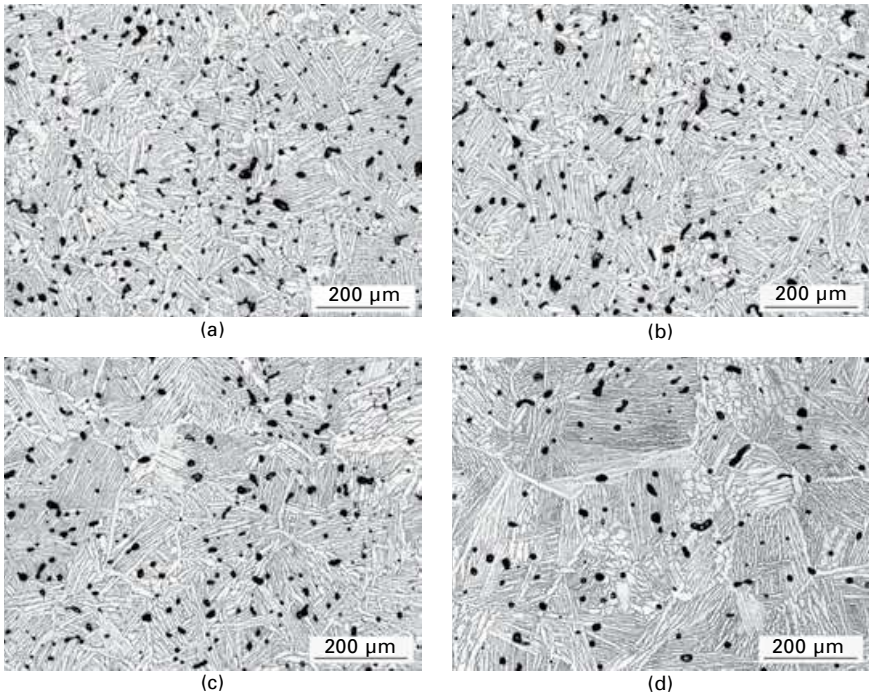

11.36 Microstructure of MIM Ti-6Al-4V, sintered at different temperatures (photos: GKSS): (a) 1250°C, (b) 1300°C, (c) 1350°C, (d)1400°C.

the microstructures of the highly corrosion resistant metals Ta and Nb are shown.

There is also a group of W-based, and to a lesser degree also Mo-based, two-phase materials, so-called 'pseudoalloys', with W and Mo as the main constituent and a binder phase formed of other metals. One example is the group of materials known as 'tungsten heavy alloys' which consist of W spheres embedded in an austenitic Ni–Cu or Ni–Fe(X) matrix. These materials are mixed from the starting powders, pressed and liquid phase sintered; the resulting microstructure, called 'heavy alloy structure', is shown above in Fig. 11.5(a); this combination of hard but fairly brittle W and soft but ductile Ni base matrix results in high strength and ductility, being one of the rare examples in which the optimum properties of different materials are effectively combined.

The other group of two-phase materials is formed by combination of refractory metals with Cu (occasionally also Ag). This aims at combining the high conductivity of Cu and Ag with the high arc resistance of W, for high current switches, or the low thermal expansion of W and Mo, for heat sink applications in electronics. Traditionally these materials have been

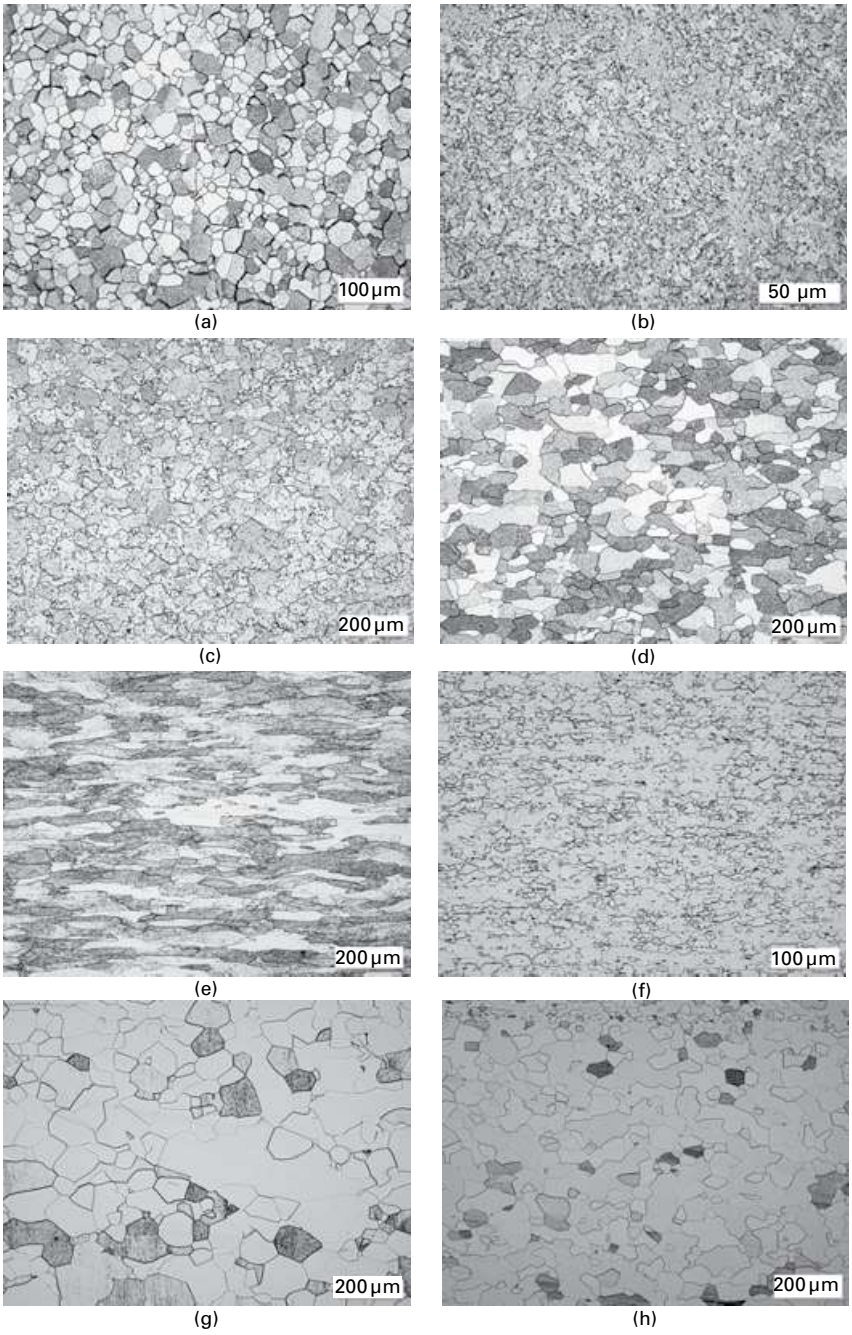

11.37 Microstructures of various refractory metals (photos: Plansee SE): (a) plain W, recrystallized, (b) W–La_2O_3, bar, (c) W–Re, sintered, (d) Mo, recrystallized, (e) Mo rolled, (f) Mo–Y_2O_3–CeO_2, wire, (g) plain Ta, sintered, (h) plain Nb, recrystallized.

manufactured by infiltrating a porous skeleton with liquid Cu or Ag; by using composite powders or ultrafine W powder coated with Cu, the press-and-sinter route can be used which for standard powder mixes yields poor densification during sintering. In Fig. 11.38 the microstructure of a W–20% Cu pseudoalloy is shown in the rolled condition.

11.4.5 Microstructures of hard metals

For hard metals, there are two major groups to be distinguished regarding composition and microstructure: the WC-based ones – the 'traditional' hard metals – and the TiCN-based grades, also known as 'cermets'. One principal difference is that WC is a compound with a precisely defined composition while TiCN may vary in composition: on one hand there is a complete phase field from plain TiC to plain TiN, and on the other hand, metallic elements may be taken into the lattice. Therefore, cermets are less critical regarding composition, in particular carbon content, than WC-based grades and they offer a wider variety of microstructures. In Fig. 11.39, the two microstructural types are shown.

For WC–Co hard metals, the WC grain size is a very important criterion, as is the binder content. For metal cutting, fine and ultrafine grades with low to moderate binder content are mostly used (Fig. 11.40(a) and (b)) which may contain cubic carbides such as TiC, NbC and TaC, while for rock drilling or chipless forming operations, coarser microstructures and higher binder contents are preferred (Fig. 11.40(c) and (d)). For ultrafine grades not only do correspondingly fine WC and Co powders have to be employed, but the

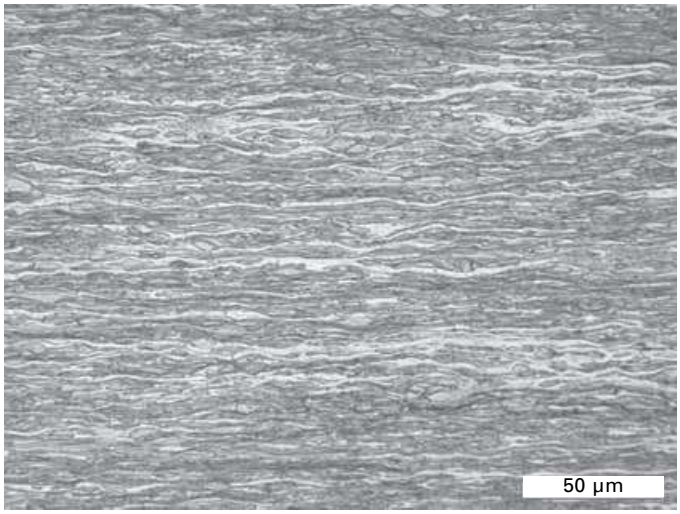

11.38 W–20% Cu, rolled.

(a)

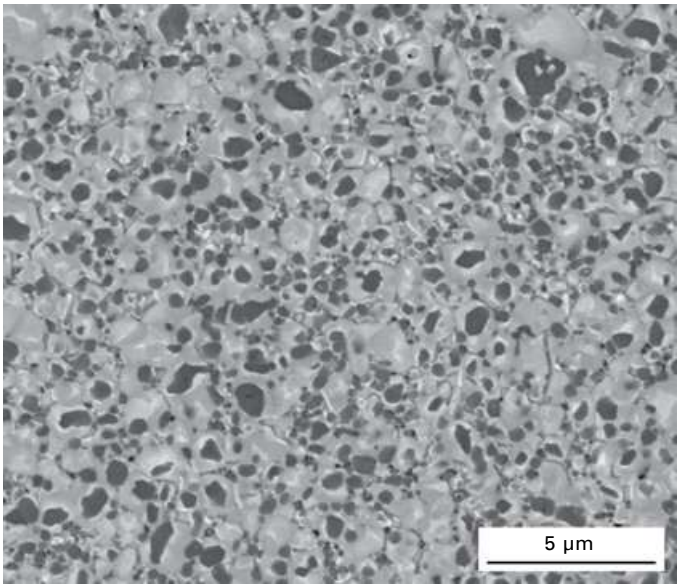

(b)

11.39 Microstructures of classical WC–Co hard metal and of cermet: (a) WC–Co hard metal, (b) TiCN base cermet.

WC grain growth during sintering, which is a problem with ultrafine grades although not with standard hard metals, has to be prevented by addition of grain refining additives such as VC or Cr_3C_2. A most critical effect is the formation of isolated very large WC grains in an otherwise ultrafine microstructure which greatly lowers the mechanical properties; this effect

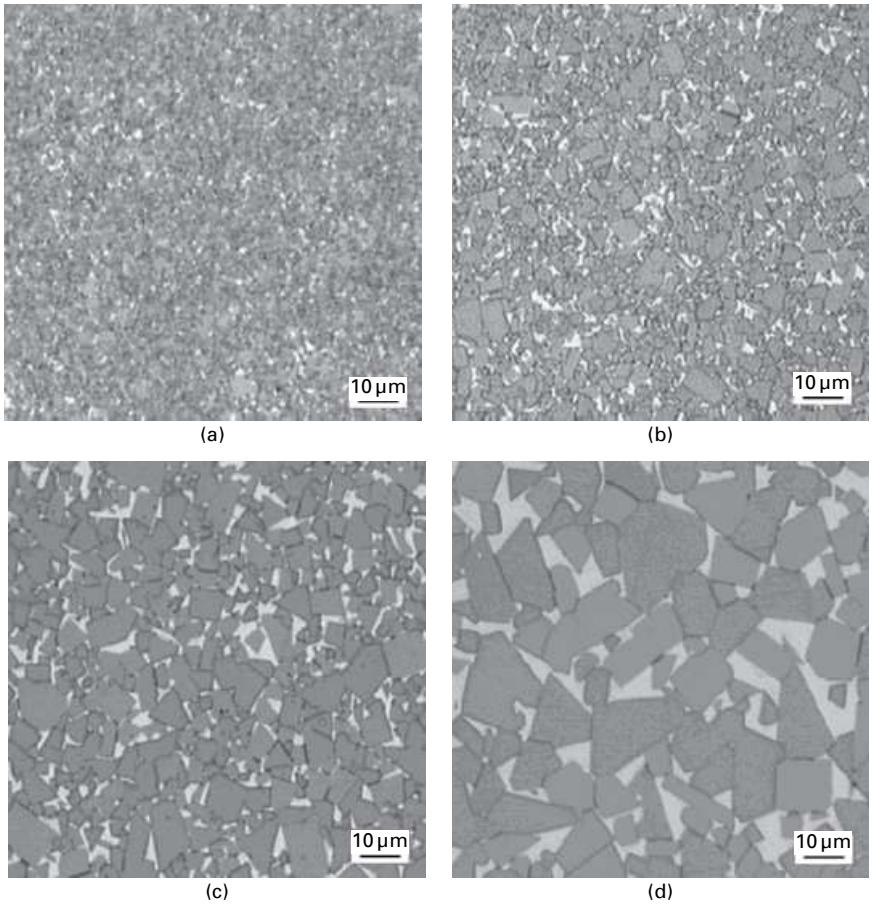

11.40 Microstructure of WC–10 mass% Co hard metal with identical binder content but different WC grain sizes: (a) sub micrometre, (b) fine, (c) coarse, (d) extra coarse.

must be prevented by very careful control of processing and in particular of the chemistry.[45]

By suitable selection of the binder composition, also Ni–Co and Fe–Ni–Co binders being used, different microstructures with their resulting properties are obtained, for example for improved corrosion resistance. Non-conventional WC morphologies are also accessible, for example platelets, as shown in Fig. 11.41; such hard metal grades may offer improved toughness properties. Even hard metals with rounded WC grains can be obtained (Fig. 11.42).

The 'cermet' type hard metals offer the unique chance to produce graded microstructures,[46,47] by changing the C–N ratio in the main hard phase TiCN. By modifying the atmosphere during sintering, either N can be removed from the surface, resulting in plain TiC there, or enriched, forming a high-TiN

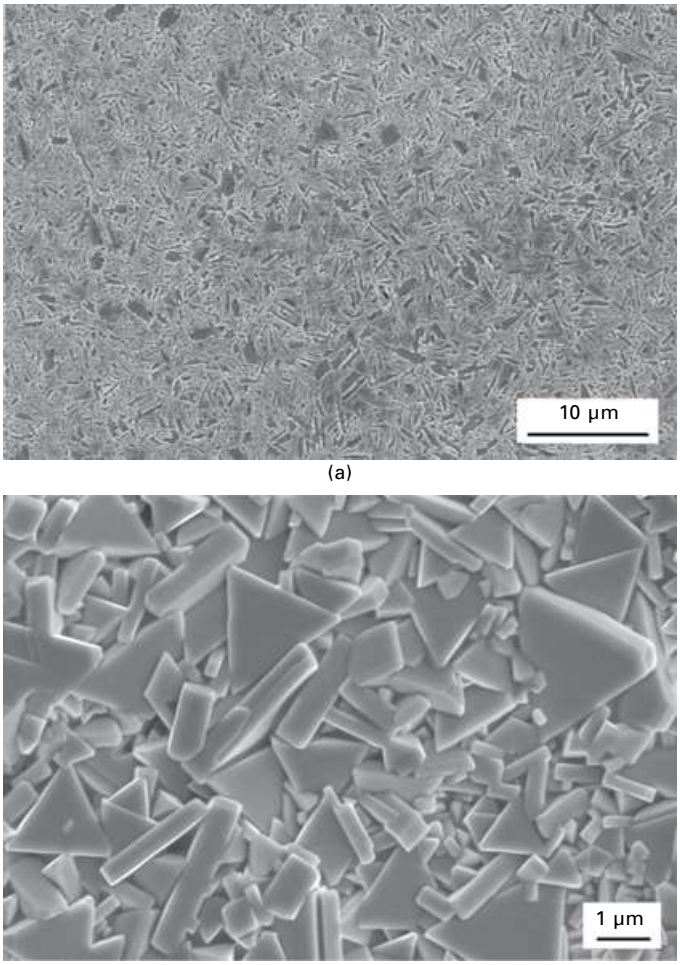

11.41 Microstructure of WC–Co hard metal with platelets: (a) metallographic section, (b) sintered surface.

surface region that exhibits cutting properties similar to those of TiN-coated hard metals but without the problem of a sharp transition between substrate and coating. Recently it has been shown that this technique can also be applied to WC–Co hard metals that contain some Ti.[48]

11.5 Trends in microstructures of powder metallurgy products

For ferrous PM materials one major direction is lowering the total porosity in order to improve the mechanical properties which strongly depend on the

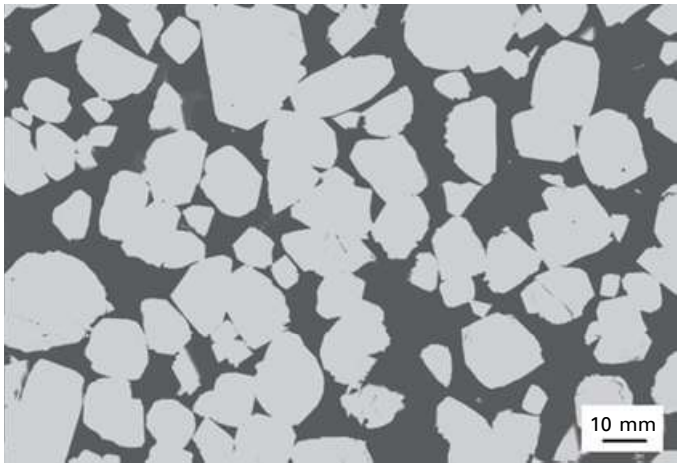

(a)

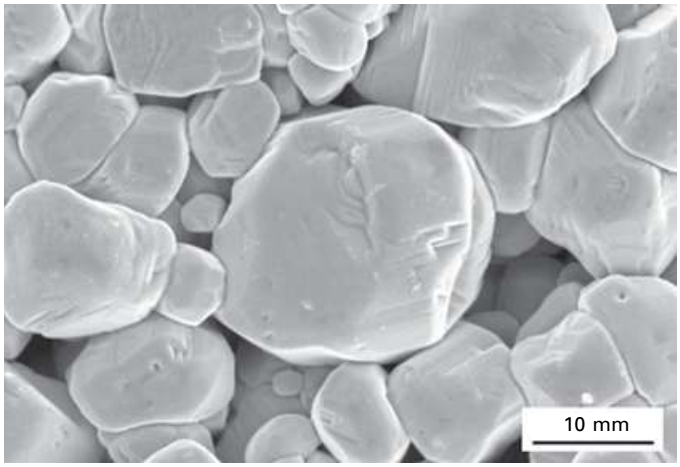

(b)

11.42 Microstructure of WC–Co hard metal with rounded WC: (a) metallographic section, (b) section etched with HCl over a long period.

density/total porosity. In particular, combining high relative density with intense sintering can be expected to result in fully closed pores, which, as shown above, significantly improves the mechanical behaviour, increasing the effective load-bearing cross section. For injection moulded products, the pores are isolated anyhow; here, further lowering the porosity, even fully eliminating them by a hot isostatic pressing (HIP) treatment after sintering, is attractive.

Another promising approach is to utilize fully the capabilities of the powder route with regard to the matrix, for example towards manufacturing

materials with defined compositional, and thus microstructural, inhomogeneity, concentrating alloy elements and resulting microstructural constituents in those areas where they are most effective, for example at the sintering contacts. This will result in more effective utilization of the mostly expensive alloy elements.

For the fully dense PM materials, finer, more regular microstructures are aimed at, regardless of whether the products are high strength aluminium alloys, tool steels or hard metals. In the latter case, varying the morphology of the hard phases offers significant potential. A further requirement is a decrease in singular defects such as non-metallic inclusions, pore clusters, large carbide grains, both regarding size and frequency, since these are the more probable to act as the sites of crack initiation the higher is the basic performance of the material. Therefore, the full potential of many PM materials can only be exploited in the case of a clean and regular microstructure. On the other hand, the use of PM routes to manufacture composites is still to be fully exploited, regardless of whether metal–ceramic or metal–polymer composites are produced. In general, despite the fairly long history of powder metallurgy, tailoring of specific microstructures still offers numerous opportunities for high performance structural and functional materials.

11.6 Acknowledgements

The authors wish to thank for supplying information and illustrations: W.D.Schubert, W.Lengauer, TU Wien, Vienna, Austria; B.Lindqvist, Höganäs AB, Höganäs, Sweden; M.Dlapka, G.Stetina, MIBA Sinter Austria GmbH, Vorchdorf, Austria; F.Petzoldt, Fraunhofer-IFAM, Bremen, Germany; M.Azadbeh, Sahand Univ., Tabriz, Iran; T.Ebel, GKSS, Geesthacht, Germany; K.Hummert, Powder Light Metals GmbH, Gladbeck, Germany; H.-C.Neubing, formerly Ecka Granulate GmbH, Germany; L.Sigl, Plansee SE, Reutte, Austria; J.L.Garcia, Sandvik Machining Solutions Sverige AB, Stockholm, Sweden.

11.7 Further reading

Books

ASM Handbook Vol.7: Powder Metal Technologies and Applications. ASM, Materials Park OH, 1998.

ASM Handbook Vol.9: Metallography and Microstructures. ASM, Materials Park OH, 2004.

Metals Handbook Vol.12: Fractography. 9th edn, ASM, Materials Park OH, 1987.

W.J.Huppmann and K.Dalal. *Metallographic Atlas of Powder Metallurgy*, Verlag Schmid, Freiburg, Germany, 1986.

P.Beiss, K.Dalal and R.Peters. *International Atlas of Powder Metallurgical Microstructures*, Metal Powder Industries Federation, 2002.

Höganäs Handbook for Sintered Components Vol.6 Metallography, Höganäs, 1999.

Metallographic Preparation of Powder Metallurgy Parts, www.struers.de, know how, application notes.

Journals

Praktische Metallographie / Practical Metallography, Hanser-Verlag (bilingual English–German), 12 issues/year.

11.8 References

1. W. Schatt, K.P. Wieters and B. Kieback, *Pulvermetallurgie*, 2nd edn, Springer, Berlin-Heidelberg-New York, 2007.
2. M. Drozda and W.A. Kaysser, *Pract. Metallogr.*, 1979, **16**, 578–82.
3. U. Engström, in, *Powder Metallurgy–State of the Art*, W.J. Huppmann, W.A. Kaysser and G. Petzow (eds), Verlag Schmid, Freiburg, 1986, 41–70.
4. M.W. Wu, K.S. Hwang and H.S. Huang, *Met. Mater. Trans.*, 2007, **38A**, 1598–1607.
5. F. Castro, S. Sainz, B. Lindsley, K.S. Narasimhan and W.B. James, *Proceedings EuroPM 2011*, Barcelona, EPMA, Shrewsbury, 2011, **1**, 47–53.
6. W. Garcia, S. Sainz, A. Karuppannagounder and F. Castro, *Advances in Powder Metallurgy and Particulate Materials* 2008 (Proceedings Powder Metallurgy World Congress 2008, Washington DC), compiled by R. Lawcock, A. Lawley, P.J. McGeehan, MPIF, Princeton NJ (2008) Part 5, 139–149.
7. F. Bernier, P. Plamondon, J.-P. Baillon and G. L'Esperance, *Powder Metall*, 2011, **54**(5), 559–65.
8. K.J.A. Brookes, *Hardmetals and Other Hard Materials*. International Carbide Data, East Barnet UK, 1992.
9. H. Danninger, M. Schreiner, G. Jangg, B. Lux, *Pract. Met.* 1983, **20**, 64–73.
10. M. Slesar, *Proceedings 7th International Powder Metallurgy Conference*, Dresden, 1981, **1**, 83–103.
11. M. Slesar, E. Dudrova, L. Parilak, M. Besterci, E. Rudnayova, *Sci. Sintering*, 1987, **19**, 17–30.
12. H. Danninger, D. Spoljaric, G. Jangg, B. Weiss, R. Stickler, *Prakt. Metallogr.*, 1994, **31**(2), 56–69.
13. H. Danninger, U. Sonntag, B. Kuhnert, R. Ratzi, *Prakt. Metallogr.*, 2002, **39**(8), 414–25.
14. M. Dlapka, H. Danninger, C. Gierl, B. Lindqvist, *Met. Powder Rep.*, 2010, **65**(2), 30–33.
15. G. Straffelini, A. Molinari, *La Metallurgia Italiana*, 2002, **10**, 31–36.
16. L. Blanco, M. Campos, J.M. Torralba, D. Klint, *Powder Metall.*, 2005, **48**(4), 315–22.

17. B. Kieback, W. Schatt, *Planseeber. Pulvermet.*, 1980, **28**, 204–15.
18. H. Danninger, *Powder Metall. Int.*, 1988, **20**(1), 21–5.
19. D. Spoljaric, H. Danninger, D. Chen, B. Weiss, R. Stickler, *Proceedings PM'94 Powder Metallurgy World Congress 1994 Paris*, SF2M, EPMA, Paris (1994) Vol. II, 827–30.
20. [illegible] *Int. J. Powder Metall.*, 1997, **33**(4), 43–53.
21. M. Dlapka, S. Strobl, H. Danninger, C. Gierl, *Prakt. Metallogr.*, 2010, **47**(12), 686–99.
22. M. Momeni, *PhD thesis*, Vienna University of Technology, 2010.
23. H. Danninger, G. Frauendienst, K.-D. Streb and R. Ratzi, *Mater. Chem. Phys.*, 2001, **67**, 72–7.
24. L. Alzati, R. Gilardi, G. Pozzi, S. Fontana, *Advances in Powder Metallurgy and Particulate Materials* 2011 (Proceedings Powder Met 2011, San Francisco), compiled by I.E. Anderson, T.W. Pelletiers, MPIF, Princeton NJ, 2011, **7**, 11–18.
25. *Höganäs Handbook for Sintered Components Vol.6 Metallography*, Höganäs (1999).
26. M. Kupkova, M. Kupka, S. Strobl, C. Gierl, J. Wagesreither, *Powder Metall. Progr. 7*, 2007, **1**, 35–43.
27. H. Danninger, S. Strobl, R. Guertenhofer, E. Dudrova, *Proceedings 2000 Powder Metallurgy World Congress*, Kyoto, K. Kosuge and H. Nagai (eds), The Japan Society of Powder and Powder Metallurgy, 2001, Part I, 394–397.
28. M. Dlapka, *PhD Thesis*, Vienna University of Technology, [illegible] *Hüttenmaenn. Mh.*, 2009, **154**, 200–204.
30. E. Santuliana, C. Menapace, S. Libardi, G. Lorenzi, A. Molinari, *Int. J. Powder Metall.*, 2011, **47**(6), 38–45.
31. W.V. Knopp, *Advances in Powder Metallurgy and Particulate Materials* 1996 (Proceedings Powder Metallurgy World Congress 1996, Washington DC) T.M. Cadle, K.S. Narasimhan eds., MPIF, Princeton NJ, 1996, **11**, 176–170.
32. H. Danninger, J.M. Garmendia, R. Ratzi, *Powder Metall. Progr.*, 2010, **10**(3), 121–132.
33. C. Sohar, *Lifetime Controlling Defects in Tool Steels*. Springer, Heidelberg-Dordrecht-London-New York, 2011.
34. M. Azadbeh, H. Danninger, C. Gierl, *Proceedings EuroPM2011 Barcelona*, EPMA, Shrewsbury, 2011, **3**, 99–104.
35. S. Storchheim, *Progr. Powder Metall.*, 1962 **18**, 124–130.
36. W. Kehl, H.F. Fischmeister, *Powder Metall.*, 1980, **23**(3), 113–119.
37. H.-C. Neubing, G. Jangg, *Met. Powder Rep.*, 1987, **42**, 354–358.
38. H.-C. Neubing, in, *Pulvermetallurgie in Wissenschaft und Praxis Bd.20*, H. Kolaska (ed), Fachverband Pulvermetallurgie, Hagen, 2004, 3–29.
39. T. Schubert, T. Pieczonka, S. Baunack, B. Kieback, *Proceedings EuroPM2005 Prague*, EPMA, Shrewsbury, 2005, **1**, 3–8.
40. D. Kent, J. Drennan, G. Schaffer, *Acta Mater.*, 2011, **59**, 2469–80.
41. G.B. Sercombe, G.B. Schaffer, *Acta Mater.*, 1999, **47**, 689–97.
42. G.C. Obasi, O.M. Ferri, T. Ebel, R. Bormann, *Mat. Sci. Eng. A*, 2010, **527**, 3929–35.
43. E. Lassner, W.D. Schubert, *Tungsten*. Kluwer Academic/Plenum Publishers, New York, 1999.

44. P.K. Johnson, *Int. J. Powder Metall.*, 2008, **44**(4), 43–8.
45. M. Sommer, W.D. Schubert, E. Zobetz, P. Warbichler, *Int. J. Refract. Met. Hard Mater.*, 2002, **320**, 41–50.
[illegible] *J. Alloys Comp.*, 2002, 1–2 **338**, 193–212.
[illegible] *Int. J. Refract. Met. Hard Mater.*, 2006, **24**, 155–161.
48. J.L. Garcia, *Int. J. Refract. Met. Hard Mater.*, 2011, **29**, 306–311.